WESTERDIJK FUNGALBIO DIVERSITY INSTITUTE

Chemodiversity of *Penicillium* isolated from alpine and arctic environments, including ten new species

D.P. Overy[1,3*], J.C. Frisvad[2], T.E. Witte[1], C.L. Hicks[1], A. Hermans[1], A. Sproule[1], G. Louis-Seize[1], K.A. Seifert[1,3], N. Yilmaz[4], J. Price[4], N.I. van Vuuren[4], C.M. Visagie[4*]

[1]Ottawa Research and Development Centre, Agriculture and Agri-Food Canada, 960 Carling Avenue, Ottawa, ON, Canada, K1A 0C6; [2]Department of Systems Biology, Building 221, Technical University of Denmark, DK-2800 Kgs. Lyngby, Denmark; [3]Department of Biology, Carleton University, Ottawa, ON, Canada, K1S 5B6; [4]Department of Biochemistry, Genetics and Microbiology, Forestry and Agricultural Biotechnology Institute (FABI), University of Pretoria, Pretoria, South Africa

**Corresponding authors*: D.P. Overy, david.overy@agr.gc.ca; C.M. Visagie, cobus.visagie@fabi.up.ac.za

Abstract: Polar, high altitude montane and cold desert environments harbour only sparse plant life and often remain frozen for extended periods. Because of their remoteness, often combined with restricted access, such regions are rarely visited and the fungal biodiversity of the soils is scarcely studied. Despite this, when such studies are undertaken, psychrophilic *Penicillium* species are often reported and the isolates exhibit a high spectrum of biologically active compounds of biotechnological interest. Small molecule profiling by mass spectrometry (often called 'metabolomics') can supplement phylogenetic species concepts and provide information to characterize variation within species or populations. During large scale fungal isolation surveys exploring new psychrophilic fungi from high altitude alpine and arctic tundra soils, several undescribed *Penicillium* species were discovered. A polyphasic taxonomic approach was adopted to formally describe ten new species using multigene phylogenetic analyses and phenotypic characterizations including secondary metabolite production, colony characters, and microscopic analysis of morphological structures. Using untargeted metabolomics and molecular networking tools, an emphasis was made to characterize, compare and discuss in depth, the chemical diversity associated with these new *Penicillium* species.

Key words: Extrolites, *Fasciculata*, GCPSR, new taxa, *Ramosum*, *Robsamsonia*, taxonomy.

Taxonomic novelties: New species: *Penicillium algidum* Visagie, Overy, Seifert & Frisvad, *Penicillium aquamarinum* Visagie, Overy, Seifert & Frisvad, *Penicillium discoense* Visagie, Overy, Seifert & Frisvad, *Penicillium hesseltinei* Visagie, Overy, Seifert & Frisvad, *Penicillium jugorum* Visagie, Overy, Seifert & Frisvad, *Penicillium marthae* Visagie, Overy, Seifert & Frisvad, *Penicillium oreophilum* Visagie, Overy, Seifert, Christensen & Frisvad, *Penicillium rivulorum* Visagie, Overy, Seifert & Frisvad, *Penicillium turcosum* Visagie, Overy, Seifert & Frisvad, *Penicillium wyomingense* Visagie, Overy, Seifert & Frisvad.

Citation: Overy DP, Frisvad JC, Witte TE, Hicks CL, Hermans A, Sproule A, Louis-Seize G, Seifert KA, Yilmaz N, Price J, van Vuuren NI, Visagie CM (2025). Chemodiversity of *Penicillium* isolated from alpine and arctic environments, including ten new species. *Studies in Mycology* **112**: 75–116. doi: 10.3114/sim.2025.112.03

Received: 3 February 2025; **Accepted:** 23 July 2025; **Effectively published online:** 1 August 2025.

Corresponding editor: R.A. Samson

INTRODUCTION

Terrestrial cold-temperature environments – habitats often comprised of exposed soils, bare rocks, permafrost, glaciers and snow, such as regions found in extreme polar latitudes, areas of high altitude, and cold deserts – are often frozen for extended periods of time over the year and support sparse plant life. In common with temperate and tropical ecosystems, fungi are the primary decomposers of herbaceous and wood residues in polar and high-altitude alpine soils and play a crucial role in soil development and nutrient cycling (Donhauser & Frey 2018). Fungi in cold ecosystems are subjected to environmental extremes, such as extensive freeze-thaw cycling, extreme UV / solar radiation and low nutrient availability; selective pressures that may influence adaptive evolution of incumbent fungal species. Species of fungi that have adapted to growth in cold habitats are termed psychrophiles, or psychrotrophs, if they exhibit growth at or near 0 °C; a psychrophile has a growth optimum at 15 °C, whereas a psychrotroph has a growth optimum at or greater than 20 °C (Hassan *et al.* 2016). Due to restricted accessibility, fungal biodiversity in polar and high-altitude soils remain largely understudied. Snow and ice deposits act as reservoirs of fungal spores, in which various genera of ubiquitous fungi (i.e. *Penicillium*) are typically found (Ma *et al.* 2000), probably transported in the atmosphere and deposited during periods of precipitation.

The genus *Penicillium* is cosmopolitan and speciose, with over 598 accepted species (Houbraken *et al.* 2020, Visagie *et al.* 2024) classified in subgenus *Aspergilloides* (with 20 sections, which are further subdivided into 66 series) and subgenus *Penicillium* (with 13 sections and 38 series). When describing new *Penicillium* species, a polyphasic taxonomic approach is preferred, where new species are characterised based on phenotypic characters such as colony appearance, microscopic morphology descriptions and secondary metabolite profiles in concert with the comparison and correlation of multigene phylogenies that include other known taxa (Frisvad & Samson 2004, Visagie *et al.* 2014b, 2024). Psychrophilic *Penicillium* species are reported from polar and high-altitude ecosystems, including soils (Azmi & Spepelt 1997, Frisvad *et al.* 2006, Litova *et al.* 2014), glaciers (Sonjak *et al.* 2006, Sonjak *et al.* 2007), saline niches (Loque *et al.* 2009, Cantrell *et al.* 2017), lakes (Ellis-Evans 1996), and historical woodlands (Arenz *et al.* 2006). Despite consistent reports of penicillia from alpine and arctic environments, only a few new *Penicillium* species have been described (McRae *et al.* 1999, Frisvad *et al.* 2006, Sonjak *et al.* 2007).

Generally, *Penicillium* species produce a diverse range of

Studies in Mycology

secondary metabolites (also referred to as extrolites) which, apart from their taxonomic utility, are of interest to natural product discovery programs. Psychrophilic and psychrotrophic fungi often produce unique molecules with potential biotechnological and pharmaceutical applications, including biologically active secondary metabolites, exopolysaccharides, and cold-active enzymes (Zuconni *et al.* 2020, dos Santos *et al.* 2021). Profiling small molecule production using mass spectrometry is an effective and refined approach used to investigate or characterise variations in secondary metabolite production within and between fungal species (Witte & Overy 2022). To assess variations within mass spectrometry data sets, untargeted metabolomics workflows break down the metabolite composition of culture extracts into representative mass features (associated with a chromatographic retention time (RT) and observed ion mass to charge ratio (*m/z*)); where data matrices of mass feature abundance are evaluated in an "unbiased" manner using multivariate and univariate statistics. Additionally, mass feature content can further be evaluated using molecular networking of MS/MS experiments, where observed molecular fragmentation spectra are used to annotate metabolites and organise the data into discrete networks linking together similar molecules and molecular families (Yang *et al.* 2013). As secondary metabolite production can be growth condition dependent, multiple different metabolite profiles can be consolidated into a consensus phenotype to represent a given strain or species (Witte & Overy 2022). Together, untargeted metabolomics and molecular networking workflows can be used to holistically assess and compare the secondary metabolite diversity produced by collections of fungal isolates, where both known and "unknown" molecules are incorporated into the analysis (Witte & Overy 2022).

Our previous study of four psychrotolerant *Penicillium* species from arctic and alpine soils documented a high chemical diversity, including a broad spectrum of biologically active compounds of pharmaceutical interest that included griseofulvin, asperfuran, compactin, pseurotin and several pyripyropenes, benzomalvins, and fumagillins (Frisvad *et al.* 2006). The pyschrophilins and cycloaspeptides are examples of cyclic peptide secondary metabolites that were first discovered from several *Penicillium* species derived from arctic soils (Dalsgaard *et al.* 2004, 2005). During large scale surveys searching for novel psychrophilic fungi in samples from high altitude alpine and arctic tundra soils, we isolated several undescribed *Penicillium* species. Here, ten new species are formally described using the polyphasic taxonomic approach and combined with untargeted metabolomics to explore their chemical diversity.

MATERIALS AND METHODS

Strains, sampling and isolations

The *Penicillium* strains under study are derived from historical soil sampling surveys carried out in 1973, 1988, 1993, 1994, 1996, and 1999–2002. Multiple soil samples were obtained from various collection sites that included southern portions of the Rocky Mountains in North America (Wyoming, USA: Wind River Mountain Range and Snowy Mountain Range – Routt National Forest (Medicine Bow), Lake Marie, Libby Flats, Hanging Lakes, North Platte River (Fort Steele), & Table Rock road; Colorado, USA: Front Mountain Range - Cache la Poudre River; New Mexico, USA: Chihuahuan Desert - Sevilleta National Wildlife Refuge), from Denmark (Greenland: Zackenberg, Jameson Land peninsula, Disco Island, & Qeqertarsuaq (historically known as Godhavn); Faroe Islands: Eiði), and from Norway (Svalbard). Soil samples were streaked onto the selective low-water-activity medium DG18 using a serial dilution technique and incubated at 15 and 25 °C. Streak plates were monitored routinely for fungal growth; emerging fungal colonies were excised as they appeared and transferred to new growth medium to isolate axenic cultures. Strains were preserved as spore suspensions in 10 % glycerol and stored at -80 °C. Strains were accessioned in various collections as indicated in Table 1.

DNA extraction, sequencing and phylogenetic analysis

Genomic DNA extractions were made from 7-d-old colonies grown on malt extract agar (MEA) using the Ultraclean™ Microbial DNA isolation Kit (MoBio, Solano Beach, USA). The DNA was stored at -20 °C until used for PCR amplification. The 5.8S rDNA and flanking internal transcribed spacer regions (ITS), partial beta-tubulin (*BenA*), partial calmodulin (*CaM*) and partial RNA polymerase II second largest subunit (*RPB2*) gene regions were amplified using the primer pairs V9G & LS266 for ITS (de Hoog & Gerrits van den Ende 1998, Masclaux *et al.* 1995), Bt2a & Bt2b for *BenA* (Glass & Donaldson 1995), cmd5 & cmd6 for *CaM* (Hong *et al.* 2005) and RPB2-F1 & RPB2-7CR_1 for *RPB2* (Houbraken *et al.* 2020), while amplification conditions as proposed by Visagie *et al.* (2014b) and Houbraken *et al.* (2020) were used. The PCR's were prepared in 25 µL volumes and consisted of 0.5 µL dNTP's, 0.04 µL for each primer (20 µM), 1 µL 10× Titanium *Taq* buffer (Clontech, California, USA), 0.1 µL 50× Titanium *Taq* enzyme, 0.5 µL template DNA and 7.82 µL sterile distilled water. The BigDye Terminator Cycle Premix Kit (Applied Biosystems, Waltham, USA) and primers used for PCRs were subsequently used to prepare sequencing reactions. Products were run on an ABI PRISM™ 310 DNA automated sequencer (Applied Biosystems). Contigs were assembled and edited in Geneious Prime v. 2021.1 (BioMatter Ltd., Auckland, New Zealand). Obtained sequences were compared to a locally curated reference sequence dataset based on sequences published for all accepted species (Houbraken *et al.* 2020). Based on these results, a subset of sequences was prepared for phylogenetic comparisons (Table 1). Newly generated sequences were deposited to GenBank (www.ncbi.nlm.nih.gov/genbank/) and accessions are listed in Table 1.

For phylogenetic analyses, datasets were aligned in MAFFT v. 7.453 (Katoh & Standley 2013) using the G-INS-i algorithm. Alignments were trimmed and concatenated in Geneious. Concatenated datasets were divided into gene regions and subdivided into introns and exons with each treated as separate partitions. Single gene datasets were divided into exons and introns, with these treated as separate partitions. The general time reversible model with gamma distribution and invariable sites (GTR+G+I) was applied to each partition (Abadi *et al.* 2019). Phylogenetic analyses were based on Maximum Likelihood (ML) performed in IQ-TREE v. 2.3.4. and bootstrap analyses using 1000 replicates (Minh *et al.* 2020). Tree figures were created using TreeViewer v. 2.2.0 and edited in Affinity Publisher v. 2.5.2 (Serif (Europe) Ltd, Nottingham, UK).

Morphology

Morphological characters were recorded using standardised protocols as proposed in Visagie *et al.* (2014b). Growth rates and colony characters were observed from Czapek yeast autolysate agar

Table 1. Strains used for phylogenetic comparisons. Names in **bold** represent new species described in this study.

Species	Section	Series	Strains	GenBank accession nr			
				ITS	*BenA*	*CaM*	*RPB2*
P. algidum	***Ramosum***	***Lanosa***	**DAOMC 256945 = IBT 21988 = CMW 57197 = CN093E9**	**KY989166**	**KY989041**	**KY989102**	**MZ984119**
	Ramosum	***Lanosa***	**IBT 22020 = CMW 57198 = CN093F1**	**KY989167**	**KY989042**	**KY989103**	**MZ984120**
	Ramosum	***Lanosa***	**DAOMC 256946 = IBT 22067 = IBT 24414 = CBS 102886 = CMW 57199 = CN093F2 (ex-type)**	**KY989168**	**KY989043**	**KY989104**	**MZ984123**
P. americanum	*Ramosum*	*Soppiorum*	NRRL 66819 (ex-type)	MK791278	MK803427	MK803428	—
P. aquamarinum	***Robsamsonia***	***Robsamsonia***	**DAOMC 251672 = IBT 16643 = CMW 57210 = CN093A4 (ex-type)**	**KY989143**	**KY989018**	**KY989083**	**KY989204**
	Robsamsonia	***Robsamsonia***	**DAOMC 251673 = IBT 17669 = CMW 57211 = CN093A5**	**KY989146**	**KY989021**	**KY989085**	**KY989206**
	Robsamsonia	***Robsamsonia***	**DAOMC 251680 = IBT 22760 = CMW 57212 = CN093A6**	**KY989182**	**KY989057**	**KY989116**	**KY989218**
P. aurantiogriseum	*Fasciculata*	*Viridicata*	CBS 324.89 (ex-type)	AF033476	MN969372	KU896822	JN406573
	Fasciculata	*Viridicata*	CBS 792.95	JN942749	AY674298	—	JN985381
	Fasciculata	*Viridicata*	CV0048	JX091395	JX091501	JX141571	MK450820
	Fasciculata	*Viridicata*	IBT 35659	—	GCA019977855	GCA019977855	GCA019977855
P. beceitense	*Ramosum*	*Lanosa*	CBS 142989 (ex-type)	LT899780	LT898229	LT899764	LT899798
P. brevistipitatum	*Robsamsonia*	*Robsamsonia*	AS 3.6887 (ex-type)	DQ221696	DQ221695	KU896824	JN406528
	Robsamsonia	*Robsamsonia*	IBT 31321	—	GCA002072405	GCA002072405	GCA002072405
P. chroogomphum	*Ramosum*	*Soppiorum*	CBS 136204 (ex-type)	KC594043	KP684056	KP684057	MN969167
P. compactum	*Robsamsonia*	*Robsamsonia*	AS 3.15411 (ex-type)	KM973207	KM973203	KM973200	KT698909
P. concentricum	*Robsamsonia*	*Robsamsonia*	CBS 477.75 (ex-type)	KC411763	AY674413	DQ911131	KT900575
	Robsamsonia	*Robsamsonia*	IBT 3081	—	GCA028827145	GCA028827145	GCA028827145
	Robsamsonia	*Robsamsonia*	PPRI 25884	MK951933	MK951812	MK951881	—
P. coprobium	*Robsamsonia*	*Robsamsonia*	CBS 280.97	—	AY674423	—	—
	Robsamsonia	*Robsamsonia*	CBS 561.90 (ex-type)	DQ339559	AY674425	KU896830	KT900576
	Robsamsonia	*Robsamsonia*	CBS 562.90	—	AY674424	—	—
P. coprophilum	*Robsamsonia*	*Robsamsonia*	CBS 110760 (ex-type)	AF033469	AY674421	KU896831	JN406645
	Robsamsonia	*Robsamsonia*	IBT 35676	—	GCA028826855	GCA028826855	GCA028826855
P. crustosum	*Fasciculata*	*Camembertiorum*	CBS 115503 (ex-type)	AF033472	MN969379	DQ911132	MN969114
	Fasciculata	*Viridicata*	CBS 101136	JN942747	AY674308	—	JN985383
	Fasciculata	*Viridicata*	CBS 144.45 (ex-type)	JN097811	MN969380	KU896832	JN985388
	Fasciculata	*Viridicata*	CBS 477.84	JN942737	AY674309	—	JN985393
	Fasciculata	*Viridicata*	IBT 34249	—	GCA028828185	GCA028828185	GCA028828185

Table 1. (Continued).

Species	Section	Series	Strains	GenBank accession nr			
				ITS	*BenA*	*CaM*	*RPB2*
P. discoense	***Ramosum***	***Soppiorum***	**DAOMC 251813 = IBT 22667 = CMW 57213 = CN093B2 (ex-type)**	**KY989178**	**KY989053**	**KY989112**	**MZ984138**
	Ramosum	***Soppiorum***	**DAOMC 251814 = IBT 22668 = CMW 57214 = CN093B3**	**KY989179**	**KY989054**	**KY989113**	**MZ984139**
	Ramosum	***Soppiorum***	**DAOMC 251815 = IBT 22669 = CMW 57215 = CN093B4**	**KY989180**	**KY989055**	**KY989114**	**MZ984140**
P. fimorum	*Robsamsonia*	*Robsamsonia*	CBS 140575 (ex-type)	KU904342	KT698887	KT698896	KT698906
	Robsamsonia	*Robsamsonia*	CBS 140576	—	KT698888	KT698897	KT698907
	Robsamsonia	*Robsamsonia*	DTO 159-F1	—	KT698889	KT698898	KT698908
	Robsamsonia	*Robsamsonia*	IBT 29495	—	GCA028828255	GCA028828255	GCA028828255
P. freii	*Fasciculata*	*Viridicata*	CBS 101486	JN942735	AY674291	—	JN985395
	Fasciculata	*Viridicata*	CBS 112292	JN942731	AY674292	—	JN985397
	Fasciculata	*Viridicata*	CBS 476.84 (ex-type)	MN431389	KU896813	KU896836	JN985430
	Fasciculata	*Viridicata*	CMW 59922	—	PP993238	PP993245	PP993252
	Fasciculata	*Viridicata*	CMW 59951	—	PP993239	PP993246	PP993253
	Fasciculata	*Viridicata*	DAOMC 242723	—	GCA001513925	GCA001513925	GCA001513925
	Fasciculata	*Viridicata*	IBT 34325	—	GCA028827385	GCA028827385	GCA028827385
P. hesseltinei	***Fasciculata***	***Viridicata***	**DAOMC 251664 = IBT 12396 = CMW 57228 = CN093B5 (ex-type)**	**KY989128**	**KY989003**	**KY989070**	**KY989195**
P. jamesonlandense	*Ramosum*	*Lanosa*	CBS 102888 (ex-type)	DQ267912	DQ309448	KJ866985	MN969121
	Ramosum	*Lanosa*	IBT 21985 = CMW 57180 = CN093B6	KY989164	KY989039	KY989101	KY989214
	Ramosum	*Lanosa*	IBT 22068 = CMW 57181 = CN093B7	KY989169	KY989044	KY989105	MZ984124
	Ramosum	*Lanosa*	IBT 24408 = IBT 22663 = CMW 57182 = CN093B8	KY989176	KY989051	MZ984165	MZ984126
	Ramosum	*Lanosa*	IBT 24453 = CMW 57183 = CN093B9	KY989193	KY989068	KY989126	MZ984125
P. jugorum	***Ramosum***	***Lanosa***	**DAOMC 251817 = IBT 22778 = CMW 57185 = CN093C2 (ex-type)**	**KY989184**	**KY989059**	**KY989118**	**MZ984129**
	Ramosum	***Lanosa***	**DAOMC 256962 = IBT 22779 = CMW 57184 = CN093C1**	**KY989183**	**KY989058**	**KY989117**	**MZ984127**
	Ramosum	***Lanosa***	**DAOMC 256963 = IBT 22780 = CMW 57186 = CN093C3**	**KY989186**	**KY989061**	**KY989120**	**MZ984134**
	Ramosum	***Lanosa***	**DAOMC 256964 = IBT 22792 = CMW 57187 = CN093C4**	**KY989188**	**KY989063**	**KY989121**	**MZ984128**
P. kojigenum	*Ramosum*	*Lanosa*	CBS 345.61 (ex-type)	AF033489	KJ834463	KJ867011	JN406564
P. lanosum	*Ramosum*	*Lanosa*	CBS 106.11 (ex-type)	DQ304540	DQ285627	FJ530974	KU904356
	Ramosum	*Lanosa*	IBT 4172	DQ267919	DQ285619	—	—
	Ramosum	*Lanosa*	IBT 6619	DQ267908	DQ285612	—	—
P. lenticrescens	*Ramosum*	*Soppiorum*	CBS 138215 (ex-type)	KJ775675	KJ775168	KJ775404	MN969123

Table 1. (Continued).

Species	Section	Series	Strains	GenBank accession nr			
				ITS	*BenA*	*CaM*	*RPB2*
	Ramosum	*Soppiorum*	CNUFC JCW3-5	MZ687466	OK105099	—	OK539663
P. lusitanum	*Ramosum*	*Soppiorum*	IBT 22478 = CMW 57217 = CN093C6	KY989173	KY989048	KY989108	MZ984142
	Ramosum	*Soppiorum*	IBT 22479 = CMW 57218 = CN093C7	KY989174	KY989049	KY989109	MZ984143
	Ramosum	*Soppiorum*	IBT 22992 = CMW 57219 = CN093C8	KY989189	KY989064	KY989122	MZ984144
	Ramosum	*Soppiorum*	IBT 24418 = IBT 22356 = CN093C5 (ex-type)	KY989172	KY989047	KY989107	MZ984141
	Ramosum	*Soppiorum*	MUM 18.49 (ex-type)	MK702084	MK702085	—	—
P. marthae	***Fasciculata***	***Viridicata***	**DAOMC 251665 = IBT 12661 = CMW 57220 = CN103F6**	**KY989129**	**KY989004**	**KY989071**	**KY989196**
	Fasciculata	***Viridicata***	**DAOMC 251666 = IBT 12662 = CMW 57221 = CN103F7**	**KY989130**	**KY989005**	**KY989072**	**KY989197**
	Fasciculata	***Viridicata***	**DAOMC 251667 = IBT 12685**	**KY989131**	**KY989006**	**KY989073**	**KY989198**
	Fasciculata	***Viridicata***	**DAOMC 251668 = IBT 12687 = CMW 57222 = CN103F8**	**KY989132**	**KY989007**	**KY989074**	**KY989199**
	Fasciculata	***Viridicata***	**DAOMC 251669 = IBT 12691**	**KY989133**	**KY989008**	**KY989075**	**KY989200**
	Fasciculata	***Viridicata***	**DAOMC 251670 = IBT 13054 = CMW 57223 = CN103F9 (ex-type)**	**KY989134**	**KY989009**	**KY989076**	**KY989201**
P. melanoconidium	*Fasciculata*	*Viridicata*	CBS 115506 (ex-type)	MN431393	MN969387	KU896843	KU904358
	Fasciculata	*Viridicata*	CV1331	JX091410	JX091545	JX141587	MK450844
	Fasciculata	*Viridicata*	CBS 101135	JN942722	AY674299	—	JN985406
	Fasciculata	*Viridicata*	CBS 101468	JN942721	—	—	JN985407
	Fasciculata	*Viridicata*	CBS 101472	JN942720	—	—	JN985408
	Fasciculata	*Viridicata*	CBS 110343	JN942719	AY674300	—	JN985409
	Fasciculata	*Viridicata*	CBS 169.87 (ex-type)	JN942722	MN969388	KU896844	JN985406
P. oreophilum	***Ramosum***	***Lanosa***	**DAOMC 251821 = IBT 23951 = CMW 57190 = CN093D2 (ex-type)**	**KY989190**	**KY989065**	**KY989123**	**MZ984135**
	Ramosum	***Lanosa***	**DAOMC 256947 = IBT 22341 = CMW 57188 = CN093C9**	**KY989171**	**KY989046**	**KY989106**	**KY989215**
	Ramosum	***Lanosa***	**DAOMC 256961 = IBT 22541 = CMW 57189 = CN093D1**	**KY989175**	**KY989050**	**KY989110**	**MZ984130**
	Ramosum	***Lanosa***	**DAOMC 256948 = IBT 22909 = CMW 57192 = CN093D5**	**—**	**MZ984156**	**MZ984166**	**MZ984131**
	Ramosum	***Lanosa***	**DAOMC 256965 = IBT 24500 = CMW 57191 = CN093D3**	**KY989194**	**KY989069**	**KY989127**	**KY989220**
P. polonicum	*Fasciculata*	*Viridicata*	CBS 101479	JN942718	JN398145	—	JN985410
	Fasciculata	*Viridicata*	CBS 222.28 (ex-type)	AF033475	MN969392	KU896848	JN406609
	Fasciculata	*Viridicata*	CGMCC 3.5272	—	GCA025589915	GCA025589915	GCA025589915
	Fasciculata	*Viridicata*	CMW 59905	—	PP993237	PP993244	PP993251
	Fasciculata	*Viridicata*	CMW 59955	—	PP993236	PP993243	PP993250
	Fasciculata	*Viridicata*	IBT 4502	—	GCA002072265	GCA002072265	GCA002072265

Table 1. (Continued).

Species	Section	Series	Strains	GenBank accession nr			
				ITS	*BenA*	*CaM*	*RPB2*
	Fasciculata	*Viridicata*	PB2502	—	GCA025768265	GCA025768265	GCA025768265
	Fasciculata	*Viridicata*	PM3203	—	GCA025768295	GCA025768295	GCA025768295
	Fasciculata	*Viridicata*	PPRI 11295	—	MK450898	MK451635	MK450846
	Fasciculata	*Viridicata*	PPRI 11326	—	MK450935	MK451637	MK450848
	Fasciculata	*Viridicata*	PPRI 13653	—	MK450899	MK451636	MK450847
P. raistrickii	*Ramosum*	*Raistrickiorum*	CBS 261.33 (ex-type)	AY373927	KJ834485	KJ867006	JN406592
P. ribis	*Ramosum*	*Lanosa*	CBS 127809 = DAOM 234091 = IBT 16537 = IBT 24431 (ex-type)	DQ267916	MN969395	KJ866995	JN406631
	Ramosum	*Lanosa*	IBT 21215 = CMW 57205 = CN093E7	KY989163	KY989038	KY989100	MZ984112
	Ramosum	*Lanosa*	IBT 24403 = IBT 17760 = CMW 57201 = CN093E2	KY989147	KY989022	KY989086	MZ984111
P. rivulorum	***Ramosum***	***Lanosa***	**DAOMC 251681 = IBT 24420 = IBT 17740 = CMW 57228 = CN022E3 (ex-type)**	**KY989192**	**KY989067**	**KY989125**	**MZ984109**
P. robsamsonii	*Robsamsonia*	*Robsamsonia*	CBS 140573 (ex-type)	KU904339	KT698885	KT698894	KT698904
	Robsamsonia	*Robsamsonia*	CBS 140574	—	KT698886	KT698895	KT698905
	Robsamsonia	*Robsamsonia*	IBT 29466	—	GCA028829455	GCA028829455	GCA028829455
P. sajarovii	*Ramosum*	*Raistrickiorum*	CBS 277.83 (ex-type)	KC411724	MN969397	MN969295	JN406588
P. scabrosum	*Ramosum*	*Scabrosa*	CBS 683.89 (ex-type)	DQ267906	DQ285610	FJ530987	JN406541
	Ramosum	*Scabrosa*	CN047G8	—	OR241737	OR241826	OR241881
P. simile	*Ramosum*	*Raistrickiorum*	CBS 129191 (ex-type)	FJ376592	FJ376595	GQ979710	MN969137
P. soppii	*Ramosum*	*Soppiorum*	CBS 144.83	KC411676	MN395873	MN402468	—
	Ramosum	*Soppiorum*	CBS 226.28 (ex-type)	AF033488	MN969399	KJ867002	JN406606
	Ramosum	*Soppiorum*	CBS 438.88	KC411760	MN395874	MN402471	—
	Ramosum	*Soppiorum*	CBS 869.70	DQ267909	DQ285613	—	—
	Ramosum	*Soppiorum*	IBT 19343	DQ267920	DQ285620	—	—
P. swiecickii	*Ramosum*	*Lanosa*	CBS 119391 (ex-type)	AF033490	KJ834494	KJ866993	JN406635
	Ramosum	*Lanosa*	CMW 57208 = CN093F4	KY989170	KY989045	MZ984167	MZ984132
	Ramosum	*Lanosa*	CMW 57209 = CN093F5	KY989187	KY989062	MZ984168	MZ984133
	Ramosum	*Lanosa*	DAOMC 214755	DQ267904	DQ285608	—	—
	Ramosum	*Lanosa*	DTO 244-H3	KJ775695	KJ775188	—	—
	Ramosum	*Lanosa*	IBT 16536	KY989139	KY989014	KY989080	—
	Ramosum	*Lanosa*	IBT 16545 = IBT 24425	KY989140	KY989015	KY989081	—
	Ramosum	*Lanosa*	IBT 18311 = CMW 57207 = CN093F3	KY989155	KY989030	MZ984158	MZ984137

Table 1. (Continued).

Species	Section	Series	Strains	GenBank accession nr			
				ITS	*BenA*	*CaM*	*RPB2*
	Ramosum	*Lanosa*	IBT 18945 = KAS2430	KY989157	KY989032	KY989094	—
	Ramosum	*Lanosa*	IBT 20705 = KAS2435	KY989161	KY989036	KY989098	PP993259
	Ramosum	*Lanosa*	IBT 22666 = KAS2458	KY989177	KY989052	KY989111	KY989216
	Ramosum	*Lanosa*	IBT 22735 = KAS2463	KY989181	KY989056	KY989115	KY989217
	Ramosum	*Lanosa*	IBT 22773 = KAS2467	KY989185	KY989060	KY989119	—
	Ramosum	*Lanosa*	IBT 23954 = KAS2480	KY989191	KY989066	KY989124	—
P. tricolor	*Fasciculata*	*Viridicata*	CBS 101488	JN942705	—	—	JN985421
	Fasciculata	*Viridicata*	CBS 635.93 (ex-type)	JN942704	MN969403	KU896852	JN985422
	Fasciculata	*Viridicata*	CBS 636.95	—	AY674311	—	—
	Fasciculata	*Viridicata*	CBS 637.93	JN942703	AY674312	—	JN985423
	Fasciculata	*Viridicata*	CMW 57231 = CN093D7	—	MZ984155	MZ984163	MZ984147
	Fasciculata	*Viridicata*	CMW 57232 = CN093D6	—	MZ984154	MZ984162	MZ984146
	Fasciculata	*Viridicata*	DAOMC 251674 = IBT 18159 = CMW 57229 = CN093G1	KY989151	KY989026	KY989089	KY989207
	Fasciculata	*Viridicata*	DAOMC 251676 = IBT 18292 = CMW 57230 = CN093G2	KY989153	KY989028	KY989091	KY989209
	Fasciculata	*Viridicata*	DAOMC 251678	KY989159	KY989034	KY989096	PP993257
P. tunisiense	*Ramosum*	*Soppiorum*	MUM 17.62 (ex-type)	MG586956	MG586970	MG586974	—
	Ramosum	*Soppiorum*	MUM 17.80	MG586957	MG586971	MG586975	—
P. turcosum	***Ramosum***	***Lanosa***	**DAOMC 256942 = IBT 17778 = CMW 57195 = CN093E3**	**KY989148**	**KY989023**	**KY989087**	**MZ984122**
	Ramosum	***Lanosa***	**DAOMC 256941 = IBT 24419 = IBT 16625 = CMW 57193 = CN093D9 (ex-type)**	**KY989142**	**KY989017**	**KY989082**	**MZ984117**
P. virgatum	*Ramosum*	*Virgata*	CBS 114838 (ex-type)	AJ748692	KJ834500	KJ866992	JN406641
	Ramosum	*Virgata*	IBT 19272 = CMW 57220 = CN093F6	KY989158	KY989033	KY989095	KY989211
	Ramosum	*Virgata*	IBT 20823 = CMW 57222 = CN093F8	KY989162	KY989037	KY989099	KY989213
	Ramosum	*Virgata*	IBT 24423 = IBT 14166 = CMW 57221 = CN093F7 (ex-type)	KY989137	KY989012	KY989078	KY989202
	Ramosum	*Virgata*	IBT 24449 = IBT 16998 = CMW 57223 = CN093F9	KY989144	KY989019	KY989084	KY989205
P. viridicatum	*Fasciculata*	*Viridicata*	CBS 101034	—	AY674293	—	JN985424
	Fasciculata	*Viridicata*	CBS 101475	JN942701	—	—	JN985425
	Fasciculata	*Viridicata*	CBS 109826	JN942700	AY674294	—	JN985426
	Fasciculata	*Viridicata*	CBS 112052	JN942699	—	—	JN985427
	Fasciculata	*Viridicata*	CBS 264.29	JN942698	—	—	JN985428
	Fasciculata	*Viridicata*	CBS 390.48 (ex-type)	AY373939	MN969406	KU896856	JN121511
	Fasciculata	*Viridicata*	CMW 59940	—	PP993242	PP993249	PP993256

Table 1. (Continued).

Species	Section	Series	Strains	GenBank accession nr			
				ITS	*BenA*	*CaM*	*RPB2*
	Fasciculata	*Viridicata*	CMW 59952	—	PP993240	PP993247	PP993254
	Fasciculata	*Viridicata*	CMW 59957	—	PP993241	PP993248	PP993255
P. vulpinum	*Robsamsonia*	*Claviformia*	CBS 126.23 (ex-type)	AF506012	KJ834501	KU896857	KU904367
P. wyomingense	***Ramosum***	***Lanosa***	**DAOMC 256943 = IBT 17868 = CMW 57202 = CN093E4**	**KY989149**	**KY989024**	**MZ984160**	**MZ984114**
	Ramosum	***Lanosa***	**DAOMC 256944 = IBT 18067 = CMW 57203 = CN093E5**	**KY989150**	**KY989025**	**KY989088**	**MZ984115**
	Ramosum	***Lanosa***	**DAOMC 256940 = IBT 24433 = IBT 14073 = CMW 57231 (ex-type)**	**KY989136**	**KY989011**	**KY989077**	**PP993258**
P. xyleborini	*Ramosum*	*Soppiorum*	CMW 56800 (ex-type)	MW504356	MW480817	MW480823	MW480824

Table 2. *Penicillium* section *Ramosum* series *Lanosa* species morphologically characterised in this study.

Species	Conidia walls	Stipe walls	Growth rates after 7 d (mm)											
			CYA 10 °C	CYA 15 °C	CYA 20 °C	CYA 25 °C	CYA 30 °C	CYAS	MEA	MEA 20 °C	YES	DG18	OA	CREA
P. algidum	smooth	rough	5–8	13–17	18–21	21–22	no growth to microcolonies	22–23	19–21	21–22	27–29	17–19	22–24	13–14
P. jamesonlandiense	rough	smooth	8–9	14–16	17–18	10–13	no growth	15–16	8–12	16–22	12–16	11–13	9–11	5–9
P. jugorum	rough	finely roughened	5–8	12–14	16–18	4–6	no growth	6–8	4–6	16–20	11–16	9–11	4–6	4–6
P. lusitanum	smooth	smooth to finely roughened	6–10	7–9	16–18	19–20	no growth	15–20	5–7	14–16	15–18	17–19	5–7	4–5
P. oreophilum	rough	rough	7–10	16–17	17–22	15–20	no growth	16–20	15–18	20–24	20–24	15–17	12–13	10–12
P. ribis	smooth	rough	9–10	16–17	19–21	19–24	no growth	18–24	18–21	20–23	25–27	16–18	20–22	10–12
P. rivulorum	smooth	rough	10–11	18–19	25–27	26–28	3–4	25–27	29–31	28–30	34–36	22–24	26–28	15–20
P. swiecickii	smooth	smooth	13–16	22–23	26–28	25–27	no growth	21–25	21–24	27–30	25–30	15–18	20–23	11–14
P. turcosum	smooth	smooth and rough	9–11	16–17	20–21	24–25	microcolonies	25–26	20–23	22–24	28–30	17–18	21–23	13–14
P. wyomingense	smooth	rough	8–9	15–16	18–19	21–22	5–8	23–24	20–21	19–21	28–30	20–21	23–25	12–14

(CYA), CYA with 5 % NaCl (CYAS), DG18 (Oxoid CM0729), MEA (Oxoid CM0059), oatmeal agar (OA), yeast extract sucrose agar (YES) and creatine sucrose agar (CREA). Media were prepared in 90-mm-diam. Petri dishes. Inoculations were made in three-point fashion and plates were incubated in the dark for 7 d at 25 °C. Additional CYA plates were incubated at 5, 10, 15, 20, 30 and 37 °C. Additional MEA plates were incubated at 20 °C. Colour names and codes used in descriptions follow Kornerup & Wanscher (1967). Colonies were captured with a Sony a6400 camera equipped with a Sony FE 90mm f/2.8 Macro G OSS Lens. Microscopic observations were made using an Olympus SZX12 dissecting and Olympus BX50 compound microscopes equipped with Infinity3 and InfinityX cameras run by Infinity Analyze v. 6.5.1 software (Lumenera Corp., Ottawa, Canada). Extended Depth of Field stacking of colony texture micrographs was performed using Helicon Focus v. 7.6.1 (HeliconSoft, Kharkiv, Ukraine). Plates were prepared in Affinity Photo v. 2.5.2 [Serif (Europe) Ltd, Nottingham, UK]. For aesthetic purposes, micrographs were edited using the "inpainting brush tool" without altering areas of scientific significance.

Untargeted metabolomics profiling

The extraction and metabolomic profiling of strains using ultra-high pressure liquid chromatography coupled to high resolution mass spectrometry (UPLC-HRMS) was performed as detailed in Witte & Overy (2022). In brief, strains were three-point inoculated onto CYA, YES and DG18 agar and incubated for 14 d in the dark at 25 °C; after which, six plug explants were removed from across the diameter of a single culture, solvent extracted, shaking in 15 mL of EtOAc for 2 h, the solvent removed and dried under vacuum. Dried extracts were reconstituted in methanol and analysed on a Thermo Ultimate 3000 UPLC coupled to a Thermo LTQ Orbitrap XL high resolution mass spectrometer and a Thermo Dionex Ultimate 3000 Diode array detector (190–800 nm). Chromatography was performed on a Phenomenex C18 Kinetex column (50 mm × 2.1 mm ID, 1.7 µm) with a flow rate of 0.35 mL/min, running a gradient of water (+ 0.1 % formic acid) and acetonitrile (+ 0.1 % formic acid): starting at 5 % acetonitrile increasing to 95 % acetonitrile by 4.5 min, held at 95 % acetonitrile until 8 min, returning to 5 % acetonitrile by 9 mins and held to 10 mins to equilibrate the column to starting conditions. The HRMS was operated in ESI^+ mode (monitoring a range of 100–2000 *m/z*) using the following parameters: sheath gas (40), auxiliary gas (5), sweep gas (2), spray voltage (4.2 kV), capillary temperature (320 °C), capillary voltage (35 V), and tube lens (100 V).

Mass spectrometry data preprocessing was performed using MZmine v. 2.37 (Pluskal *et al.* 2010) with parameters as detailed in Witte & Overy (2022), with the following exceptions: mass features were kept in the analysis if at least one sample exhibited an intensity over 1×10^7, and were filtered out from sample rows if their intensities were less than 1×10^6. Additionally, the 'gap-filling' and 'normalisation' steps were omitted. The pre-processed raw data files were converted into a data matrix of discriminate variables, referred to as mass features, consisting of retention time (RT) and *m/z*. Mass features representing associated adducts and in-source fragments of the same parent ion were grouped using Pearson correlation analysis over a sliding window of elution time (using an in-house R script). Mass feature data were converted to binary form, and then summed across the three media conditions to form a 'pseudo-binary' matrix of detection frequencies for each mass feature. Heatmaps were produced using the ComplexHeatMap R package (Gu *et al.* 2016).

Mass feature annotation

Representative extracts were selected based on untargeted metabolomics results for LC-HRMS/MS profiling by nanoLC coupled to the Q-Exactive Plus mass spectrometer (Thermo Fisher Scientific). Chromatographic separation of metabolites was performed on a Proxeon EASY nLC II System (Thermo Fisher Scientific) equipped with a Thermo Scientific™ Acclaim™ PepMap™ RSLC C18 column (P/N ES800A), 15 cm × 75 µm ID, 3 µm, 100 Å employing a water/acetonitrile/0.1 % formic acid gradient for 60 min at a flow rate of 0.25 µL/min. Compounds were separated using a linear gradient from 10 to 100 % of acetonitrile for 45 min. The HRMS was operated in ESI^+ mode with an ion source temperature of 250 °C and an ion spray (Thermo Scientific™ EASY spray) voltage of 2.1 kV. The FTMS scan type was full MS/data dependent (dd)-MS^2; with full mass scan parameters as follows: a resolution of 70000, an auto gain control target under 3×10^6, a maximum isolation time of 100 ms, and an *m/z* range of 100–1500. The parameters of the dd-MS^2 scan were as follows: a resolution of 17500, an auto gain control target under 1×10^5, a maximum isolation time of 100 ms, a loop count of top 10 peaks, an isolation window of *m/z* 2, a normalised collision energy of 35 and dynamic exclusion duration of 10 s.

Preprocessing of the acquired Xcalibur raw data files was completed using MZmine v. 3.5.0. Masses were detected with a noise threshold of 1×10^4. Chromatogram building was completed with the ADAP algorithm using a minimum group size of 10, a minimum intensity for consecutive scans of 1×10^6 and a minimum absolute height 5×10^6. RT and *m/z* tolerances were consistently set to 0.2 min and 0.01 *m/z* respectively, throughout pre-processing. Chromatogram deconvolution was carried out using ADAP feature resolver with a signal to noise threshold of 30, a minimum feature height of 5×10^6, and a coefficient/area threshold of 40, a peak duration range of 0.00–10.0 and an RT wavelet range of 0.00–1.0. Isotopic peaks were then removed followed by alignment of peaks using the JOIN aligner method and a 2:1 ratio for *m/z* to RT weight. Correlation grouping was then applied to group together adducts and in source fragments present within the dataset, using an intensity threshold for correlation of 1×10^6. Ion identity networking was completed using a minimum height of 1×10^5 (Schmid *et al.* 2021). Peaks missing from the data matrix were then back filled using the same RT and *m/z* range gap-filling algorithm before applying feature filtering to remove peaks that were not associated with MS^2 spectra. The mass features were then networked together using GNPS feature-based molecular network analysis using default parameters (Wang *et al.* 2016) with the following modification: MS^2 spectra were linked into networks if they have at least 10 shared fragments and a cosine score greater than 0.75.

Associated mass feature chemical formulas were predicted based on high resolution exact masses of $[M+H]^+$ or $[M+Na]^+$ ions (< 5 ppm) combined with isotope abundance patterns (analysed using MassWorks, Cerno Bioscience). All compound annotations matched exact *m/z* (< 5 ppm) to reported compounds in *Penicillium* literature. Annotations were supported wherever possible by analysis of MS^2 fragmentation patterns using MS-FINDER for rules-based filtering of structure databases using *in silico* fragmentation analysis (Tsugawa *et al.* 2016), with hypothesised annotations accepted if they were within the top 3 structural matches. Annotations were further supported by the GNPS workflow for comparison to experimentally derived MS^2 spectral databases during the feature-based molecular network analysis (Wang *et al.* 2016), and/or by MS-DIAL workflow for MS^2 spectral database matching (Tsugawa

et al. 2015). MS^2 spectral databases queried included all databases available at the Massbank of North America (https://mona.fiehnlab.ucdavis.edu, accessed April 1, 2024) which included the GNPS MS^2 databases. Lastly, annotations were supported wherever possible by comparison of UV absorbance spectral signatures from literature and in house databases.

RESULTS

Phylogenetic analyses

Comparisons with our curated reference dataset resolved strains into section *Fasciculata* series *Viridicata*, section *Ramosum*

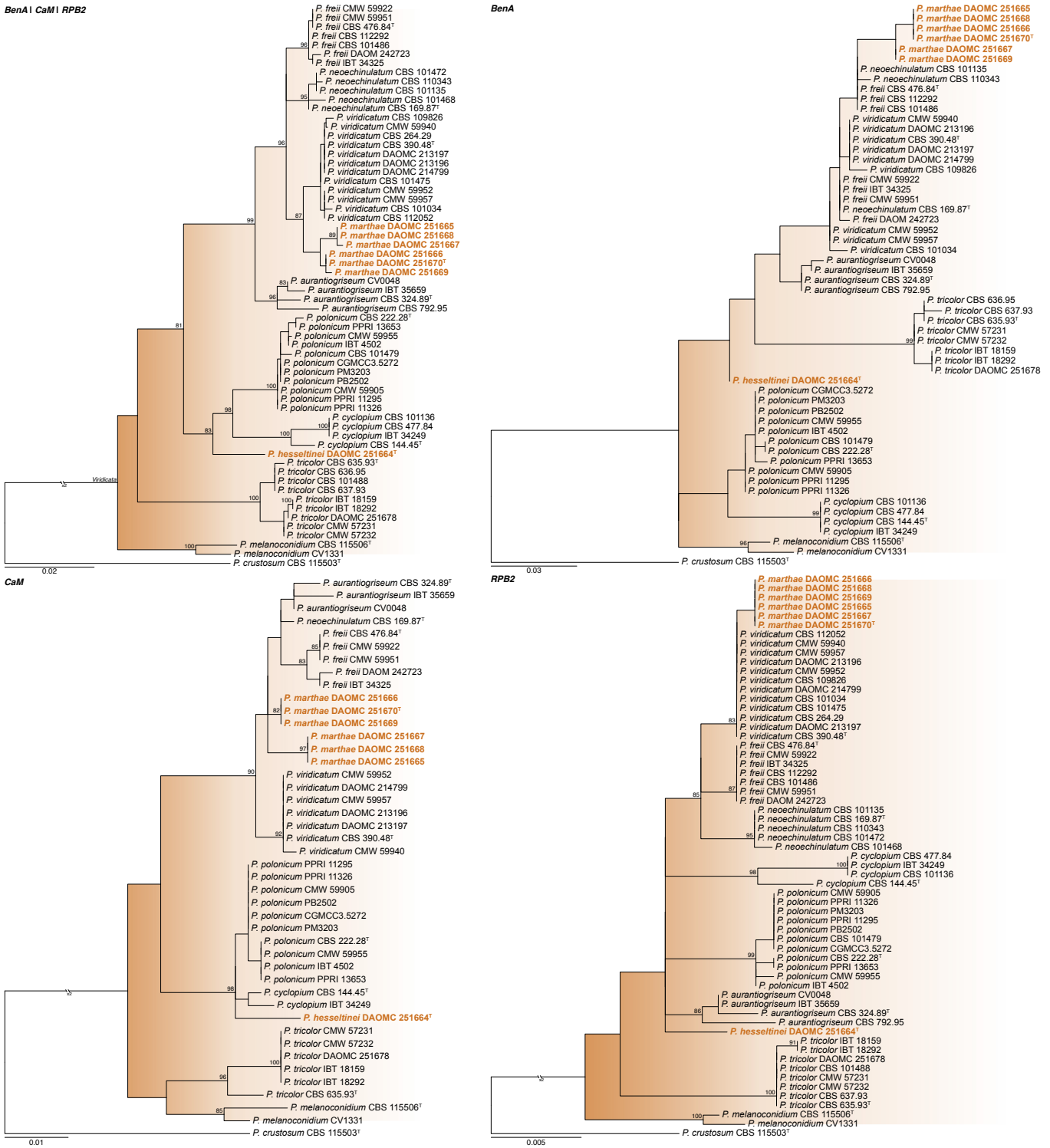

Fig. 1. Multi- and single gene phylogenetic trees of section *Fasciculata* series *Viridicata* based on *BenA*, *CaM* and *RPB2*. *Penicillium crustosum* was selected as outgroup. Branches supported by bootstrap values higher than 80 % are indicated at relevant branches. Strains of new species are shown in **bold** coloured text. Ex-type strains are indicated by ^{T}.

series *Lanosa* and *Soppiorum*, and section *Robsamsonia* series *Robsamsonia* for which phylogenies were subsequently calculated. The ITS region showed poor resolution at species level and was thus omitted from analyses. Aligned datasets, partitioning schemes and tree files were uploaded to the University of Pretoria's research data repository hosted on Figshare (doi: 10.25403/UPresearchdata.27117037).

Section Fasciculata series Viridicata (Fig. 1): Series *Viridicata* currently contains eight accepted species (Houbraken *et al.* 2020), but sequence similarities between them is generally high. Our phylogenetic analyses, more specifically the *BenA* phylogeny, showed that *P. neoechinulatum* and *P. freii* might represent one species. However, it will be premature to synonymize them based on *P. freii* conidia that are smooth in contrast to the rough walled conidia of *P. neoechinulatum*, while they also differ chemically (Frisvad & Samson 2004). Analyses revealed two new species in the series, described below as *P. marthae* and *P. hesseltinei*. *Penicillium hesseltinei* shares an identical ITS with *P. polonicum*, but *BenA* differs by at least 5 bp, *CaM* by 6 bp and *RPB2* by 6 bp from other species. *Penicillium marthae* shares identical ITS sequences with *P. neoechinulatum* and *P. viridicatum*, but its *BenA* differs by at least 2 bp, *CaM* by 3 bp and *RPB2* by 5 bp from other species. The concatenated tree places *P. hesseltinei* as a close relative of *P. polonicum* and *P. cyclopium*. *Penicillium marthae* is resolved in a clade with *P. freii*, *P. neoechinulatum* and *P. viridicatum*.

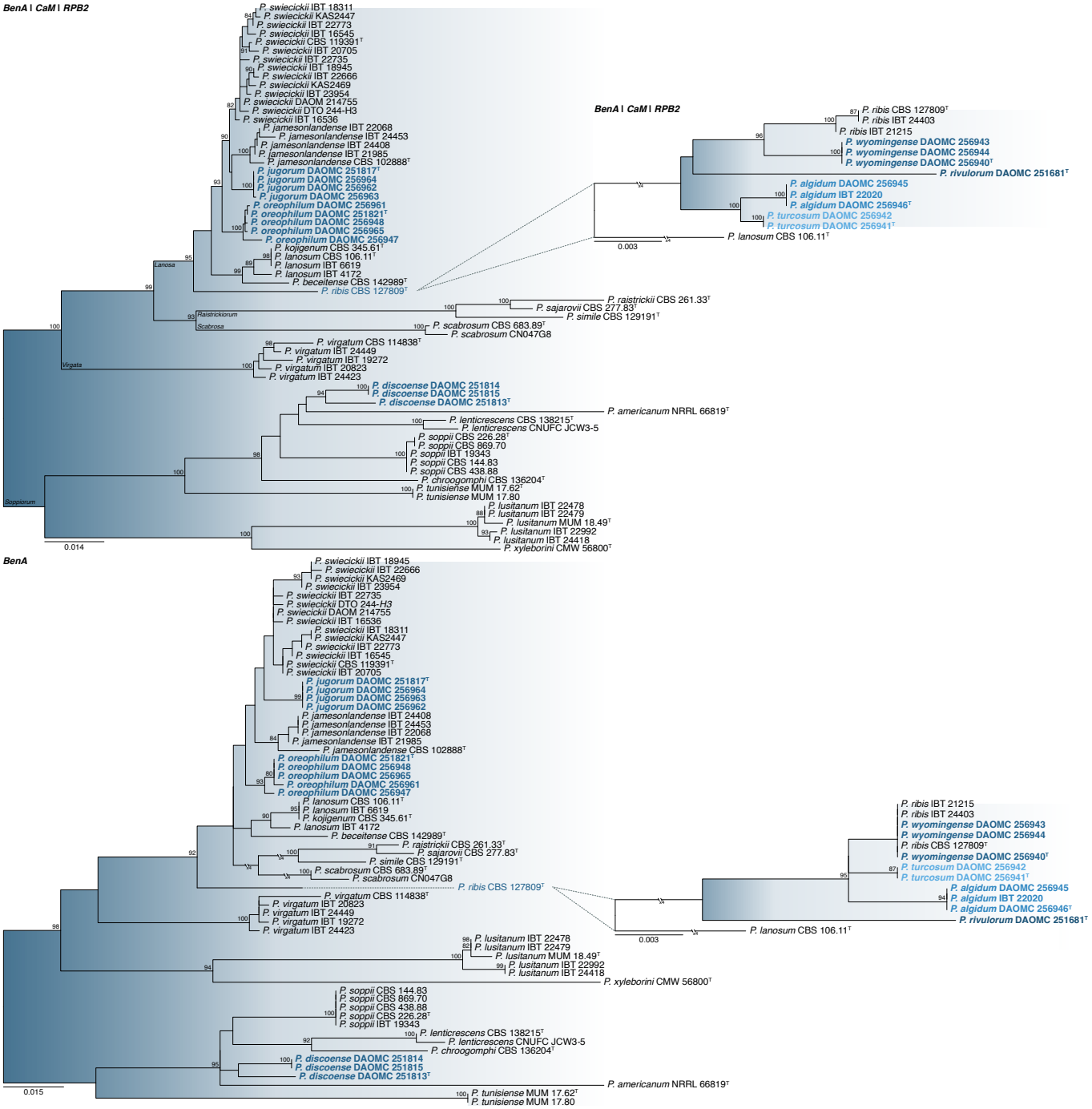

Fig. 2. Multi- and single gene phylogenetic trees of section *Ramosum* based on *BenA*, *CaM* and *RPB2*. The midpoint rooting option was used for the main tree, while *P. lanosum* was selected as outgroup for the tree calculated for the *P. ribis* species complex. Branches supported by bootstrap values higher than 80 % are indicated at relevant branches. Strains of new species are shown in **bold** coloured text. Ex-type strains are indicated by T.

Section Ramosum (Fig. 2): Houbraken *et al.* (2020) accepted 18 species in section *Ramosum* [*P. xyleborini* since described in Crous *et al.* (2021)] and divided it into five series, including series *Lanosa*, *Raistrickiorum*, *Scabrosa*, *Soppiorum* and *Virgata*. *Penicillium beceitense*, *P. jamesonlandense*, *P. kojigenum*, *P. lanosum*, *P. ribis* (syn. *P. ribium*) and *P. swiecickii* belong to the series *Lanosa*. Based on phylogenetic data presented here, it is our opinion that *P. kojigenum* is a synonym of *P. lanosum*. Six of our newly proposed species belong to this series. Two of the species, described below as *P. oreophilum* and *P. jugorum*, are clearly resolved as distinct species in all phylogenies. *Penicillium oreophilum* differs from other species by at least 7 bp based on *BenA*, 9 bp based on *CaM*, 3 bp based on *RPB2*, and 1 bp based on ITS. *Penicillium jugorum* differs from other species by at least 6 bp based on *BenA*, 2 bp based on *CaM*, 6 bp based on *RPB2*, and 2 bp based on ITS. In section *Ramosum*, we also introduce four new species in the *P. ribis* species complex as *P. algidum*, *P. rivulorum*, *P. turcosum* and *P. wyomingense*. This group is very similar with *BenA* and *CaM* not able to distinguish between all species. The ITS of *P. ribis*, *P. algidum*, *P. turcosum* and *P. wyomingense* are identical, with *P. rivulorum* that has at least 4 bp differences from other species. Comparing the other gene regions, *P. algidum* has at least 4 bp differences based on *BenA*, 1 bp based on *CaM*, and 2 bp based on *RPB2*; *P. turcosum* has at least 2 bp differences based on *BenA*, 1 bp based on *CaM*, and 2 bp based on *RPB2*; *P. wyomingense* is identical to *P. ribis* based on *BenA* and *CaM*, but differs at least 13 bp based on *RPB2*; and *P. rivulorum* has at least 10 bp differences based on *BenA*, 4 bp based on *CaM*, and 11 bp based on *RPB2*. Sequence variation is thus low in both *BenA* and *CaM*, but *RPB2* performs better. Future work will be focused on the isolation of more strains and sequencing their genomes in order to better explain the relationships within this clade. However, as discussed below,

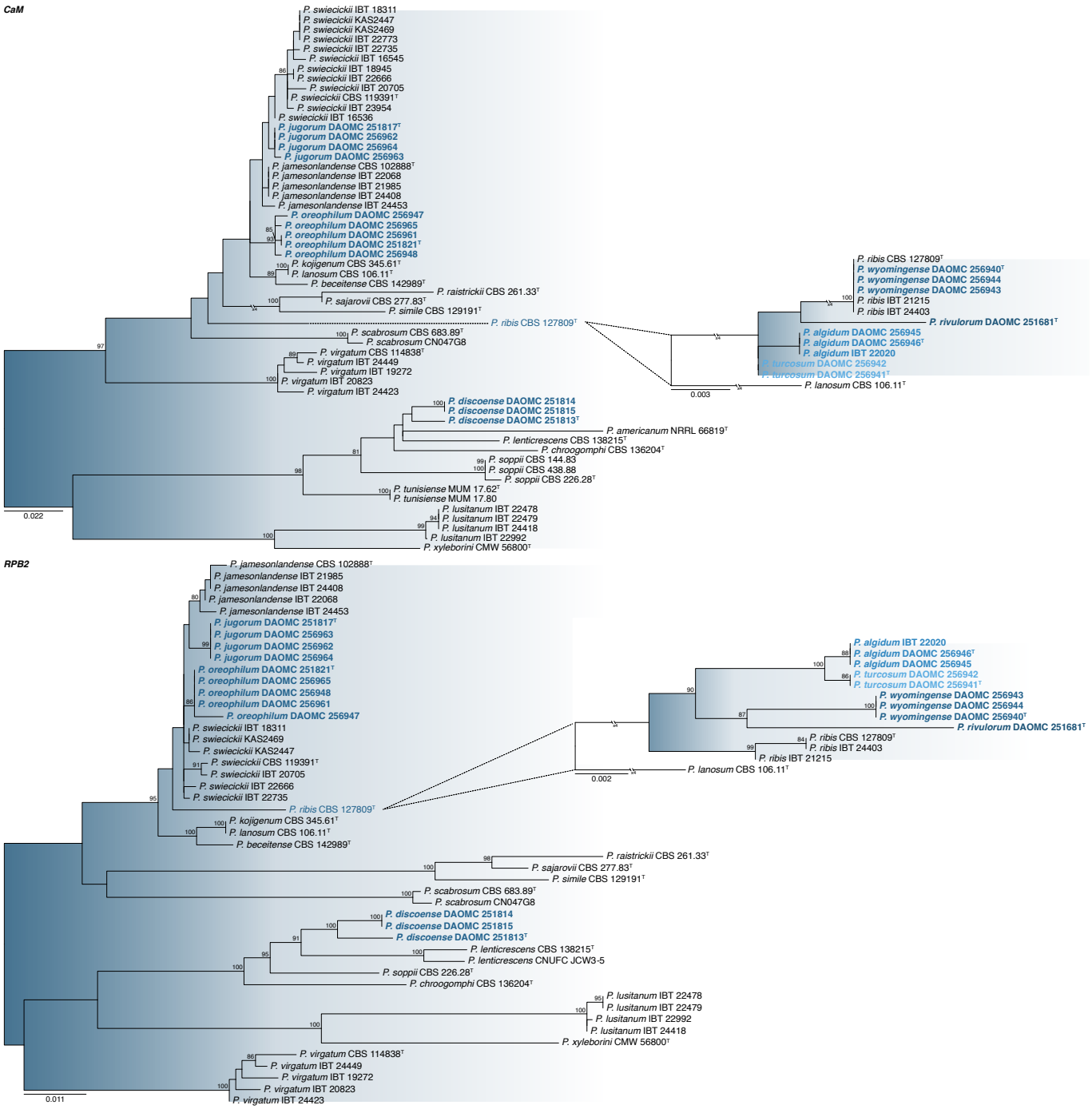

Fig. 2. (Continued).

chemical profiles of these strains are very unique and follow the grouping revealed by the multigene phylogeny. Additionally, we introduce a new species in series *Soppiorum* as *P. discoense*. Phylogenetically, it is most closely related to *P. chroogomphum*, *P. lenticrescens* and *P. soppii*. *Penicillium discoense* differs from other species by at least 15 bp based on *BenA*, 23 bp based on *CaM*, 34 bp based on *RPB2*, and 3 bp based on ITS. Strain DAOMC 251813 shows a large degree of variation from the other two strains. Other species identified during this study includes *P. virgatum* and the recently described *P. lusitanum* (Gonçalves *et al.* 2019).

Section Robsamsonia (Fig. 3): One new species is introduced in section *Robsamsonia* series *Robsamsonia* as *P. aquamarinum*. All genes resolved this species as a close relative of *P. robsamsonia* and *P. fimorum*. *Penicillium aquamarinum* differed from other species by at least 10 bp based on *BenA*, 16 bp based on *CaM* and 6 bp based on *RPB2*. The ITS region is identical to that of *P. robsamsonia* and *P. concentricum*.

Morphology

Ten new *Penicillium* species are formally described in the Taxonomy section below. They belong to section *Fasciculata* series *Viridicata*, section *Ramosum* series Lanosa and *Soppiorum*, and section *Robsamsonia* series *Robsamsonia*. Strains generally conformed to the typical characters of other close relatives. Section *Ramosum* species were found to be psychrophilic, growing as well or better at lower temperatures (Table 2). Notes on morphological similarity between new species and their close relatives are provided in the Taxonomy section.

Secondary metabolite production

Untargeted metabolomic profiling was used to construct a phenotype for each of the new species, presented in the Fig. 4 as a heatmap representing metabolite production based on a cumulative mass feature occurrence frequency by media. Each of the new species as delineated by phylogenetic and morphological phenotyping produced a unique expression of secondary metabolites that can be considered as diagnostic for each species (refer to Taxonomy Section). Over 80 secondary metabolites were annotated from the metabolomic phenotypes (of the ten new species and the additional inclusion of *P. ribis*), representing a diverse range of chemistry that included secondary metabolite products derived from non-ribosomal peptide synthases (NRPS), polyketide synthases (PKS), hybrid NRPS-PKS biosynthesis, and terpenoid biosynthesis (associated mass spectrometry data are summarized in Supplemental Information Table S1 and corresponding MS2 mirror plots in Figs S1–S30). Of particular note, metabolite annotation was not possible for several mass features that also contributed to a considerable portion of the metabolomic phenotype of each species – in some cases, unannotated mass features constituted entire phenotype blocks shared between species (i.e. block 7 in the metabolomic phenotype with shared production by *P. discoense* and *P. wyomingense*).

NRPS-derived secondary metabolites (Figs 5, 6): Numerous cyclodipeptides contributed to the metabolomic phenotype of several of the *Penicillium* species. In particular, *P. aquamarinum* was a prolific producer of cyclodipeptides and associated prenylated analogues, as observed from the large block of mass features in block 22 of the heatmap (Fig. 4). Marcfortines A–C (**1**–**3**), peniciherquamide B (**4**), and mangrovamide F (**5**) produced by *P. aquamarinum*; mangrovamide G (**6**) produced by *P. aquamarinum* and *P. ribis*; chrysogenamide A (**7**) produced by *P. discoense*; and paraherquamide B (**8**) produced by *P. turcosum*, are structurally similar, complex heptacyclic dipeptides – several of which are known bioactive molecules due to their spirooxindole moiety (Panda *et al.*, 2023). Numerous cyclodipeptide diketopiperazines, also recognized for their associated biological activities, such as the roquefortines C & D (**9**, **10**) by *P. aquamarinum*; rhinocladin A (**11**) produced by *P. turcosum*; tryprostatin B (**12**) produced by *P. ribis*; amauromine (**13**) and fellutanines A–C (**14**–**16**) produced by *P. aquamarinum*, *P. jugorum*, *P. oreophilum*; and the structurally related aurantiamine (**17**), pre-aurantiamine (**18**), and viridamine (**19**) produced *P. marthae*, contributed greatly to the chemical diversity of the metabolomic phenotype of each species. The remaining cyclodipeptides identified were the communesins A, F–H (**20**–**23**) produced by *P. rivulorum*; complex cytotoxic heptacyclic molecules

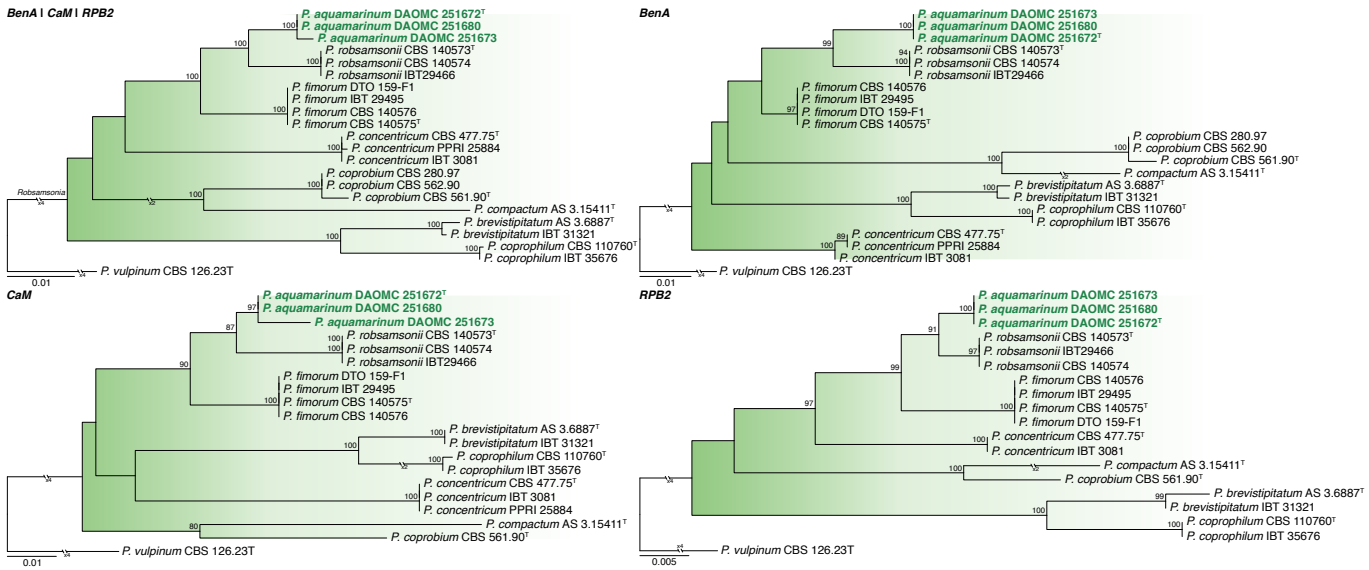

Fig. 3. Multi- and single gene phylogenetic trees of section *Robsamsonia* based on *BenA*, *CaM* and *RPB2*. *Penicillium chrysogenum* was selected as outgroup. Branches supported by high bootstrap values (> 80 %) and/or posterior probabilities (> 0.95) are indicated at relevant branches (* = 100 % or 1 pp). Strains of new species are shown in **bold** coloured text. Ex-type strains are indicated by T.

that are often functionalized by prenylated and acylated side chains. Penigequinolone A (**24**) and yaequinolones B, F, & J1 (**25**–**27**) produced by *P. oreophilum*, are oxidized prenylated alkaloids containing a bicyclic quinolone backbone formed by the NRPS mediated condensation of anthranilate and o-methyltyrosine (Zou *et al.* 2015). *Penicillium marthae* produced a unique block of mass features in the metabolomic phenotype (block 6, Fig. 4) representing the quinazolinobenzodiazepine alkaloids, sclerotigenin (**28**) and circumdatin F (**29**), molecules that contain 3 amino acid residues and are also associated with known insecticidal activity. Additional mass features associated with the NRPS-derived, N-methylated linear peptides viridic acid (**30**) were observed in block 5 of the metabolomic phenotype associated with *P. marthae*. Production of the quinolone-γ-lactam alkaloids quinolactacins A-C (**31**–**33**) was unique to *P. algidum*, where biosynthesis of the quinolone-γ-lactam scaffold is mediated by two single module NRPSs (Zhao *et al.*, 2020). Production of the cytotoxic NRPS-derived amino acid ester, asperphenamate (**34**) and a hydroxyl analogue (**35**), represented by mass features in block 2 of the metabolomic phenotype (Fig. 4) was common to most of the *Penicillium* species examined, including *P. discoense*, *P. jugorum*, *P. oreophilum*, *P. wyomingense*, *P. ribis*, *P. algidum*, *P. turcosum*, *P. rivulorum*.

A variety of different macrocyclic peptides were also observed to be produced by most of section *Ramosum* species. Production of the γ-aminobutyric acid (GABA)-containing cyclic heptapeptides unguisin A & C (**36**, **37**) were unique to *P. turcosum*. Psychrophilins A–D (**38**–**41**), α-nitro-containing cyclic tripeptides produced through the combined action of a dimodular and monomodular NRPSs (Zhao et al, 2016), were observed to be produced from *P. rivulorum* and *P. turcosum*, while psychrophilins A, B & D were observed from *P. algidum*, psychrophilin A & D from *P. ribis* and psychrophilin A from *P. wyomingense*. The N-methylated cyclic pentapeptides known as the cycloaspeptides (**42**–**48**) were produced by *P. jugorum*, *P. oreophilum*, *P. ribis*, *P. algidum*, and *P. turcosum* (block 9 of the metabolomic phenotype, Fig. 4). Cycloaspeptides A (**42**) and D (**45**) were the most predominant cycloaspeptide analogues produced (based on mass feature relative abundance); however, due to the unique biosynthesis of the cycloaspeptides – in terms of *N*-methylation and NRPS promiscuity of amino acid incorporation (de Mattos-Shipley *et al.* 2018) – numerous additional cycloaspeptide analogues were also observed [i.e. cycloaspeptides E, G & H* (**46**–**48**)]. Ion molecular networking (presented in Fig. 7) further revealed new, additional analogues of cycloaspeptides D, E, and G, suggestive of incorporation of phenylalanine or tyrosine

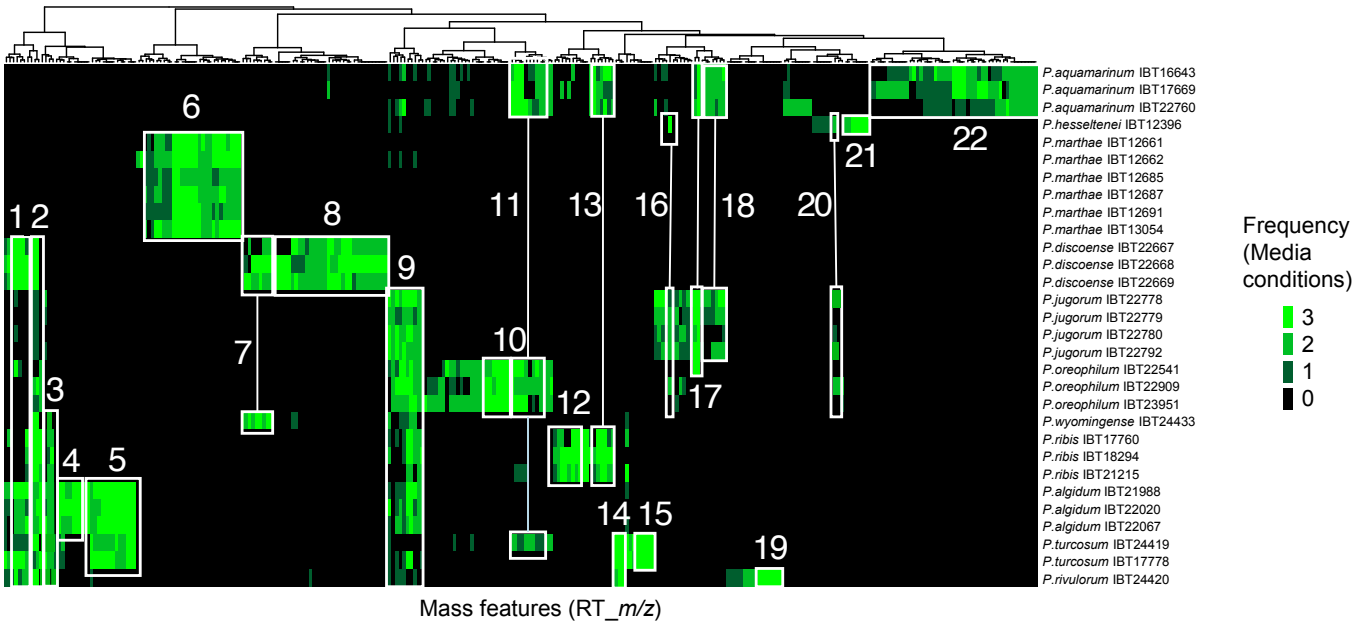

1. Griseofulvin, dechlorogriseofulvin, norlichexanthone
2. Asperphenamate (and analog)
3. Psychrophilins A-D, asperfuran
4. Penitrems A, B, D, E, F, quinolactacins A, B, C
5. Funiculosin, melearoride A/PF1163B
6. Xanthomegnins (viomellein, vioxanthin, xanthomegnin), sclerotigenin, circumdatin F, viridic acid, aurantiamines/viridamines
7. Unknowns
8. Unknowns, chrysogenamide A
9. Cycloaspeptides A, B/C/D, E, G
10. Phenylquinolines (e.g. yaequinoline J1)
11. Compactins, lovastatin, mevastatin
12. Tryprostatin B, atlantinones A, B, andrastin E
13. Mangrovamide G
14. Unguisins A, C
15. Paraherquamide B, rhinocladin A
16. Pseurotin A
17. Amauromine/fellutanines
18. Chaetoglobosins A, B, E, cytoglobosin D
19. Communesins A, F, G, H
20. Synerazol
21. Viridicatol
22. Roquefortines, mangrovamides, marcfortines, peniciherquamide B, pyripyropenes A, deacetyl A, dehydroxy-A, B/C/D, E, F

Fig. 4. Consensus metabolomic phenotypes derived from UPLC-HRMS profiling of culture extracts for representative strains of the ten new *Penicillium* species and *P. ribis*. Heatmap colours represent the number of media conditions on which a given mass feature (column) was detected for a specific strain (row), ranging from 0 (black) to 3 (bright green). The dendrogram on the top axis represents a hierarchical cluster analysis of detection frequencies that was used to align mass features within the heatmap based on similar production patterns. Particular groupings of mass features for which metabolite annotation was achieved are "boxed" with an associated number that correspond with metabolite names listed below the heatmap.

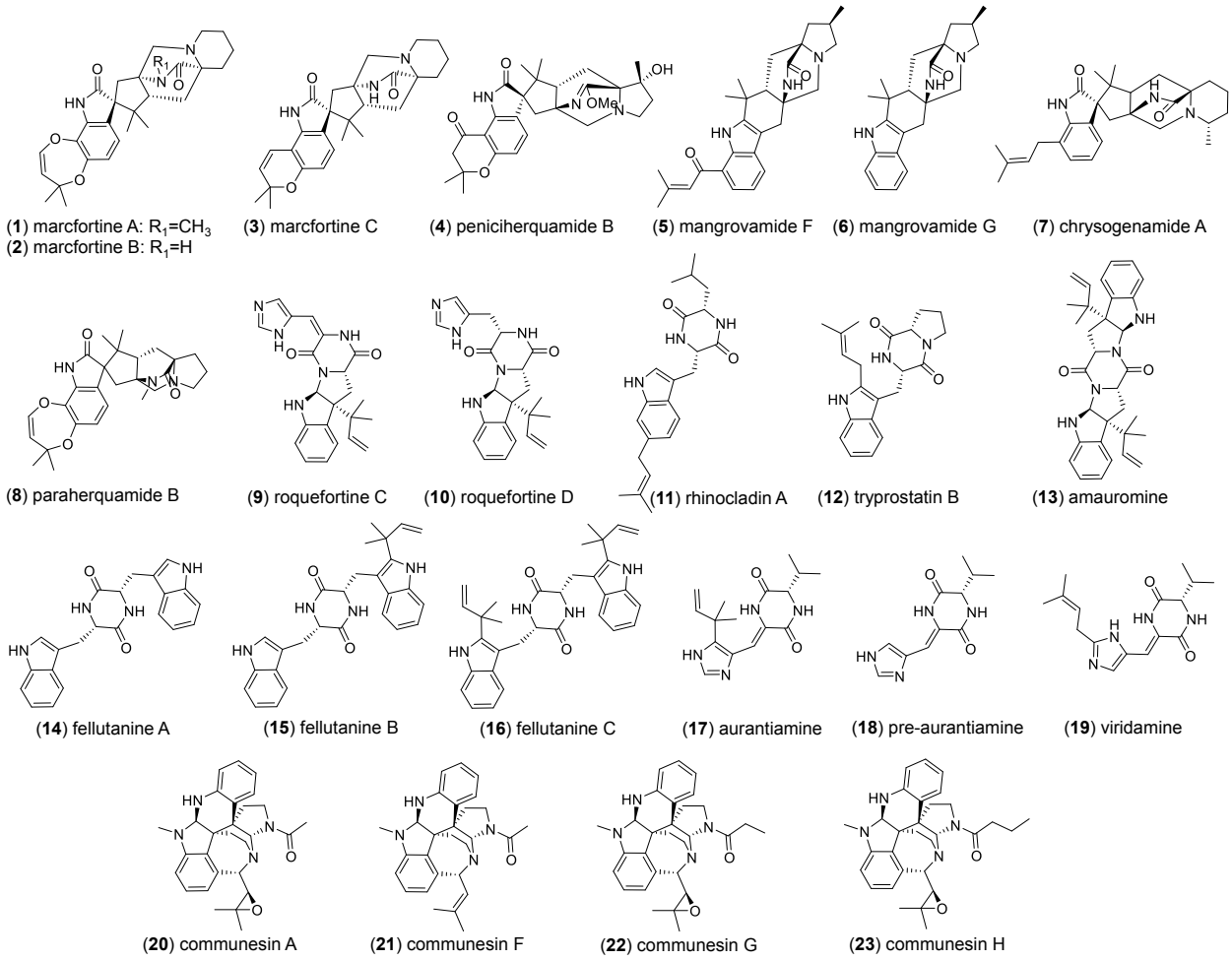

Fig. 5. Molecular structures of the cyclodipeptides annotated from the untargeted metabolomics phenotyping.

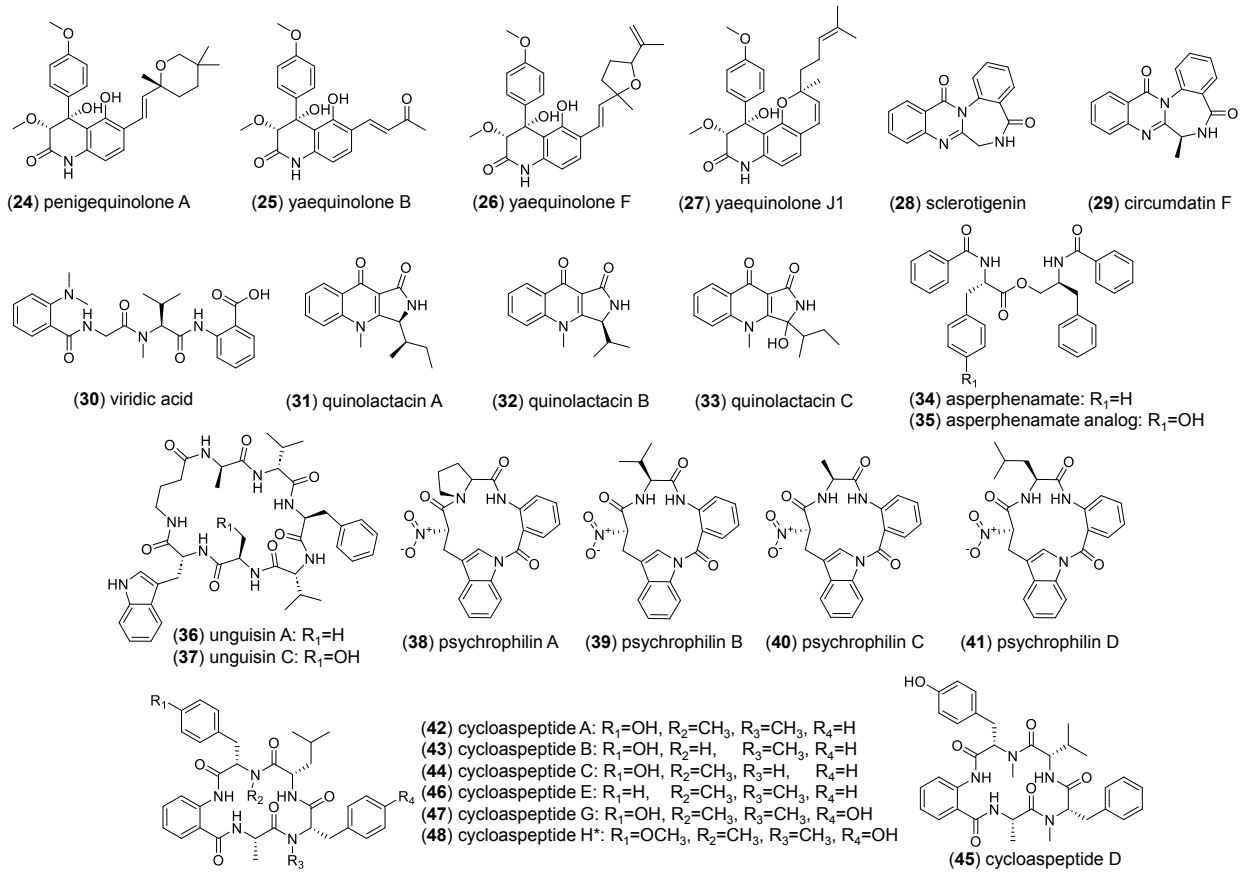

Fig. 6. Molecular structures of the NRPS-derived secondary metabolites annotated from the untargeted metabolomics phenotyping.

residues lacking *N*-methylation [similar to cycloaspeptides B and C (**43**, **44**)], and structural variants of cycloaspetide A in which the tyrosine phenol is methylated (similar to cycloaspeptide H*).

NRPS-PKS derived secondary metabolites (Fig. 8): Production of a selection of NRPS-PKS derived secondary metabolites were observed to be shared between many of the *Penicillium* species studied. For example, production of the cytochalasin alkaloids, cytoglobosin D (**49**) and chaetoglobosins A, B, and E (**50**–**52**) were observed (block 18 of the metabolomic phenotype) from both *P. aquamarinum* and *P. jugorum*. Production of funiculosin (**53**) and a funiculosin analog (**54**) (unique substituted pyridones having a cyclopentanetetrol and a cyclopentanetriol moieties respectively) and the macrolide lactams melearoride A (**55**) and PF 1163B (**56**) were shared between both *P. algidum* and *P. turcosum* (block 5 of the metabolomic phenotype heatmap). The highly functionalized, azaspirocyclic γ-lactams pseurotin A (**57**) and synerazol (**58**) were produced by a combination of *P. hesseltenei*, *P. jugorum*, and *P. oreophilum*.

PKS derived secondary metabolites (Fig. *9)*: The halogenated, spirocyclic hexaketide molecule griseofulvin (**59**) and the biosynthetic precursor dechloro-griseofulvin (**60**) were produced by *P. discoense*, *P. algidum*, *P. turcosum*, and *P. rivulorum*, along with norlichexanthone

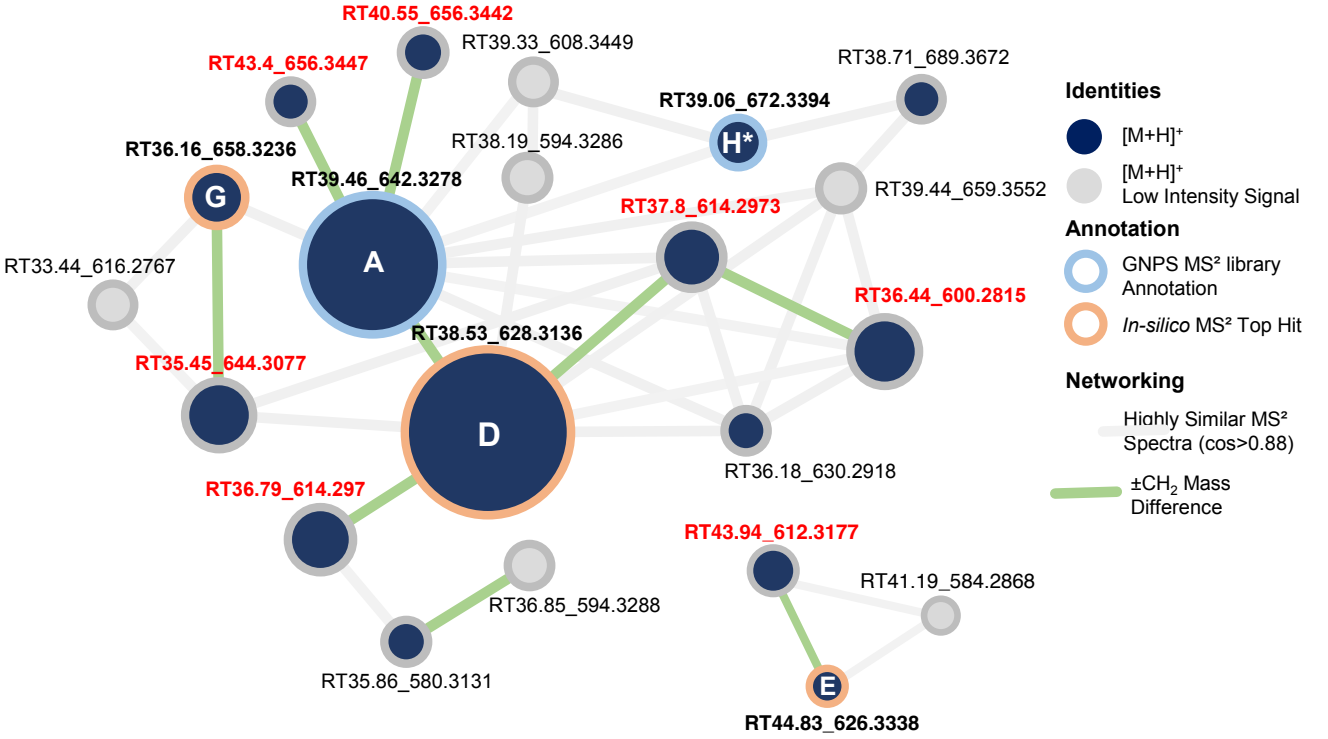

Fig. 7. Molecular networking maps of cycloaspetides detected in culture extracts from nanoLC-HRMS/MS experiments. Nodes represent observed $[M+H]^+$ precursor ions and lines connecting nodes represent highly similar cosine scores (> 0.88) comparing MS^2 scans. Cycloaspeptides mass features appear in bold and are labelled as: A (cycloaspeptide A), D (cycloaspeptide D), E (cycloaspeptide E), G (cycloaspeptide G), and H* (cycloaspeptide H_130057). Mass features in red **bold** text represent predicted, structurally new cycloaspeptide analogues with variations in N-methylation and O-methylation patterns (as denoted by green lines).

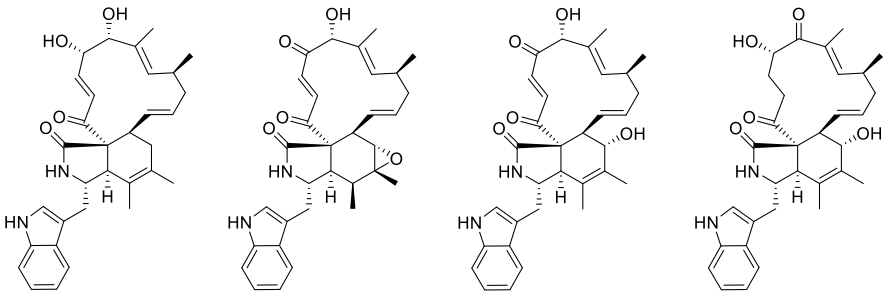

(**49**) cytoglobosin D (**50**) chaetoglobosin A (**51**) chaetoglobosin B (**52**) chaetoglobosin E

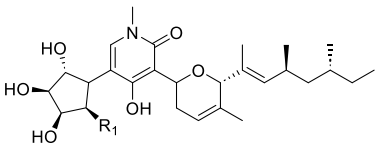

(**53**) funiculosin R_1=OH
(**54**) funiculosin analog R_1=H

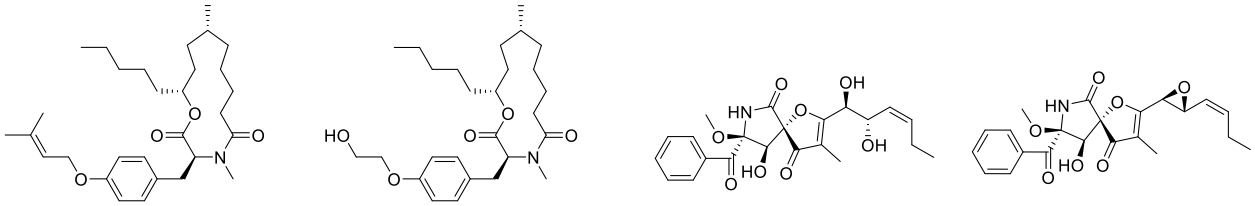

(**55**) melearoride A (**56**) PF 1163B (**57**) pseurotin A (**58**) synerazol

Fig. 8. Molecular structures of secondary metabolites derived from hybrid NRPS-PKS biosynthesis observed from the untargeted metabolomics phenotyping.

(**61**), which is believed to be a shunt metabolite formed early on from the benzophenone precursor offloaded from the PKS during griseofulvin biosynthesis (Petersen *et al.* 2014). Interestingly, norlichexanthone was observed to be produced by *P. ribis*; however, production of griseofulvin was not observed. Of the studied species, *P. marthae* was the only species to produce the structurally similar, homodimeric naphthoquinone pigment molecules, viomellein (**62**), vioxanthin (**63**) and xanthomegnin (**64**) (observed in block 6 of the metabolomic phenotype that was characteristic for *P. marthae*). *Penicillium ribis*, *P. algidum*, *P. wyomingense* and *P. turcosum* all produced the dihydro-benzofuran derivative asperfuran (**65**) (block 3 of the metabolomic phenotype). Various 'fungal statins' and their associated biosynthetic intermediates were observed (block 11 of the metabolomic phenotype) to be produced by *P. aquamarinum*, *P. oreophilum*, and *P. turcosum*. Each of the species produced compactin (**66**,**67**) and ML236 A (**68**,**69**) (for which both open and closed forms were observed), pravastatin (**70**), and lovastatin (**71**). To aid in data interpretation, ion identity network analysis (Fig. 10) revealed additional mass features associated with various 'statin' biosynthetic intermediates and potential shunt pathway metabolites

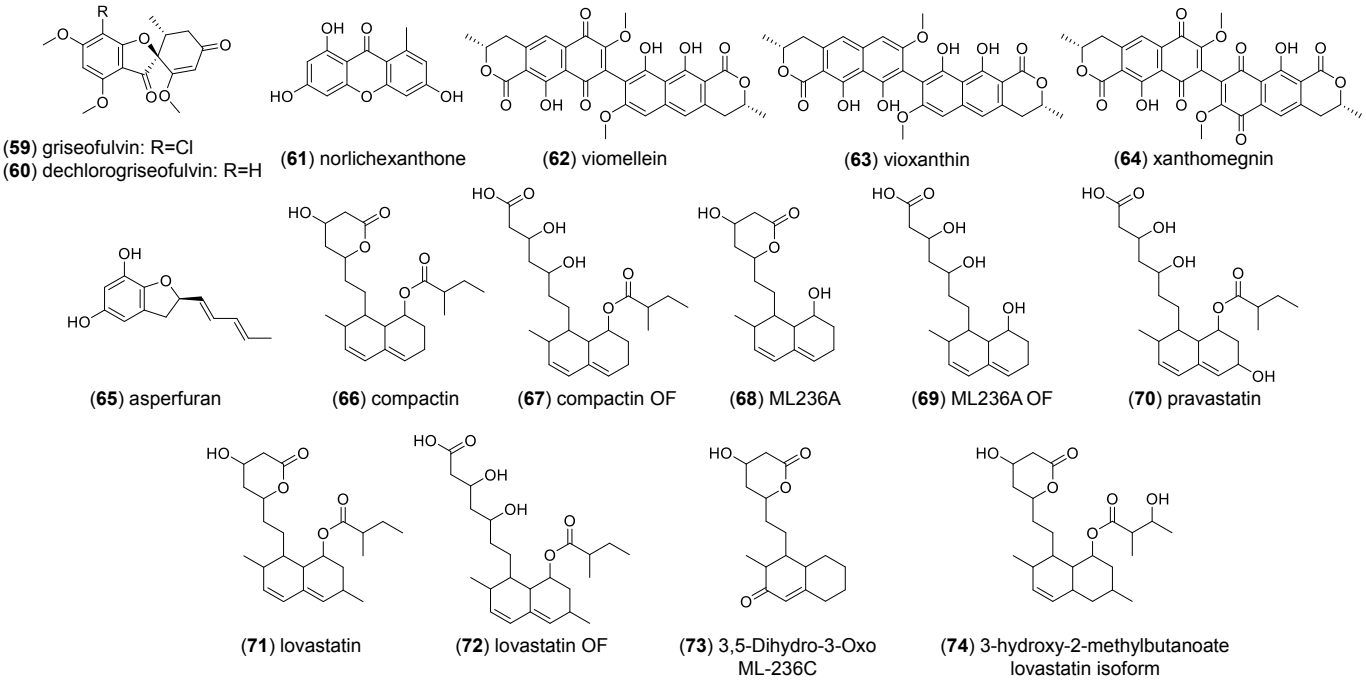

Fig. 9. Molecular structures of the PKS-derived secondary metabolites annotated from the untargeted metabolomics phenotyping.

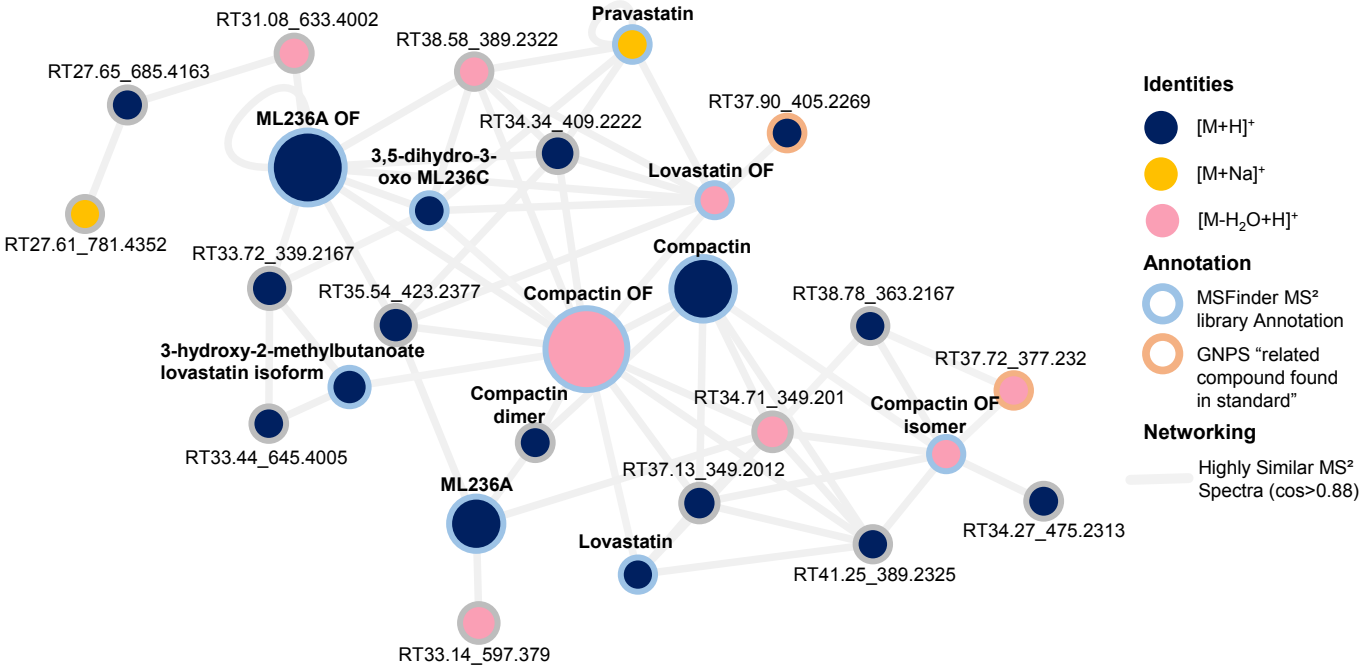

Fig. 10. Molecular networking maps of fungal statin associated secondary metabolites detected in culture extracts from nanoLC-HRMS/MS experiments. Blue nodes represent observed $[M+H]^+$ precursor ions, yellow nodes represent $[M+Na]^+$ precursor ions, and pink nodes represent $(M-H2O+H]^+$ precursor ions and lines connecting nodes represent highly similar cosine scores (> 0.88) comparing MS^2 scans. Mass feature annotations made based on MS^2 fragmentation pattern database matches are provided in bold text.

[i.e. lovastatin open form (**72**), 3,5-dihydro-3-oxo ML236C (**73**), and a 3-hydroxy-2-methylbutanoate lovastatin derivative (**74**)] associated with 'statin" production. Further investigation into extracted ion chromatograms revealed that compactin and compactin-associated intermediates (such as ML236A) were the predominant 'statin' analogues observed (in terms of relative ion abundance) as compared to lovastatin and pravastatin analogues from all three producing species.

Terpenoid secondary metabolites (Fig. 11): Indole diterpenoid alkaloids represent a large class of fungal secondary metabolites, often associated with biological activity. The penitrems A–F (**75**–**79**), produced by *P. algidum*, consist of a cyclic diterpenoid backbone and an indole moiety derived from tyrptophan, however, penitrem biosynthesis does not involve a NRPS (Hou *et al.*, 2022). The meroterpenoid pyripyropenes consist of a triketide–sesquiterpenoid molecular scaffold fused with a pyridine ring derived from nicotinic acid and differ based on hydroxylations and acetylations at various points on the molecular scaffold. Production of the pyripyropenes were limited to *P. aquamarinum*, from which pyripyropene A (**80**), dihydroxyl-pyripyropene A (**81**), deacetyl-pyripyropene A (**82**), pyripyropene E (**83**) and mass features associated with either pyripyropene B, C, or D were observed (block 22 of the metabolomic phenotype unique to *P. aquamarinum*). Atlantinones A & B (**84**, **85**) and andrastin E (**86**) are meroterpenoids produced by *P. ribis* (block 12 of the metabolomic heatmap) that are biosynthetically related to the pyripyropenes, as both metabolite classes are derived from farnesylated 3,5-dimethylorsellinic acid; however, neither atlantinone A, B, or andrastin E were observed from any of the other described *Penicillium* species under study.

TAXONOMY

Penicillium algidum Visagie, Overy, Seifert & Frisvad, ***sp. nov.*** MB 855913. Fig. 12.

Etymology: Latin, *algidum*, meaning cold or chilly, referring to the psychrotrophic nature of the species.

Subgeneric classification: *Penicillium* section *Ramosum* series *Lanosa.*

Colony diam. (7 d, at 25 ºC, *in mm)*: CYA 21–22; CYA 10 °C 5–8; CYA 15 °C 13–17; CYA 20 °C 18–21; CYA 30 °C no growth to microcolonies; CYA 37 °C no growth; CYAS 22–23; MEA 19–21; MEA 20 °C 21–22, YES 27–29; DG18 17–19; OA 22–24; CREA 13–14.

Colony characters: CYA (25 °C, *7 d)*: Colonies low, raised centrally, radially lightly sulcate, sectoring; margins low, narrow, entire; mycelia white; texture velutinous; sporulation moderately dense, conidia *en masse* Greenish Grey (26C2), Greyish to Dull Green (26B4–E4); soluble pigments absent; exudates absent; reverse Yellowish White (2A2), Greenish Grey (1C3), Dull to Greyish Yellow (3B3–4B3). *CYA (20* °C, *7 d)*: Colonies resembling those incubated at 25 °C. *MEA (25* °C, *7 d)*: Colonies low, raised centrally, radially lightly sulcate, sectoring typical; margins low, narrow, entire; mycelia white; texture velutinous; sporulation moderately dense, conidia *en masse* Greenish Grey (26C2), Greyish to Dull Green (26B4–E4); soluble pigments absent; exudates absent; reverse Yellowish White (2A2), Greenish Grey (1C3), Dull to Greyish Yellow (3B3–4B3). *MEA (20* °C, *7 d)*: Colonies resembling those incubated at 25 °C. *DG18 (25* °C, *7 d)*: Colonies low, plane to sulcate; margins low, wide, entire; mycelia white; texture velutinous and floccose; sporulation moderately dense, conidia *en masse* Greenish to Dull Green (25C4–D4–5); soluble pigments absent; exudates absent; reverse Yellowish White (2A2), Greyish Green (1D3–4). *YES (25* °C, *7 d)*: Colonies low, raised centrally, radially lightly sulcate; margins low, narrow, entire; mycelia white; texture velutinous and floccose; sporulation moderately dense, conidia *en masse* Greyish to Dull Green (26C3–D3–5); soluble pigments absent; exudates absent; reverse Pale Yellow to Greyish Yellow (4A3–B3–6). *CREA (25* °C, *7 d)*: Colonies exhibiting weak growth; acid not produced.

Conidiophores terverticillate, a minor proportion biverticillate; *stipes* rough, 150–1500 × 3–5 µm; *branches* 2–3 per stipe, divergent, 12–25(–32) µm; *metulae* appressed, 3–6 per branch, 10–14(–17) × 3–4 µm; *phialides* ampulliform, 4–8 per metula, 8–10(–11) × (2.5–)3–4

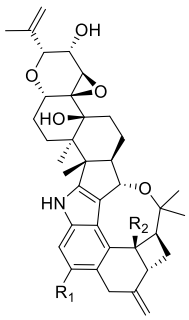

(**75**) penitrem A: R_1=Cl, R_2=OH
(**76**) penitrem B: R_1=H, R_2=H
(**77**) penitrem F: R_1=Cl, R_2=H

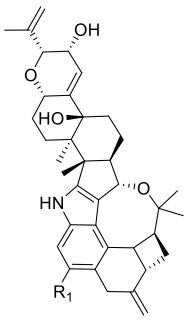

(**78**) penitrem D: R_1=Cl
(**79**) penitrem E: R_1=H

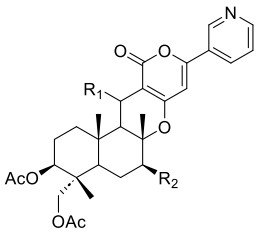

(**80**) pyripyropene A: R_1=OH, R_2=OAc
(**81**) dehydroxypyripyropene A: R_1=H, R_2=OAc
(**82**) deacetylpyripyropene A: R_1=OH, R_2=OH

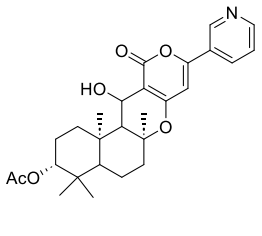

(**83**) pyripyropene E

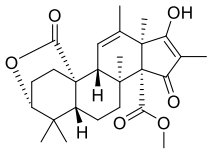

(**84**) atlantinone A

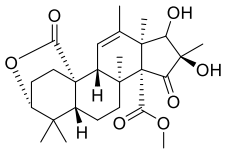

(**85**) atlantinone B

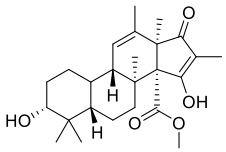

(**86**) andrastin E

Fig. 11. Molecular structures of the terpenoid secondary metabolites annotated from the untargeted metabolomics phenotyping.

Fig. 12. *Penicillium algidum sp. nov*. (DAOMC 256946). **A.** Colonies on CYA, MEA, DG18, YES and OA. **B.** Colony texture on MEA. **C.** Conidia. **D–I.** Conidiophores. Scale bars = 10 µm.

µm, average length metula/phialide 1.28; *conidia* smooth, globose, 2.5–3 × 2.5–3 µm ($\bar{x}$= 2.76 ± 0.17 × 2.72 ± 0.16), average width/length = 0.98, n = 54.

Extrolites: Asperfuran; asperphenamate and hydroxyl-aperphenamate; cycloaspeptides A–E, G & H; funiculosin and dehydro-funiculosin; griseofulvin and dechloro-griseofulvin; melearoride A; norlichexanthone; PF 1163B; penitrems A, B, D–F; psychrophilins A, B & D; and quinolactacins A–C.

Typus: **Greenland**, Zackenberg, east of Oksestien, red/brown clay like soil proximal to *Calluna* sp. (heather) and *Salix* sp. (willow), 1999, *E.K. Lyhne* (**holotype** DAOM 985253, dried specimen, ex-type culture DAOMC 256946 = IBT 22067 = IBT 24414 = CBS 102886 = CMW 57199 = CN093F2).

DNA barcodes: ITS = KY989168, *BenA* = KY989043, *CaM* = KY989104, *RPB2* = MZ984123.

Additional materials examined: **Greenland**, Jameson Land peninsula, near Hugin Lake, tundra soil under *Calluna* sp. (heather), 1999, *E.K. Lyhne*, culture DAOMC 256945 = IBT 21988 = CMW 57197 = CN093E9; Jameson Land peninsula, near Hugin Lake, coastal sand, 1999, *E.K. Lyhne*, culture IBT 22020 = CMW 57198 = CN093F1.

Notes: *Penicillium algidum*, *P. turcosum*, *P. wyomingense* and *P. rivulorum* are introduced as new species in the *P. ribis* species complex. Morphologically and phylogenetically distinguishing among these species is difficult (Fig. 2, Table 2). *Penicillium rivulorum* consistently grows faster than its close relatives, while it can grow at 30 °C, as do *P. turcosum* and *P. wyomingense*. Chemical profiling of strains showed patterns similar to what is observed in the groupings of the multigene phylogeny (discussed in secondary metabolite results above). *P. algidum* differs from other species of the *P. ribis* species complex by the production of penitrems A, B, D, E, & F and quinolactacins A-C along with multiple unique mass features associated with unknown chemistry.

Penicillium aquamarinum Visagie, Overy, Seifert & Frisvad, ***sp. nov.*** MB 855897. Fig. 13.

Etymology: Latin, *aquamarinum*, named after the production of green/blue (aquamarine) colonies on CYA.

Subgeneric classification: *Penicillium* section *Robsamsonia* series *Robsamsonia*.

Colony diam. (7 d, at 25 ºC, *in mm):* CYA 19–23; CYA 10 °C 12–14; CYA 15 °C 19–23; CYA 20 °C 18–23; CYA 30 °C 8–15; CYA 37 °C no growth; CYAS 16–23; MEA 25–30; MEA 20 °C 27–30; YES 37–45; DG18 25–28; OA 27–30; CREA 15–20.

Colony characters: CYA (25 °C, *7 d)*: Colonies moderately deep, radially and concentrically sulcate; margins low to moderately deep, narrow, somewhat irregular; mycelia white; texture floccose to weakly fasciculate; sporulation moderately dense, conidia *en masse* Greyish Green (25B3–D5–E5) to Greyish Turquoise (24B3–B5–E5); soluble pigments brownish, inconspicuous; exudates clear, abundant; reverse Light to Greyish Yellow (4A4–B4), to Brownish Orange (5C6). *CYA (20* °C, *7 d)*: Colonies resembling those incubated at 25 °C. *MEA (25* °C, *7 d)*: Colonies deep, radially lightly sulcate; margins low, narrow to wide, somewhat irregular; mycelia white; texture velutinous, becoming strongly fasciculate with age; sporulation dense, conidia *en masse* Greyish Green (25B3–D5–E5); soluble pigments absent; exudates clear; reverse Yellowish Brown to Brown (5C5–E7). *MEA (20* °C, *7 d)*: Colonies resembling those incubated at 25 °C, except for more floccose appearance. *DG18 (25* °C, *7 d)*: Colonies low, plane; margins low, wide, entire; mycelia white; texture velutinous, loosely floccose; sporulation dense, conidia *en masse* Greyish to Dull Green (25C4–D4–5); soluble pigments absent; exudates absent; reverse Yellowish White (3A2), Olive to Olive Brown (3D5–4D5). *YES (25* °C, *7 d)*: Colonies moderately deep, raised at centre, radially and concentrically sulcate; margins low, narrow, entire; mycelia white; texture velutinous and floccose; sporulation moderately dense, conidia *en masse* Greyish Green (25B3–26B3–27B3), darker Greyish Green (25E5) centrally; soluble pigments absent; exudates absent; reverse Light Yellow (4A4), Orange (5B6–8), Greyish Green (1C3). *CREA (25* °C, *7 d)*: Colonies moderate growth; acid weakly produced.

Conidiophores ter- to quaterverticillate, a minor proportion biverticillate, borne from surface and aerial mycelia; *stipes* rough, 150–1000 × 3–4(–5) µm; *branches* 2–4 per stipe, appressed and divergent, (8.5–)11–22(–42) µm; *metulae* appressed, 3–6 per branch, 7–11.5(–13.5) × 3–4(–4.5) µm; *phialides* ampulliform, 4–6 per metula, 6.5–8.5(–10) × 2.5–3.5 µm, average length metula/phialide 1.26; *conidia* smooth, broadly ellipsoidal, a minor proportion ovoid, 3.5–4.5 × 3–4 µm ($\bar{x}$= 3.9 ± 0.2 × 3.3 ± 0.2), average width/length = 0.84, n = 75.

Extrolites: Amauromine; chaetoglobosins A, B, & E and cytoglobosin D; fellutanines A–C; marcfortines A–C; mangrovamides F & G; peniciherquamide B; pyripyropene A, dihydroxyl-pyripyropene A, deacetyl-pyripyropene A and pyripyropene E; roquefortines C & D; and statins (compactin, lovastatin and hydroxy-2-methylbutanoate lovastatin, pravastatin, ML236A and 3,5-dihydro-3-oxo ML236C).

Typus: **USA**, Wyoming, Medicine Bow-Rout National Forest, soil near beaver dam, 26 Oct. 1994, *J.C. Frisvad* (**holotype** DAOM 749220, dried specimen, ex-type culture DAOMC 251672 = IBT 16643 = CMW 57210 = CN093A4).

DNA barcodes: ITS = KY989143, *BenA* = KY989018, *CaM* = KY989083, *RPB2* = KY989204.

Additional materials examined: **USA**, Wyoming, Medicine Bow, Pilot Hill Rd., soil, 26 Oct. 1994, *J.C. Frisvad*, culture DAOMC 251673 = IBT 17669 = CMW 57211 = CN093A5; Northwest of Lake Marie parking lot, soil beneath *Caltha leptosepala* (mountain marsh marigold), 19 Jul. 1996, *J.C. Frisvad*, culture DAOMC 251680 = IBT 22760 = CMW 57212 = CN093A6.

Notes: *Penicillium aquamarinum* is closely related to *P. fimorum* and *P. robsamsonii* (Fig. 3). On CREA, acid production is absent in *P. fimorum* and *P. robsamsonii* but present in *P. aquamarinum* (Houbraken *et al.* 2016). Also, *P. aquamarinum* colonies on CYA have a floccose to weakly fasciculate texture and produce clear exudates. Colonies on CYA of *P. fimorum* have a velvety and somewhat fasciculate texture at the centre and produce large pale brown exudates, while *P. robsamsonia* colonies on CYA are strongly fasciculate and produce large pale brown exudates. In terms of extrolite production, *P. aquamarinum* does not share any commonalities in extrolites with those reported for *P. fimorum*

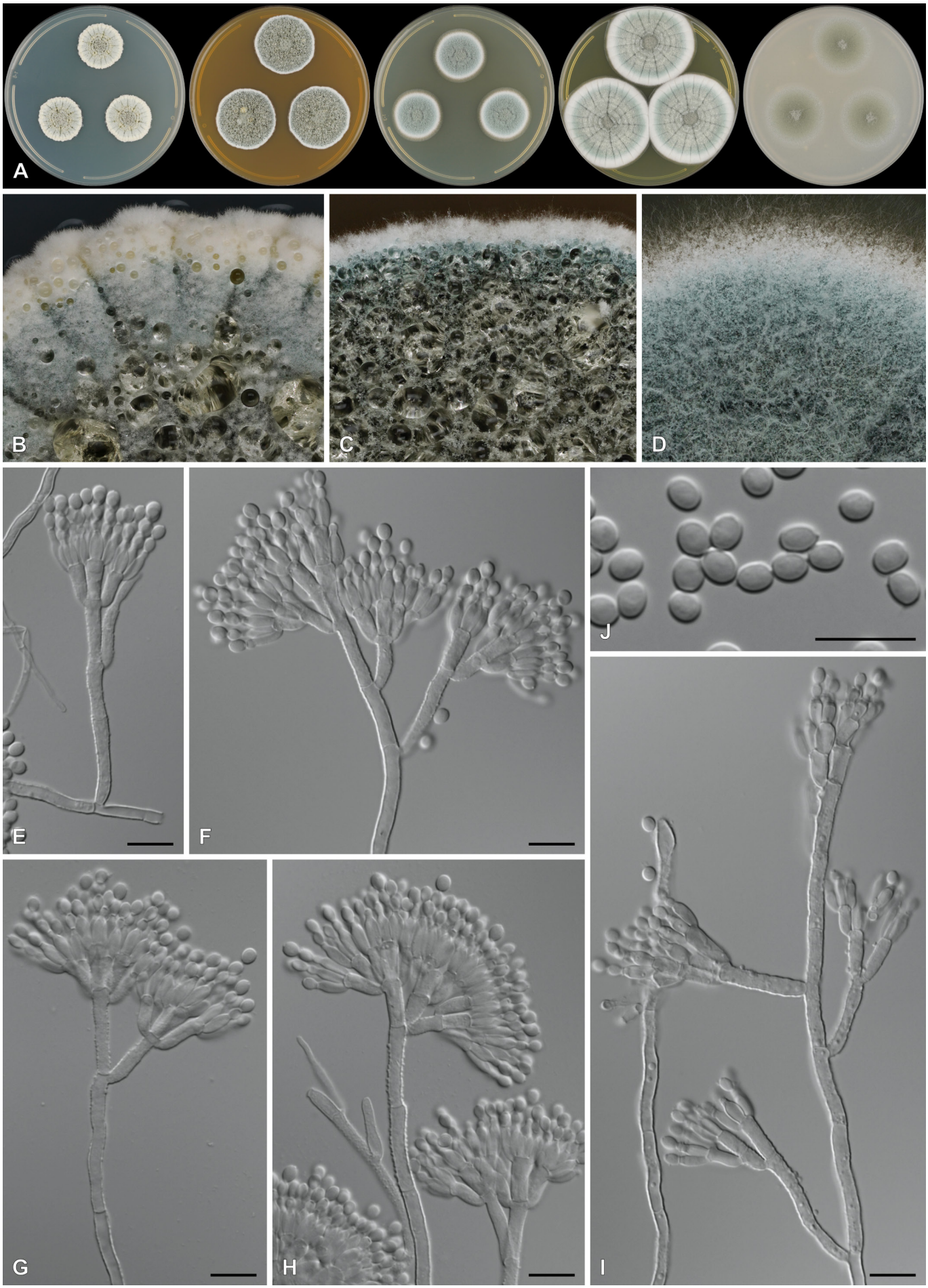

Fig. 13. *Penicillium aquamarinum sp. nov.* (DAOMC 251672). **A.** Colonies on CYA, MEA, DG18, YES and OA. **B–D.** Colony texture on CYA (B), MEA (C) and DG18 (D). **E–I.** Conidiophores. **J.** Conidia. Scale bars = 10 µm.

(Houbraken *et al.* 2016). In contrast, *P. aquamarinum* and *P. robsamsonii* both share traits in the production of chaetoglobosins, pyripyropenes, and roquefortines. However, *P. aquamarinum* is easily distinguished from *P. robsamsonii* by the production of amauromine, fellutanines A–C, marcfortines A–C, mangrovamides F & G, peniciherquamide B, and the various statin analogs listed above; while *P. robsamsonii* produces andrastin E, clavatols, quinolactacins and patulodin (Houbraken *et al.* 2016).

Penicillium discoense Visagie, Overy, Seifert & Frisvad, ***sp. nov.*** MB 855898. Fig. 14.

Etymology: Latin, *discoense*, named after Disco Island in Greenland, from where the type was isolated.

Subgeneric classification: *Penicillium* section *Ramosum* series *Soppiorum.*

Colony diam. (7 d, at 25 ºC, *in mm)*: CYA (5–)13; CYA 10 °C 5–8; CYA 15 °C 10–14; CYA 20 °C 13–16; CYA 30 °C no growth; CYA 37 °C no growth; CYAS 10–14; MEA (5–)11–12; MEA 20 °C (15–)20–21; YES (13–)18–19; DG18 13–15; OA (5–)12–13; CREA 4–7.

Colony characters: *CYA (25* °C, *7 d)*: Colonies moderately deep, radially and concentrically lightly sulcate; margins low, narrow, entire; mycelia white, inconspicuously yellow; texture floccose; sporulation absent to sparse, conidia *en masse* greyish turquoise to greyish green (24B3–25B3); soluble pigments inconspicuously yellow; exudates clear; reverse Light Yellow (4A4). *CYA (20* °C, *7 d)*: Colonies resembling those incubated at 25°C, except for inconspicuously yellow exudates. *MEA (25* °C, *7 d)*: Colonies low, plane; margins low, narrow, entire; mycelia inconspicuously yellow; texture floccose; sporulation moderately dense, conidia *en masse* Dull to Greyish Green (25D4–E5); soluble pigments absent; exudates clear to yellow; reverse Greyish Orange to Brown (6B4–E7). *MEA (20* °C, *7 d)*: Colonies resembling those incubated at 25 °C, except for sulcation plane. *DG18 (25* °C, *7 d)*: Colonies low, raised at centre, radially and concentrically lightly sulcate; margins low, narrow, entire; mycelia white; texture floccose; sporulation moderately dense, conidia *en masse* Greyish Turquoise (24B4–D5); soluble pigments inconspicuously yellow; exudates absent; reverse Yellowish White (3A2) to Yellow (3A6). *YES (25* °C, *7 d)*: Colonies moderately deep, radially and concentrically sulcate; margins low, narrow, entire; mycelia white and yellow; texture floccose; sporulation sparse to moderately dense, conidia *en masse* Dull to Greyish Green (25D4–E5); soluble pigments absent; exudates absent; reverse Orange White (5A2) to Orange (5B7). *CREA (25* °C, *7 d)*: Colonies exhibiting weak growth; acid not produced.

Conidiophores ter- to quaterverticillate, a minor proportion biverticillate, borne from surface mycelia; *stipes* smooth, 150–1000 × 3.5–5 µm; *branches* 2 per stipe, divergent, 16–38 µm; *metulae* divergent, 3–6 per branch, 10–15(–17) × 3–5(–5.5) µm; *phialides* ampulliform, 3–6 per metula, (7–)8–9 × 2.5–4 µm, average length metula/phialide 1.7; *conidia* smooth, globose, 2.5–3.5 × 2.5–3.5 µm ($\bar{x}$ = 2.55 ± 0.2 × 2.54 ± 0.2), average width/length = 1.00, n = 50.

Extrolites: Asperphenamate and hydroxyl-aperphenamate; chrysogenamide A; griseofulvin and dechlorogriseofulvin; and norlichexanthone.

Typus: **Greenland**, Disco Island, Fortune Bay, sandy soil, 26 Jul. 2000, *S. Gravesen* (**holotype** DAOM 749224, dried specimen, ex-type culture DAOMC 251813 = IBT 22667 = CMW 57213 = CN093B2).

DNA barcodes: ITS = KY989178, *BenA* = KY989053, *CaM* = KY989112, *RPB2* = MZ984138.

Additional materials examined: **Greenland**, Disco Island, Fortune Bay, sandy soil, 26 Jul. 2000, *S. Gravesen*, culture DAOMC 251814 = IBT 22668 = CMW 57214 = CN093B3; Disco Island, Fortune Bay, sandy soil, 26 Jul. 2000, *S. Gravesen*, culture DAOMC 251815 = IBT 22669 = CMW 57215 = CN093B4.

Notes: *Penicillium discoense* is classified in section *Ramosum* series *Soppiorum* and is closely related to *P. americanum*, *P. chroogomphum*, *P. lenticrescens* and *P. soppii* (Fig. 2). These species all grow restrictedly on CYA and MEA at 25 °C, with colonies typically less than 15 mm in 7 d. *Penicillium discoense* [(5–)13 mm] and *P. chroogomphum* (7–8 mm) grow slower than their close relatives on CYA at 25 °C. Also, *P. discoense* has globose to broadly ellipsoidal conidia reaching a diameter of up to 3.5 µm. This contrasts with the larger ellipsoidal conidia (4–5 × 3–4 µm) of *P. chroogomphum* (Rong *et al.* 2016). *Penicillium lenticrescens* and *P. soppii* can be distinguished from other species of the section by their conidiophore branching, typically biverticillate and never terverticillate. *Penicillium soppii* was originally reported to produce strong yellow soluble pigments (Zaleski 1927), while *P. lenticrescens* lacks soluble pigments (Visagie *et al.* 2014a). The remaining species, *P. americanum* displays similar growth rates on most media, except on CYAS (17–18 mm) (Crous *et al.* 2019). Of the extrolites identified from *P. discoense*, the products associated with asperphenamate and griseofulvin biosynthesis are fairly common in section *Ramosum* species; however, production of chrysogenamide A is unique to *P. discoense*, along with a block of unannotated mass features (Fig. 4, block 8) representing further unique extrolite chemistry associated with *P. discoense*.

Penicillium hesseltinei Visagie, Overy, Seifert & Frisvad, ***sp. nov.*** MB 855899. Fig. 15.

Etymology: Latin, *hesseltinei*, named to honour the work of C.W. Hesseltine.

Subgeneric classification: *Penicillium* section *Fasciculata* series *Viridicata.*

Colony diam. (7 d, at 25 ºC, *in mm)*: CYA 20–26; CYA 10 °C 7–8; CYA 15 °C 14–16; CYA 20 °C 20–24; CYA 30 °C 15–20; CYA 37 °C no growth; CYAS 25–28; MEA 23–27; MEA 20 °C 24–25; YES 28–30; DG18 19–22; OA 20–21; CREA 20–21.

Colony characters: *CYA (25* °C, *7 d)*: Colonies moderately deep to deep, radially sulcate; margins low to moderately deep, narrow, entire; mycelia white; texture velutinous to weakly fasciculate, some floccose mycelia; sporulation dense, conidia *en masse* Greyish to Dull Green (25C4–E4–6); soluble pigments absent; exudates clear; reverse Yellowish White to Yellowish Grey (2A2–B2), Greyish Yellow (4B5) centrally. *CYA (20* °C, *7 d)*: Colonies resembling those incubated at 25 °C. *MEA (25* °C, *7 d)*: Colonies moderately deep,

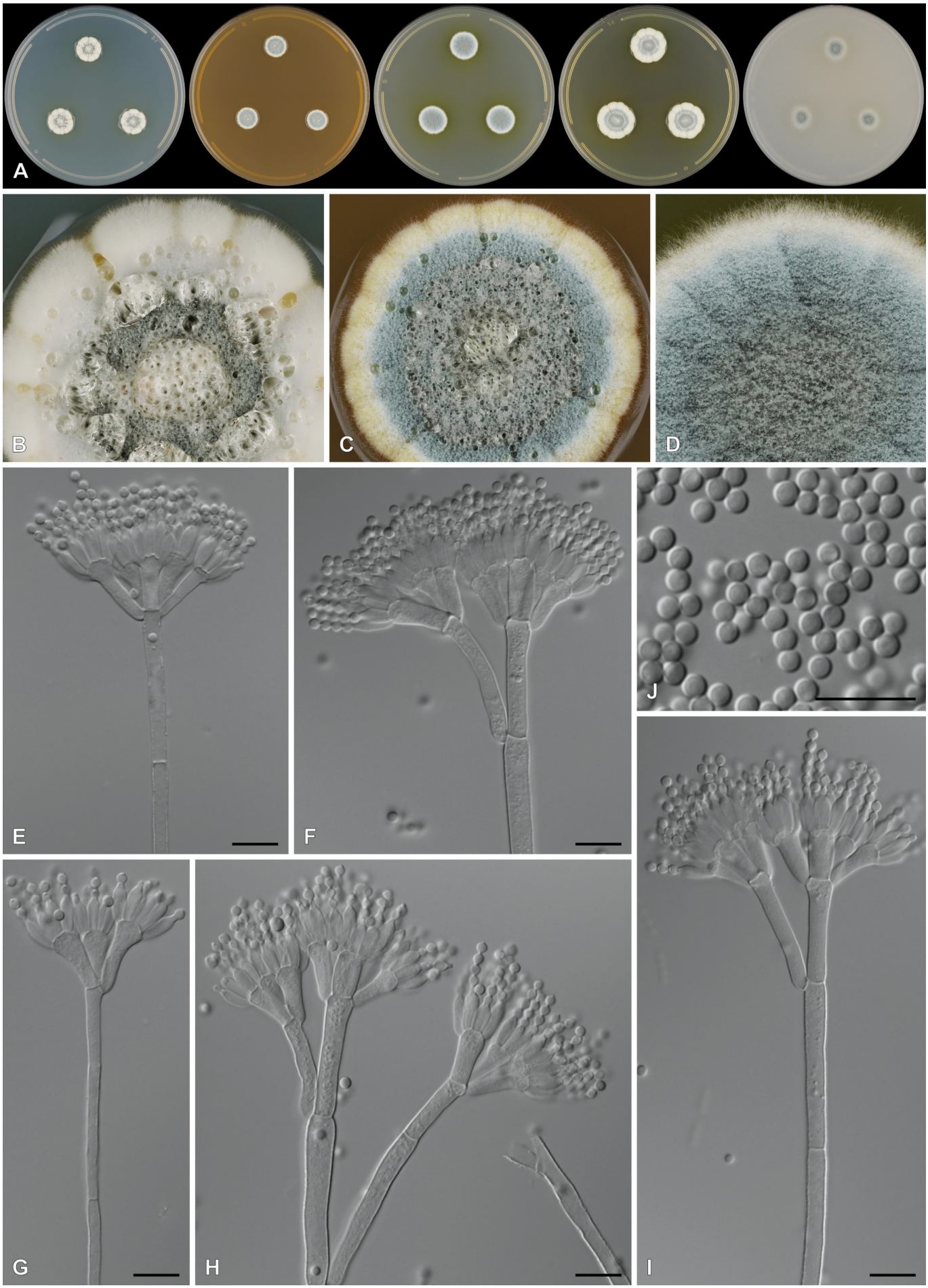

Fig. 14. *Penicillium discoense sp. nov.* (DAOMC 251813). **A.** Colonies on CYA, MEA, DG18, YES and OA. **B–D.** Colony texture on CYA (B), MEA (C) and DG18 (D). **E–I.** Conidiophores. **J.** Conidia. Scale bars = 10 µm.

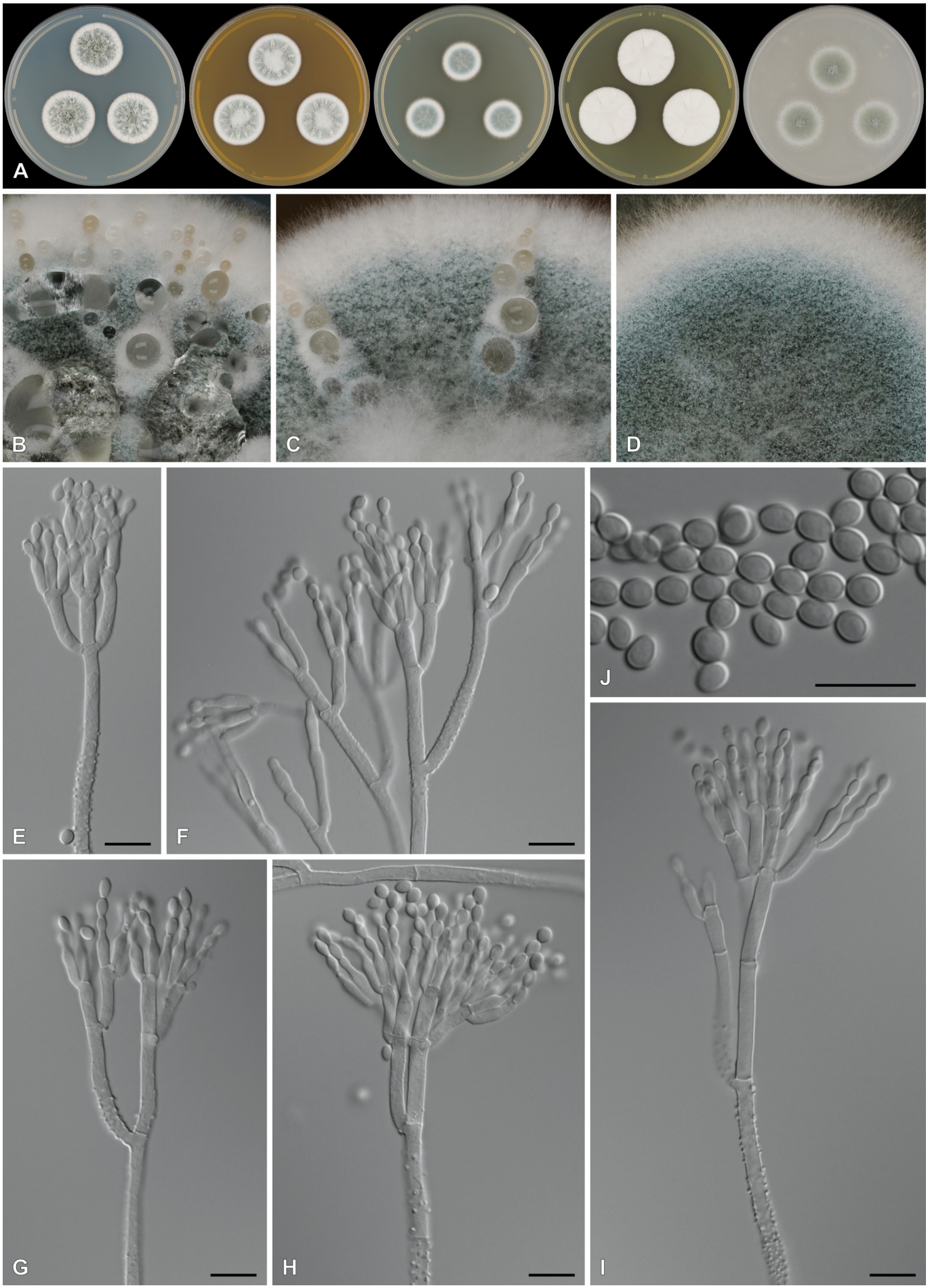

Fig. 15. *Penicillium hesseltinei sp. nov*. (DAOMC 251664). **A.** Colonies on CYA, MEA, DG18, YES and OA. **B–D.** Colony texture on CYA (B), MEA (C) and DG18 (D). **E–I.** Conidiophores. **J.** Conidia. Scale bars = 10 µm.

lightly radially sulcate; margins low, wide; mycelia white; texture velutinous, floccose centrally; sporulation moderately dense, conidia *en masse* Greyish to Dull Green (25C4–D4–5); soluble pigments absent; exudates clear; reverse Yellowish Brown to Brown (5D4–E4). *MEA (20* °C, *7 d)*: Colonies resembling those incubated at 25 °C, except for more floccose appearance centrally. *DG18 (25* °C, *7 d)*: Colonies low, plane to lightly radially sulcate; margins low, wide, entire; mycelia white; texture velutinous; sporulation dense, conidia *en masse* Greyish to Dull Green (25C4–D4–5); soluble pigments absent; exudates absent; reverse Yellowish White to Yellowish Grey (2A2–B2), Greyish Yellow (4B5) centrally. *YES (25* °C, *7 d)*: Colonies low, raised centrally, radially lightly sulcate; margins low, narrow, entire; mycelia white; texture not determined; sporulation absent; soluble pigments absent; exudates absent; reverse Light Yellow to Greyish Yellow (4A4–B5), Orange (5A6–B6). *CREA (25* °C, *7 d)*: Colonies good growth; acid strongly produced.

Conidiophores terverticillate, a minor proportion quaterverticillate; *stipes* coarsely rough, 150–1500 × 2.5–4 µm; *branches* 2–3 per stipe, divergent, 13–32 µm; *metulae* appressed, 3–6 per branch, 10–18(–22) × 2.5–4 µm; *phialides* ampulliform, 4–6 per metula, 8.5–11 × 2.5–3.5 µm, average length metula/phialide 1.38; *conidia* smooth, ellipsoidal, some ovoid, 3.5–4.5 × 2.4–4.5 µm ($\bar{x}$= 4 ± 0.2 × 3 ± 0.2), average width/length = 0.74, n = 71.

Extrolites: Pseurotin A and synerazol.

Typus: **USA**, New Mexico, Chihuahuan Desert, Sevilleta National Wildlife Refuge, cheek pouch of banner-tailed kangaroo rat (*Dipodomys spectabilis*), Mar. 1988, *J.C. Frisvad* (**holotype** DAOM 749218, dried specimen, ex-type culture DAOMC 251664 = IBT 12396 = CMW 57228 = CN093B5).

DNA barcodes: ITS = KY989128, *BenA* = KY989003, *CaM* = KY989070, *RPB2* = KY989195. *Reference genome*: JAPZBW01.

Notes: Phylogenies resolve *P. hesseltinei* basal to the clade containing *P. cyclopium* and *P. polonicum* in series *Viridicata*. *Penicillium marthae* is sister to *P. viridicatum*. Other close relatives in the series includes *P. aurantiogriseum*, *P. freii* and *P. neoechinulatum.* Comparing unique phenotypic variation between these species: *P. neoechinulatum* produces rough conidia; *P. freii* does not grow on CYA at 30 °C; *P. cyclopium* grows very slowly on CYA at 30 °C (2–6 mm); while *P. hesseltinei* grows slower than the others on CYA at 15 °C (14–16 mm) and has ellipsoidal to ovoid conidia. Comparing distinguishing phenotypic traits among the remaining species is more complicated. Stipes of *P. viridicatum* are roughened as compared to the smooth to finely roughened stipes of *P. aurantiogriseum*, *P. polonicum*, and *P. marthae*; *P. aurantiogriseum* grows more restricted on CYA at 15 °C as compared to *P. polonicum* (16–23 vs 27–30 mm); and *P. marthae* can produce an orange colony reverse on YES. Comparative data are derived from Frisvad & Samson (2004).

Penicillium jugorum Visagie, Overy, Seifert & Frisvad, ***sp. nov.*** MB 855900. Fig. 16.

Etymology: Latin, *jugorum*, meaning “from mountain ridges”.

Subgeneric classification: *Penicillium* section *Ramosum* series *Lanosa.*

Colony diam (7 d, at 25 °C, *in mm)*: CYA 4–6; CYA 10 °C 5–8; CYA 15 °C 12–14; CYA 20 °C 16–18; CYA 30 °C no growth; CYA 37 °C no growth; CYAS 6–8; MEA 4–6; MEA 20 °C 16–20; YES 11–16; DG18 9–11; OA 4–6; CREA 4–6.

Colony characters: *CYA (25* °C, *7 d)*: Colonies moderately deep, plane; margins low, narrow, entire; mycelia white; texture floccose; sporulation absent, soluble pigments absent; exudates absent; reverse Pale Yellow to Light Orange (4A3–5A4). *CYA (20* °C, *7 d)*: Colonies moderately deep, radially and concentrically lightly sulcate; margins low, narrow, entire; mycelia white; texture floccose; sporulation absent to sparse, conidia *en masse* greyish to dull green (25B3–D4); soluble pigments absent; exudates absent; reverse Pale Yellow to Light Orange (4A3–5A5). *MEA*: Colonies moderately deep, plane; margins low, narrow, entire; mycelia white; texture floccose; sporulation absent, soluble pigments absent; exudates absent; reverse Brown (6D8). *MEA (20* °C, *7 d)*: Colonies low, lightly radially sulcate; margins low, narrow, entire; mycelia white; texture floccose; sporulation moderately dense, conidia *en masse* Greyish to Dull Green (25B3–D4); soluble pigments absent to minute clear droplets; exudates absent; reverse Pale Yellow (3A3), Brownish Orange (6C8). *DG18*: Colonies moderately deep, radially and concentrically lightly sulcate; margins low, narrow, entire; mycelia white; texture floccose; sporulation sparse, conidia *en masse* Greyish Green (25B3); soluble pigments absent; exudates absent; reverse Yellowish White to Greyish Yellow (4A2–B3). *YES*: Colonies moderately deep, radially and concentrically lightly sulcate; margins low, narrow, entire; mycelia white; texture floccose; sporulation absent, soluble pigments absent; exudates absent; reverse Orange White to Greyish Orange (5A2–B4–5). *CREA*: Colonies exhibiting weak growth; acid weakly produced.

Conidiophores terverticillate, divaricate, sometimes biverticillate; *stipes* finely rough, 150–1000 × 2.5–3.5 µm; *branches* 2 per stipe, divergent, 10–35 µm; metulae divergent, (2–)3–6 per branch, 8–12(–14) × 2.5–3 µm; *phialides* ampulliform, 4–6 per metula, (6.5–)7–8 × 2–3 µm, average length metula/phialide 1.38; *conidia* rough, globose to subglobose, 2–3 × 2–3 µm ($\bar{x}$= 2.5 ± 0.1 × 2.5 ± 0.1), average width/length = 0.96, n = 87.

Extrolites: Amauromine; asperphenamate and hydroxyl-aperphenamate; chaetoglobosins A, B, & E; cycloaspeptides A–E, G & H and cytoglobosin D; fellutanines A–C; pseurotin A and synerazol.

Typus: **USA**, Wyoming, Snowy Range, Libby Flats, soil under *Picea* species, 19 Jul. 1996, *J.C. Frisvad* (**holotype** DAOM 749225, dried specimen, ex-type culture DAOMC 251817 = IBT 22778 = CMW 57185 = CN093C2 = KAS2466).

DNA barcodes: ITS = KY989184, *BenA* = KY989059, *CaM* = KY989118, *RPB2* = MZ984129.

Additional materials examined: **USA**, Wyoming, Snowy Range, Libby Flats, soil under *Picea* sp., 19 Jul. 1996, *J.C. Frisvad*, culture DAOMC 256962 = IBT 22779 = CMW 57184 = CN093C1; ibid., culture DAOMC 256963 = IBT 22780 = CMW 57186 = CN093C3; Wyoming, Snowy Range, Hanging Lakes, soil under *Pinus contorta*, 11 Sept. 1994, *J.C. Frisvad*, culture DAOMC 256964 = IBT 22792 = CMW 57187 = CN093C4.

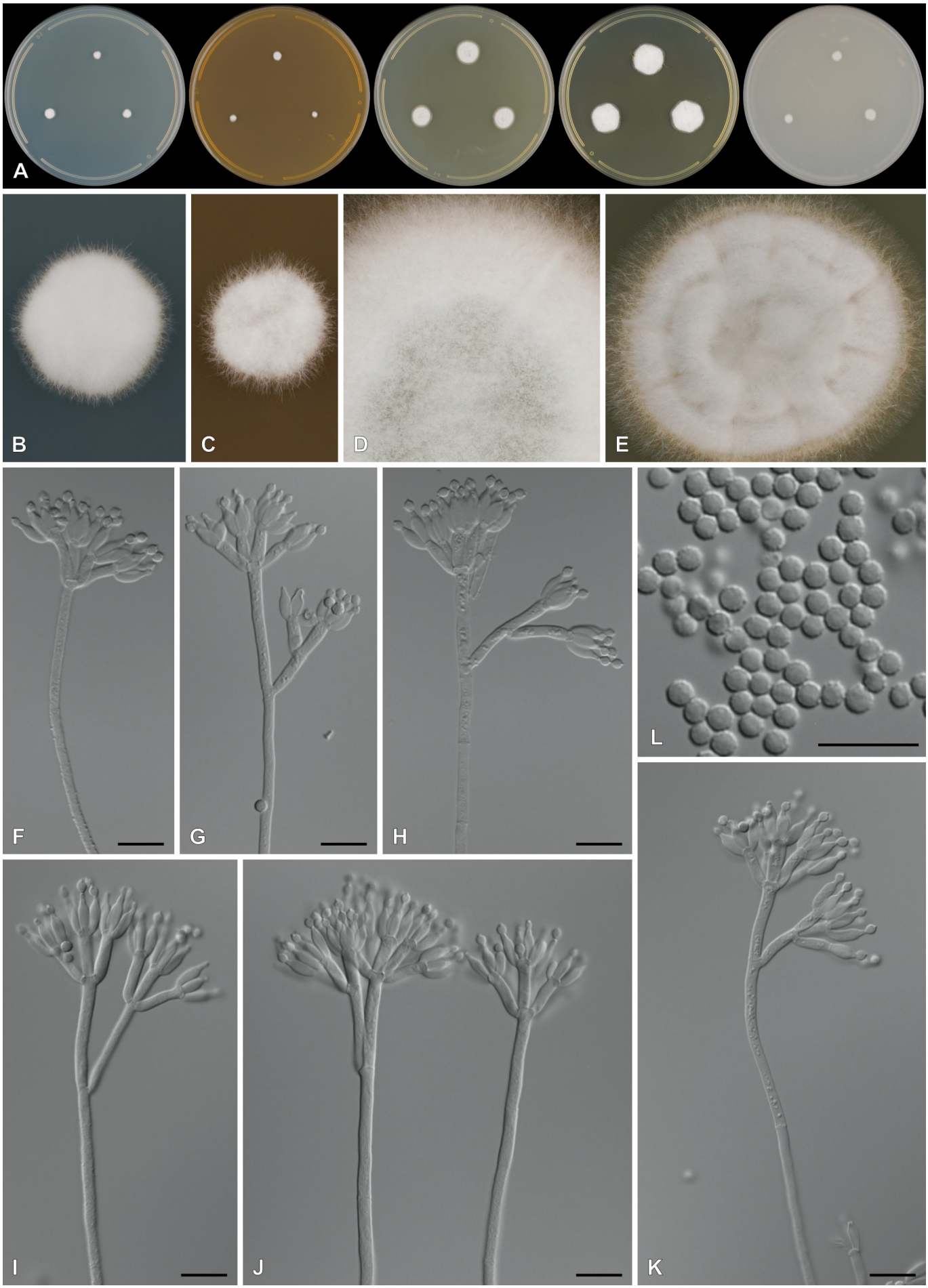

Fig. 16. *Penicillium jugorum sp. nov*. (DAOMC 251817). **A.** Colonies on CYA, MEA, DG18, YES and OA. **B–E.** Colony texture on CYA (B), MEA (C), MEA 20 °C (D) and DG18 (E). **F–K.** Conidiophores. **L.** Conidia. Scale bars = 10 µm.

Notes: *Penicillium jugorum* and *P. oreophilum* are resolved in section *Ramosum* series *Lanosa* as close relatives of *P. jamesonlandense* and *P. swiecickii* (Fig. 2). Colony growth rates on standardised media and incubation conditions, and stipe and conidia wall texture, are taxonomically informative in the series (Table 2). *Penicillium jugorum* (CYA 5–8 mm; MEA 4–6 mm) and *P. jamesonlandense* (CYA 10–13 mm; MEA 8–12 mm) grow more restrictedly than other species at 25 °C. At 20 °C, both grow significantly better (*P. jugorum* CYA 16–18 mm & MEA 16–20 mm; *P. jamesonlandense* CYA 17–18 mm & MEA 16–22 mm). The distantly related *P. lusitanum* has similar growth patterns, especially on MEA, but this species has smooth to finely roughened stipes compared to the smooth stipes of *P. jugorum* and *P. jamesonlandense*. *Penicillium oreophilum* grows relatively faster than both and produces rough walled stipes and conidia, which easily distinguishes it as a new species. *Penicillium jugorum* is easily distinguished from *P. jamesonlandense* based on extrolite production. Although both species produce pseurotin A and cycloaspeptides, *P. jugorum* produces a combination of amauromine, asperphenamates, chaetoglobosins, cytoglobsin D, fellutanines and synerazol; while *P. jamesonlandense* produces chyrogine, griseofulvins, kojic acid, and penicillic acid (Frisvad *et al.* 2006).

Penicillium marthae Visagie, Overy, Seifert & Frisvad, ***sp. nov.*** MB 855901. Fig. 17.

Etymology: Latin, *marthae*, named for Martha Christensen.

Subgeneric classification: *Penicillium* section *Fasciculata* series *Viridicata.*

Colony diam. (7 d, at 25 ºC, *in mm)*: CYA 25–33; CYA 10 °C 13–15; CYA 15 °C 24–27; CYA 20 °C 28–33; CYA 30 °C 11–18; CYA 37 °C no growth; CYAS 33–38; MEA 31–37; MEA 20 °C 30–24; YES 37–45; DG18 25–32; OA 25–29; CREA 12–15.

Colony characters: *CYA (25* °C, *7 d)*: Colonies deep, radially and concentrically very deep sulcations; margins low, narrow, irregular; mycelia white to inconspicuously yellow, sometimes yellow; texture floccose; sporulation sparse to moderately dense, conidia *en masse* Greyish to Dull Green (26C4–D4–27D4); soluble pigments brownish, inconspicuous; exudates clear; reverse Orange White (5A2) and Brownish Orange (5C4–6). *CYA (20* °C, *7 d)*: Colonies resembling those incubated at 25 °C, except for bright yellow mycelia. *MEA (25* °C, *7 d)*: Colonies moderately deep, plane to lightly sulcate, synnemata present after 4 wk; margins low, wide, entire; mycelia white and yellow; texture velutinous, fasciculate and floccose; sporulation dense, moderately dense in some isolates, conidia *en masse* Dull Green (25D4–E4–26E4); soluble pigments absent; exudates absent to minute clear droplets; reverse Greyish Orange (5B5) to Brown (6E7). *MEA (20* °C, *7 d):* Colonies resembling those incubated at 25 °C, except for more floccose appearance. *DG18 (25* °C, *7 d)*: Colonies moderately deep, plane to radially lightly sulcate; margins low, wide, entire; mycelia white; texture velutinous; sporulation dense, conidia *en masse* Greyish to Dull Green (26D4–E5–6); soluble pigments absent; exudates absent; reverse Greenish Grey (1B3–C3), Greyish Green (1C5), Olive Yellow (3F6). *YES (25* °C, *7 d)*: Colonies deep, radially and concentrically sulcate; margins moderately deep, narrow, entire; mycelia white and yellow; texture floccose; sporulation sparse to moderately dense in some isolates, conidia *en masse* Greyish Turquoise (24C4–25C4), Greyish Green (25E5–6) in denser areas; soluble pigments absent; exudates absent; reverse Light Yellow (4A4), Orange (5A6–B6–7). *CREA (25* °C, *7 d)*: Colonies good growth; acid strongly produced.

Conidiophores ter- to quaterverticillate, sometimes biverticillate, borne from surface and aerial mycelia; *stipes* commonly rough, but sometimes smooth, 135–700(–2000) × 3–5 µm; *branches* 2–4 per stipe, appressed and divergent, 11.5–32 µm; *metulae* appressed, 3–6 per branch, 8.5–15(–24) × 2.5–3.5 µm; *phialides* ampulliform, 3–8 per metula, 7–9(–13) × 2.5–3 µm, average length metula/phialide 1.40; *conidia* smooth to finely rough, globose to subglobose, 2.5–3.5 × 2.5–3.5 µm ($\bar{x}$= 3.0 ± 0.1 × 2.9 ± 0.15), average width/length = 0.94, n = 83.

Extrolites: Aurantiamine, pre-aurantiamine & viridamine; circumdatin F; sclerotigenin; viridic acid; and xanthomegnins (viomellein, vioxanthin, and xanthomegnin).

Typus: **USA**, New Mexico, Chihuahuan Desert, soil, 28 Dec. 1993, *J.C. Frisvad* (**holotype** DAOM 749219, dried specimen, ex-type culture DAOMC 251670 = IBT 13054 = CMW 57223 = CN103F9).

DNA barcodes: ITS = KY989134, *BenA* = KY989009, *CaM* = KY989076, *RPB2* = KY989201.

Additional materials examined: **USA**, New Mexico, Chihuahuan Desert, soil, 28 Dec. 1993, *J.C. Frisvad*, culture DAOMC 251665 = IBT 12661 = CMW 57220 = CN103F6 = KAS2399; ibid., culture DAOMC 251666 = IBT 12662 = CMW 57221 = CN103F7; ibid., culture DAOMC 251667 = IBT 12685; ibid., culture DAOMC 251668 = IBT 12687 = CMW 57222 = CN103F8; ibid., culture DAOMC 251669 = IBT 12691.

Notes: See notes under *P. hesseltinei* above for morphological comparison. Although *P. marthae* and *P. viridicatum* have some commonalities in extrolite production (xanthomegnins, viridamine, and viridic acid), *P. marthae* is easily distinguished by the production of circumdatin F and sclerotigenin, while *P. viridicatum* produces brevianamides and penicillic acid (Frisvad *et al.* 2004). *Penicillium marthae* was also observed to produce aurantiamine and pre-aurantiamine; however, both metabolites are likely biosynthetically co-produced with the isomeric molecule viridamine (observed from both *P. marthae* and *P. viridicatum*) and are therefore likely also associated with *P. viridicatum* (yet to be reported).

Penicillium oreophilum Visagie, Overy, Seifert, Christensen & Frisvad, ***sp. nov.*** MB 855902. Fig. 18.

Etymology: Latin, *oreophilum*, meaning “mountain loving”.

Subgeneric classification: *Penicillium* section *Ramosum* series *Lanosa.*

Colony diam. (7 d, at 25 ºC, *in mm)*: CYA 15–20; CYA 10 °C 7–10; CYA 15 °C 16–17; CYA 20 °C 17–22; CYA 30 °C no growth; CYA 37 °C no growth; CYAS 16–20; MEA 15–18; MEA 20 °C 20–24; YES 20–24; DG18 15–17; OA 12–13; CREA 10–12.

Colony characters: *CYA (25* °C, *7 d)*: Colonies moderately deep, radially and concentrically sulcate; margins low, narrow, entire; mycelia white; texture floccose; sporulation sometimes absent to sparse, sometimes moderately dense, conidia *en masse* Greenish White to Pale Green (25A2–3), Dull Green (25D3–4); soluble

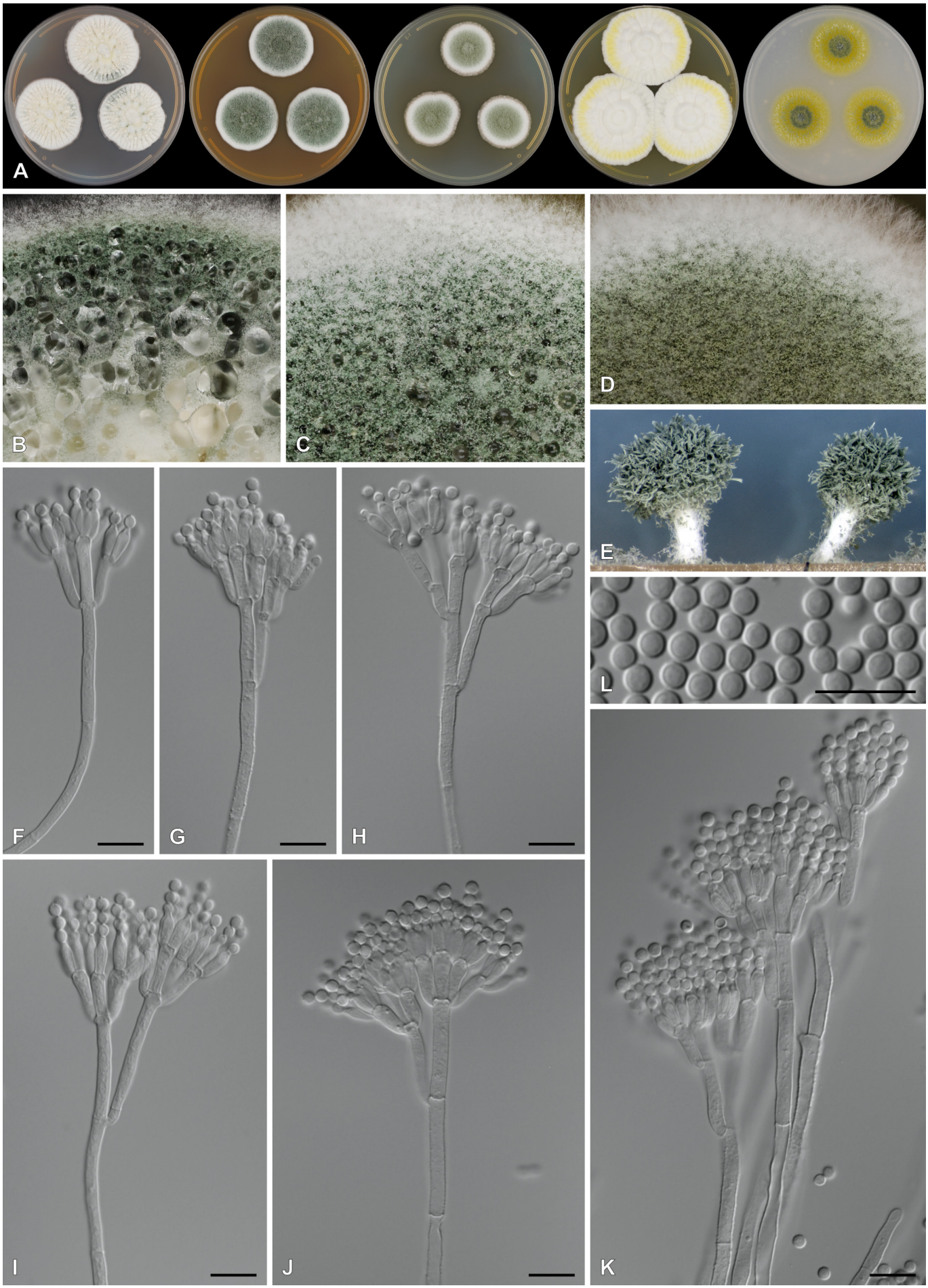

Fig. 17. *Penicillium marthae sp. nov.* (DAOMC 251670). **A.** Colonies on CYA, MEA, DG18, YES and OA. **B–D.** Colony texture on CYA (B), MEA (C) and DG18 (D). **E.** Synnema produced on MEA after 4 wk. **F–K.** Conidiophores. **L.** Conidia. Scale bars = 10 µm.

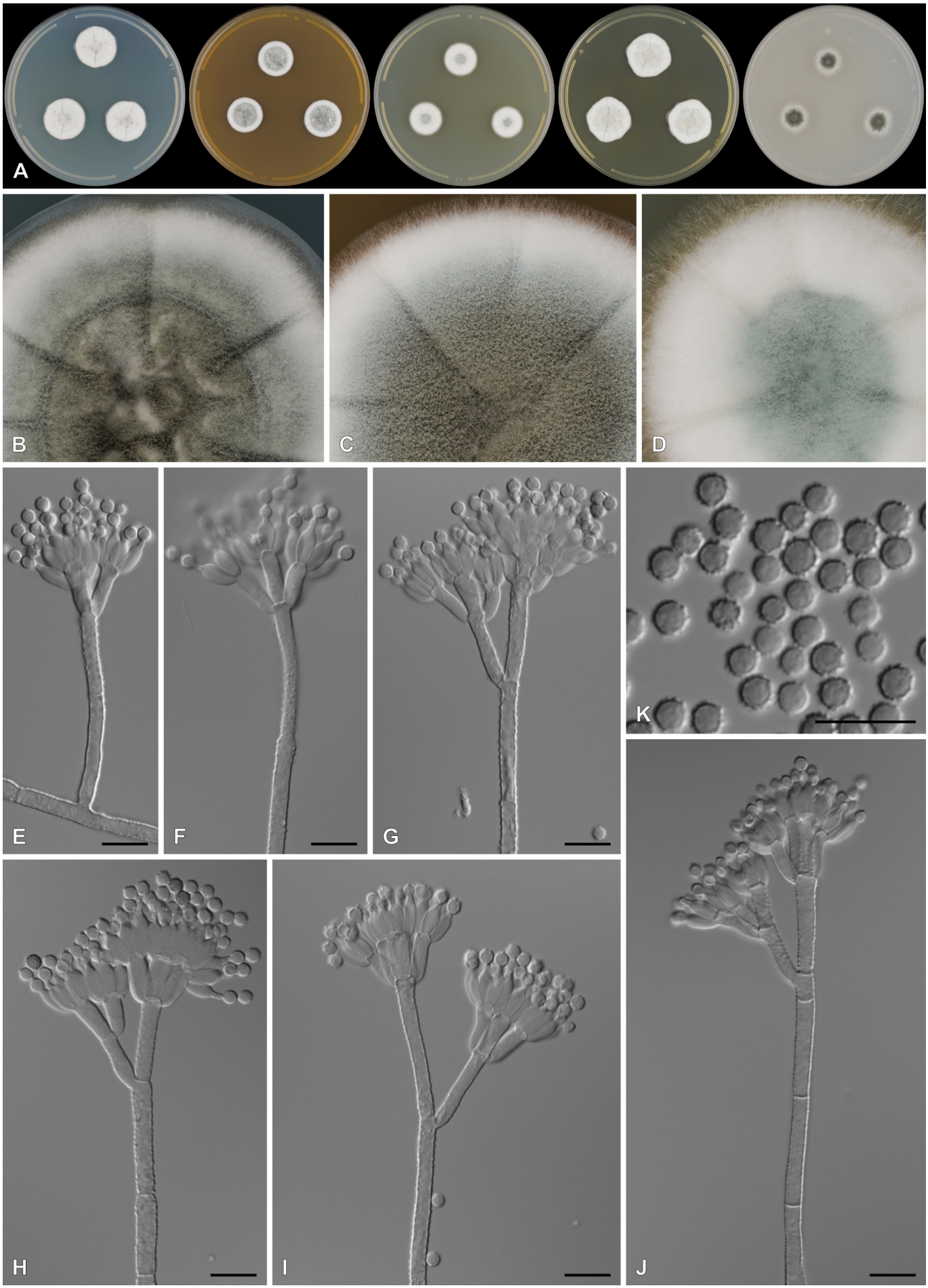

Fig. 18. *Penicillium oreophilum sp. nov*. (DAOMC 251821). **A.** Colonies on CYA, MEA, DG18, YES and OA. **B–D.** Colony texture on CYA (B), MEA (C) and DG18 (D). **E–J.** Conidiophores. **K.** Conidia. Scale bars = 10 µm.

pigments absent; exudates absent; reverse Yellowish White (3A2), Pale to Dull to Greyish Yellow (3A3–B3–4B3). *CYA (20* °C, *7 d)*: Colonies resembling those incubated at 25 °C. *MEA (25* °C, *7 d)*: Colonies low, plane to lightly sulcate; margins low, narrow, entire; mycelia white; texture floccose; sporulation sparse to moderately dense, conidia *en masse* Dull Green (25D4–E4) to Greyish Turquoise (24E4); soluble pigments absent; exudates absent to clear; reverse Light Yellow (4A4) to Yellowish Brown (6D7). *MEA (20* °C, *7 d)*: Colonies resembling those incubated at 25 °C. *DG18 (25* °C, *7 d)*: Colonies low to moderately deep, plane to very lightly sulcate; margins low, wide, entire; mycelia white; texture floccose; sporulation sparse to moderately dense in some isolates, conidia *en masse* Pale Turquoise to Greyish Turquoise (24A3–24D6); soluble pigments absent; exudates absent; reverse pale to Light Yellow (3A3–4), dull to Greyish Yellow (3B3–C4). *YES (25* °C, *7 d)*: Colonies low, raised centrally, radially and concentrically sulcate; margins low, narrow, entire; mycelia white; texture floccose; sporulation sparse, conidia *en masse* Greyish Turquoise to Greyish Green (24B3–25B3); soluble pigments absent; exudates absent; reverse Light Yellow (4A4), Orange Yellow (5A6–B6). *CREA (25* °C, *7 d)*: Colonies exhibiting weak growth; acid weakly produced.

Conidiophores terverticillate, a minor proportion biverticillate; *stipes* rough, 150–1000 × 3–4.5 µm; *branches* 2 per stipe, divergent, 13–24(–37) µm; *metulae* appressed to divergent, (2–)3–5 per branch, 9.5–15 × 3–4 µm; *phialides* ampulliform, 3–6 per metula, 7.5–9.5 × 2.5–3.5 µm, average length metula/phialide 1.38; *conidia* rough, globose to subglobose, 2.5–3.5 × 2.5–3.5 µm ($\bar{x}$= 3.28 ± 0.2 × 3.2 ± 0.2), average width/length = 0.99, n = 88.

Extrolites: Amauromine; asperphenamate and hydroxyl-aperphenamate; cycloaspeptides A–E, G & H; fellutanines A–C (only in IBT 22541); penigequinolone A; pseurotin A and synerazol; statins (compactin, lovastatin and hydroxy-2-methylbutanoate lovastatin, pravastatin, ML236A and 3,5-dihydro-3-oxo ML236C); and yaequinolones B, F, & J1.

Typus: **USA**, Wyoming, Wind River Mountain Range, alpine soil, 14 Jun. 2002, *M. Christensen* (**holotype** DAOM 749222, dried specimen, ex-type culture DAOMC 251821 = IBT 23951 = CMW 57190 = CN093D2).

DNA barcodes: ITS = KY989190, *BenA* = KY989065, *CaM* = KY989123, *RPB2* = MZ984135.

Additional materials examined: **Denmark**, Eiði, Faroe Islands, soil, 26 Jun. 1999, *E.K. Lyhne*, culture DAOMC 256947 = IBT 22341 = CMW 57188 = CN093C9; Eiði, Faroe Islands, soil, 1 Sep. 2000, *E.K. Lyhne*, culture DAOMC 256961 = IBT 22541 = CMW 57189 = CN093D1. **Greenland**, Godhavn, soil, 12 Jan. 2001, *E.K. Lyhne*, culture DAOMC 256948 = IBT 22909 = CMW 57192 = CN093D5. **Norway**, Svalbard, ice, Aug. 2001, *N. Gunde-Cimerman*, culture DAOMC 256965 = IBT 24500 = CMW 57191 = CN093D3.

Notes: See notes under *P. jugorum* above. Although the production of multiple extrolites is shared by *P. oreophilium* and *P. jugorum* (amauromine; asperphenamates, cycloaspeptides, fellutanines, pseurotin A and synerazol), *P. oreophilium* is distinguished from *P. jugorum* by the production of penigequinolone A, yaequinolones, and a variety of different fungal statins (compactin, lovastatin and hydroxy-2-methylbutanoate lovastatin, pravastatin, ML236A and 3,5-dihydro-3-oxo ML236C).

Penicillium rivulorum Visagie, Overy, Seifert & Frisvad, ***sp. nov.*** MB 855903. Fig. 19.

Etymology: Latin, *rivulorum*, meaning “from or proximal to streams”.

Subgeneric classification: *Penicillium* section *Ramosum* series *Lanosa.*

Colony diam. (7 d, at 25 ºC, *in mm)*: CYA 26–28; CYA 10 °C 10–11; CYA 15 °C 18–19; CYA 20 °C 25–27; CYA 30 °C 3–4; CYA 37 °C no growth; CYAS 25–27; MEA 29–31; MEA 20 °C 28–30; YES 34–36; DG18 22–24; OA 26–28; CREA 15–20.

Colony characters: *CYA (25* °C, *7 d)*: Colonies low, raised centrally, radially lightly sulcate, sectoring; margins low, narrow, entire; mycelia white; texture velutinous; sporulation moderately dense, conidia *en masse* Greenish Grey (26C2), Greyish to Dull Green (26B4–E4); soluble pigments absent; exudates absent; reverse Yellowish White (2A2), Greenish Grey (1C3), Dull to Greyish Yellow (3B3–4B3). *CYA (20* °C, *7 d)*: Colonies resembling those incubated at 25 °C. *MEA (25* °C, *7 d)*: Colonies low, raised centrally, radially lightly sulcate, sectoring typical; margins low, narrow, entire; mycelia white; texture velutinous; sporulation moderately dense, conidia *en masse* Greenish Grey (26C2), Greyish to Dull Green (26B4–E4); soluble pigments absent; exudates absent; reverse Yellowish White (2A2), Greenish Grey (1C3), Dull to Greyish Yellow (3B3–4B3). *MEA (20* °C, *7 d)*: Colonies resembling those incubated at 25 °C. *DG18 (25* °C, *7 d)*: Colonies low, plane to sulcate; margins low, wide, entire; mycelia white; texture velutinous and floccose; sporulation moderately dense, conidia *en masse* Greenish to Dull Green (25C4–D4–5); soluble pigments absent; exudates absent; reverse Yellowish White (2A2), Greyish Green (1D3–4). *YES (25* °C, *7 d)*: Colonies low, raised centrally, radially lightly sulcate; margins low, narrow, entire; mycelia white; texture velutinous and floccose; sporulation moderately dense, conidia *en masse* Greyish to Dull Green (26C3–D3–5); soluble pigments absent; exudates absent; reverse pale yellow to Greyish Yellow (4A3–B3–6). *CREA (25* °C, *7 d)*: Colonies exhibiting weak growth; acid not produced.

Conidiophores terverticillate, a minor proportion biverticillate; *stipes* rough, 150–1000 × 2.5–4 µm; *branches* 2 per stipe, divergent, 13–37 µm; *metulae* appressed, 3–4 per branch, 9.5–14 × 3–4 µm; *phialides* ampulliform, 5–8 per metula, 8–11 × 2.5–3.5 µm, average length metula/phialide 1.28; *conidia* smooth, broadly ellipsoidal, 3–4 × 2.5–3.5 µm ($\bar{x}$= 3.6 ± 0.2 × 3 ± 0.2), average width/length = 0.84, n = 97.

Extrolites: Asperphenamate and hydroxyl-aperphenamate; communesins A, F, G & H; griseofulvin and dechloro-griseofulvin; norlichexanthone; and psychrophilins A–D.

Typus: **USA**, Colorado, Cache la Poudre River, soil under old cottonwood, 13 Nov. 1994, *J.C. Frisvad* (**holotype** DAOM 749223, dried specimen, ex-type culture DAOMC 251681 = IBT 24420 = IBT 17740 = CMW 57228 = CN022E3).

DNA barcodes: ITS = KY989192, *BenA* = KY989067, *CaM* = KY989125, *RPB2* = MZ984109.

Notes: See notes under *P. algidum* above. *Penicillium rivulorum* differs from other species of the *P. ribis* species complex by the production of communesins A, F, G & H along with multiple unique mass features associated with unknown chemistry.

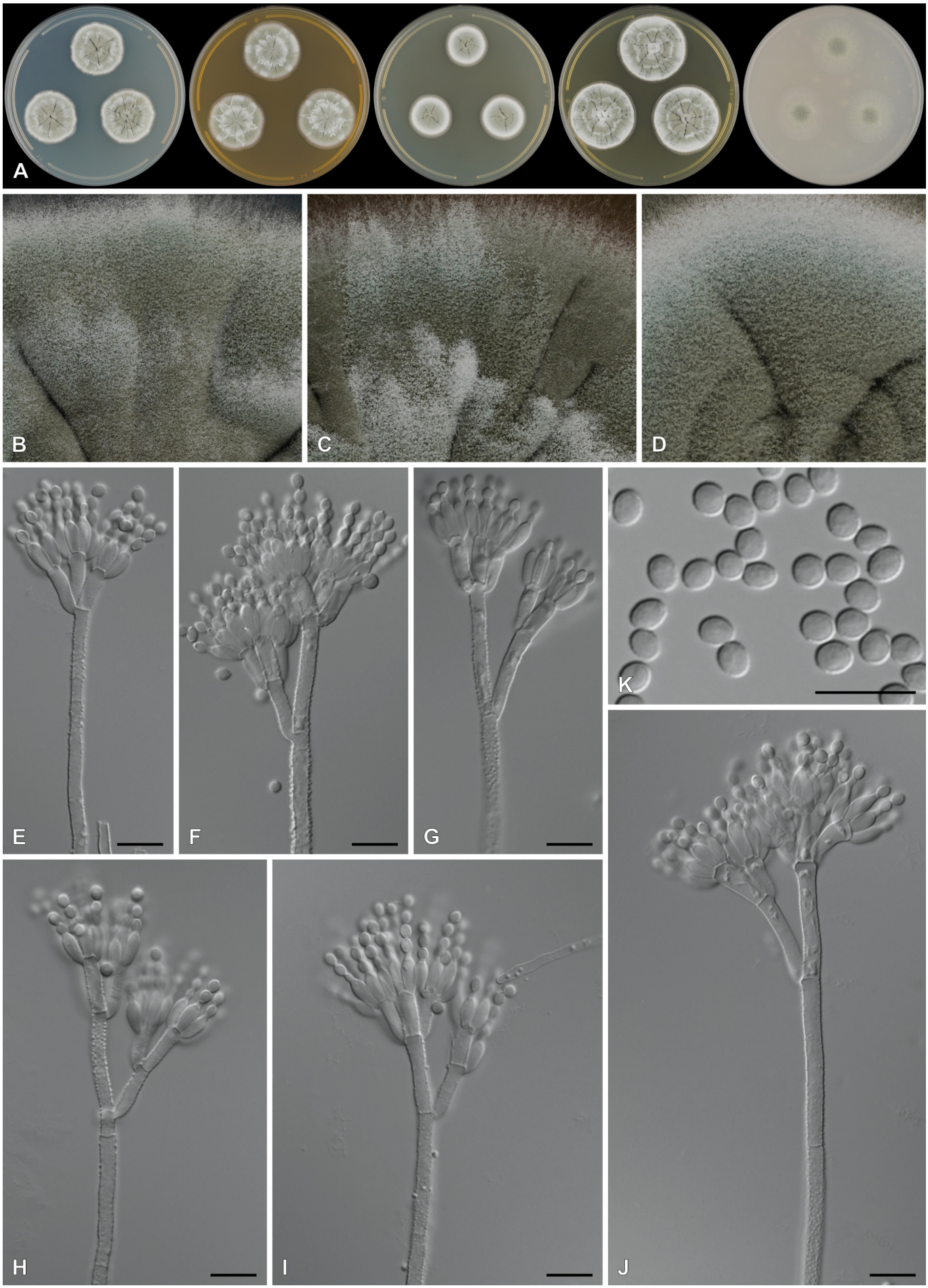

Fig. 19. *Penicillium rivulorum sp. nov*. (DAOMC 251681). **A.** Colonies on CYA, MEA, DG18, YES and OA. **B–D.** Colony texture on CYA (B), MEA (C) and DG18 (D). **E–J.** Conidiophores. **K.** Conidia. Scale bars = 10 µm.

Penicillium turcosum Visagie, Overy, Seifert & Frisvad, ***sp. nov.*** MB 855904. Fig. 20.

Etymology: Latin, *turcosum*, name in reference to the green to blue-green mineral turquoise associated with the states of Wyoming and Colorado from which the strains were isolated.

Subgeneric classification: *Penicillium* section *Ramosum* series *Lanosa.*

Colony diam. (7 d, at 25 ºC, in mm): CYA 24–25; CYA 10 °C 9–11; CYA 15 °C 16–17; CYA 20 °C 20–21; CYA 30 °C microcolonies; CYA 37 °C no growth; CYAS 25–26; MEA 20–23; MEA 20 °C 22–24, YES 28–30; DG18 17–18; OA 21–23; CREA 13–14.

Colony characters: CYA (25 °C, *7 d)*: Colonies low, raised centrally, radially lightly sulcate, sectoring; margins low, narrow, entire; mycelia white; texture velutinous; sporulation moderately dense, conidia *en masse* Greenish Grey (26C2), Greyish to Dull Green (26B4–E4); soluble pigments absent; exudates absent; reverse Yellowish White (2A2), Greenish Grey (1C3), Dull to Greyish Yellow (3B3–4B3). *CYA (20* °C, *7 d)*: Colonies resembling those incubated at 25 °C. *MEA (25* °C, *7 d)*: Colonies low, raised centrally, radially lightly sulcate, sectoring typical; margins low, narrow, entire; mycelia white; texture velutinous; sporulation moderately dense, conidia *en masse* Greenish Grey (26C2), Greyish to Dull Green (26B4–E4); soluble pigments absent; exudates absent; reverse Yellowish White (2A2), Greenish Grey (1C3), Dull to Greyish Yellow (3B3–4B3). *MEA (20* °C, *7 d)*: Colonies resembling those incubated at 25 °C. *DG18 (25* °C, *7 d)*: Colonies low, plane to sulcate; margins low, wide, entire; mycelia white; texture velutinous and floccose; sporulation moderately dense, conidia *en masse* Greenish to Dull Green (25C4–D4–5); soluble pigments absent; exudates absent; reverse Yellowish White (2A2), Greyish Green (1D3–4). *YES (25* °C, *7 d)*: Colonies low, raised centrally, radially lightly sulcate; margins low, narrow, entire; mycelia white; texture velutinous and floccose; sporulation moderately dense, conidia *en masse* Greyish to Dull Green (26C3–D3–5); soluble pigments absent; exudates absent; reverse Pale Yellow to Greyish Yellow (4A3–B3–6). *CREA (25* °C, *7 d)*: Colonies exhibiting weak growth; acid not produced.

Conidiophores terverticillate, a minor proportion biverticillate; *stipes* smooth to rough, 150–1500 × 2.5–4 µm; *branches* 2–3 per stipe, divergent, 11–30(–38) µm; *metulae* appressed, 3–6 per branch, 11–15 × 3–4 µm; *phialides* ampulliform, 4–8 per metula, 8–10 × 3–4 µm, average length metula/phialide 1.4; *conidia* smooth, globose, 2.5–3 × 2.5–3 µm ($\bar{x}$= 2.94 ± 0.15 × 2.77 ± 0.16), average width/length = 0.95, n = 50.

Extrolites: Asperfuran; asperphenamate and hydroxyl-aperphenamate; cycloaspeptides A–E, G & H; funiculosin and dehydro-funiculosin; griseofulvin and dechloro-griseofulvin; melearoride A; norlichexanthone; paraherquamide B; PF 1163B; psychrophilins A–D; rhinocladin A; statins (compactin, lovastatin and hydroxy-2-methylbutanoate lovastatin, pravastatin, ML236A, and 3,5-dihydro-3-oxo ML236C); and unguisin A & C.

Typus: **USA**, Wyoming, Fort Steele, North Platte River, alpine soil under *Populus augustifolia*, 10 May 1994, *J.C. Frisvad* (**holotype** DAOM 985254, dried specimen, ex-type culture DAOMC 256941 = IBT 24419 = IBT 16625 = CMW 57193 = CN093D9).

DNA barcodes: ITS = KY989142, *BenA* = KY989017, *CaM* = KY989082, *RPB2* = MZ984117.

Additional materials examined: **USA**, Colorado, Cache la Poudre River, alpine soil under old cottonwood, 13 Nov. 1994, *J.C. Frisvad*, culture DAOMC 256942 = IBT 17778 = CMW 57195 = CN093E3.

Notes: See notes under *P. algidum* above. *Penicillium turcosum* differs from other species of the *P. ribis* species complex by the production of paraherquamide B, rhinocladin A, fungal statins (including compactin, lovastatin & hydroxy-2-methylbutanoate lovastatin, pravastatin, ML236A, and 3,5-dihydro-3-oxo ML236C), and unguisin A & C, along with multiple unique mass features associated with unknown chemistry.

Penicillium wyomingense Visagie, Overy, Seifert & Frisvad, ***sp. nov.*** MB 855905. Fig. 21.

Etymology: Latin, *wyomingense*, named after the Wyoming big sagebrush, the shrub native to the western United States from where the species was isolated.

Subgeneric classification: *Penicillium* section *Ramosum* series *Lanosa.*

Colony diam. (7 d, at 25 ºC, in mm): CYA 21–22; CYA 10 °C 8–9; CYA 15 °C 15–16; CYA 20 °C 18–19; CYA 30 °C 5–8; CYA 37 °C no growth; CYAS 23–24; MEA 20–21; MEA 20 °C 19–21, YES 28–30; DG18 20–21; OA 23–25; CREA 12–14.

Colony characters: CYA (25 °C, *7 d)*: Colonies low, raised centrally, radially lightly sulcate, sectoring; margins low, narrow, entire; mycelia white; texture velutinous; sporulation moderately dense, conidia *en masse* Greenish Grey (26C2), Greyish to Dull Green (26B4–E4); soluble pigments absent; exudates absent; reverse Yellowish White (2A2), Greenish Grey (1C3), Dull to Greyish Yellow (3B3–4B3). *CYA (20* °C, *7 d)*: Colonies resembling those incubated at 25 °C. *MEA (25* °C, *7 d)*: Colonies low, raised centrally, radially lightly sulcate, sectoring typical; margins low, narrow, entire; mycelia white; texture velutinous; sporulation moderately dense, conidia *en masse* Greenish Grey (26C2), Greyish to Dull Green (26B4–E4); soluble pigments absent; exudates absent; reverse Yellowish White (2A2), Greenish Grey (1C3), Dull to Greyish Yellow (3B3–4B3). *MEA (20* °C, *7 d)*: Colonies resembling those incubated at 25 °C. *DG18 (25* °C, *7 d)*: Colonies low, plane to sulcate; margins low, wide, entire; mycelia white; texture velutinous and floccose; sporulation moderately dense, conidia *en masse* Greenish to Dull Green (25C4–D4–5); soluble pigments absent; exudates absent; reverse Yellowish White (2A2), Greyish Green (1D3–4). *YES (25* °C, *7 d)*: Colonies low, raised centrally, radially lightly sulcate; margins low, narrow, entire; mycelia white; texture velutinous and floccose; sporulation moderately dense, conidia *en masse* Greyish to Dull Green (26C3–D3–5); soluble pigments absent; exudates absent; reverse Pale Yellow to Greyish Yellow (4A3–B3–6). *CREA (25* °C, *7 d)*: Colonies exhibiting weak growth; acid not produced.

Conidiophores terverticillate, a minor proportion biverticillate; *stipes* rough, 150–1500 × 3.5–5 µm; *branches* 2–3 per stipe, divergent, 17–35(–50) µm; *metulae* appressed, 3–6 per branch, 10–16 × 3–4.5 µm; *phialides* ampulliform, 4–8 per metula, 8–14 × 2.5–3.5 µm, average length metula/phialide 1.09; *conidia* smooth, globose

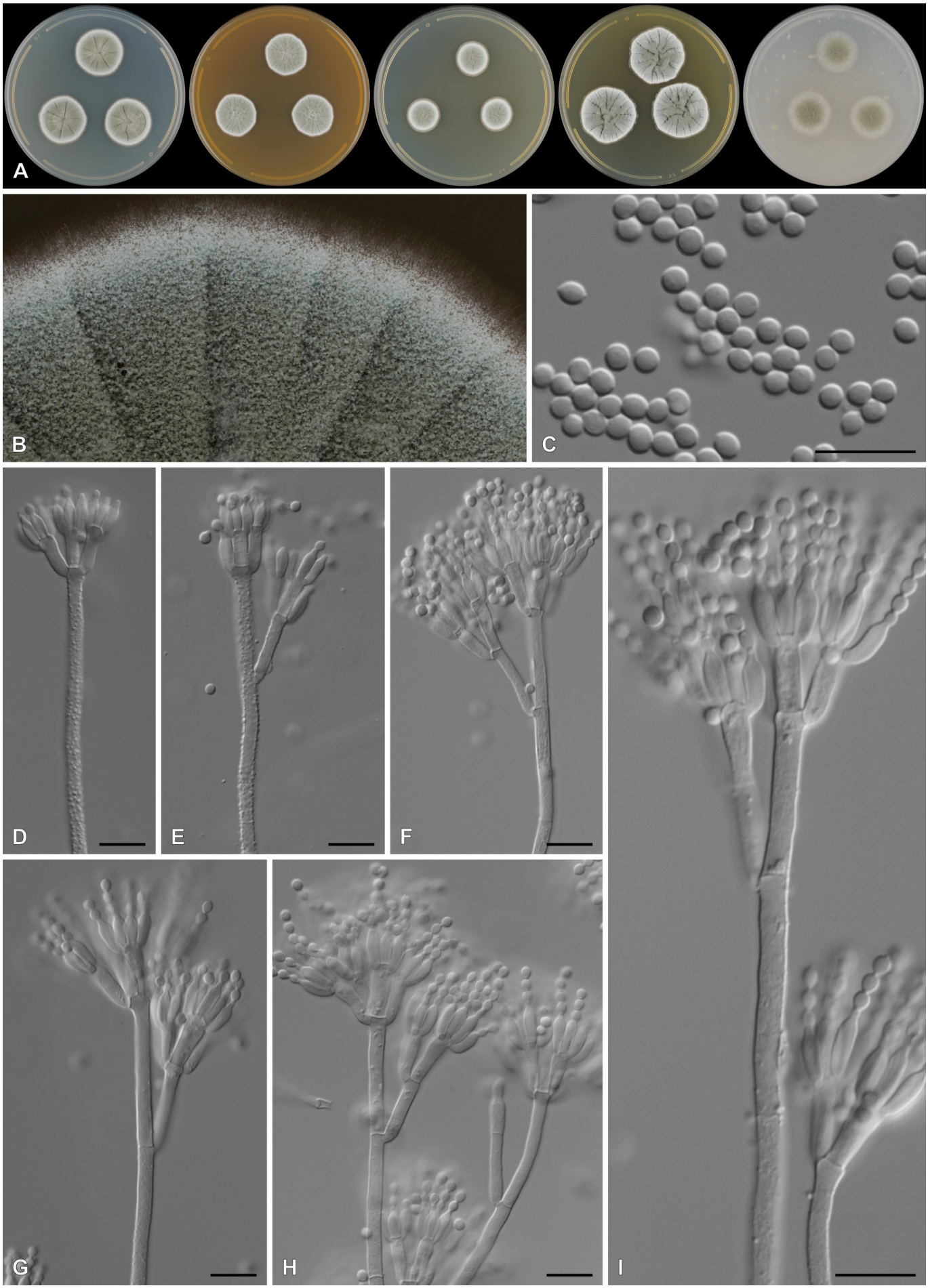

Fig. 20. *Penicillium turcosum sp. nov*. (DAOMC 256941). **A.** Colonies on CYA, MEA, DG18, YES and OA. **B.** Colony texture on MEA. **C.** Conidia. **D–I.** Conidiophores. Scale bars = 10 µm.

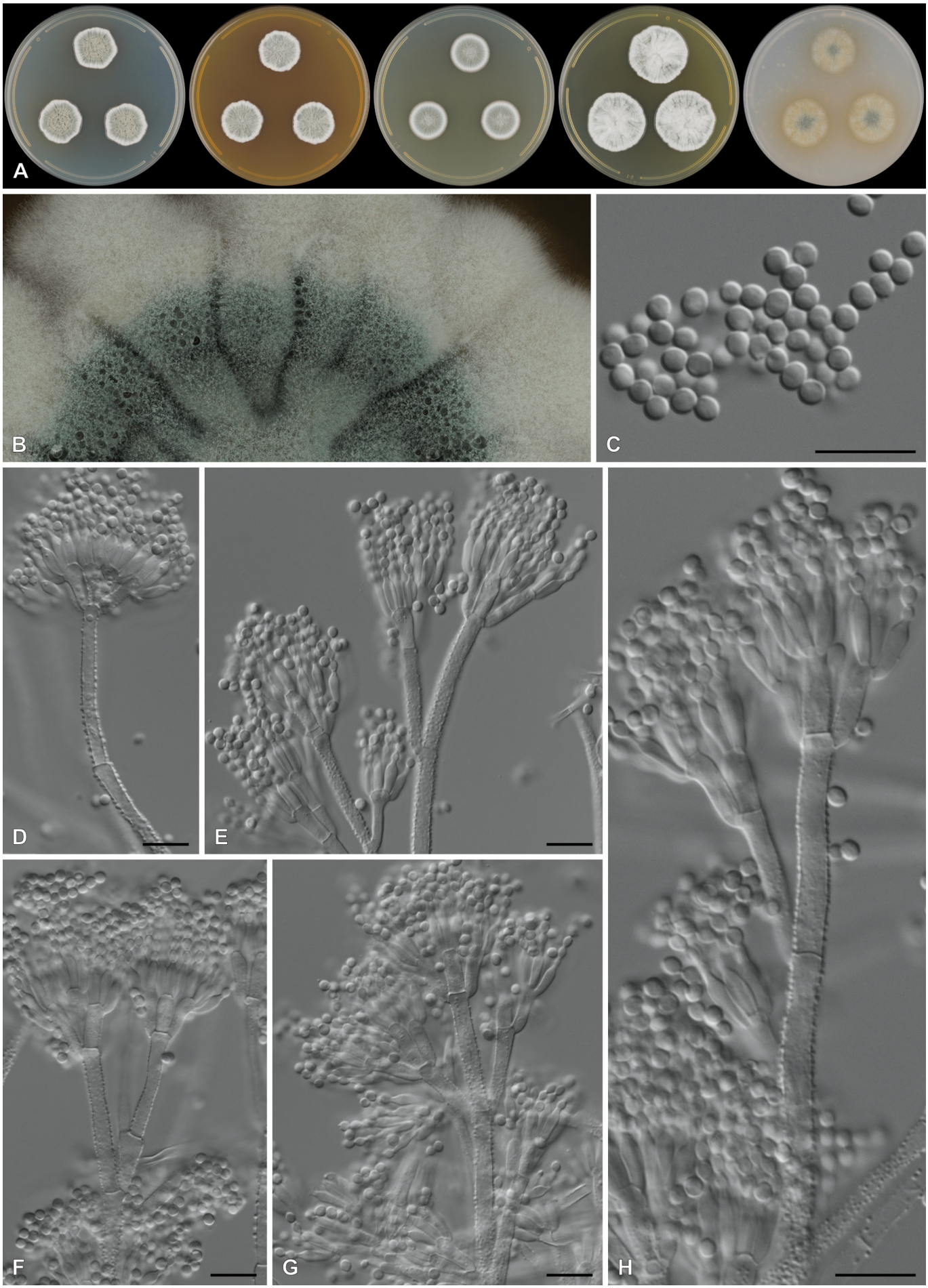

Fig. 21. *Penicillium wyomingense sp. nov*. (DAOMC 256940). **A.** Colonies on CYA, MEA, DG18, YES and OA. **B.** Colony texture on MEA. **C.** Conidia. **D–H.** Conidiophores. Scale bars = 10 µm.

to subglobose, 2.5–3 × 2.5–3 µm ($\bar{x}$= 2.93 ± 0.15 × 2.73 ± 0.13), average width/length = 0.94, n = 51.

Extrolites: Asperfuran; asperphenamate and hydroxyl-aperphenamate; and psychrophilin A.

Typus: **USA**, Wyoming, Rock Springs, alpine soil under *Artemisia tridentata* subspecies *wyomingensis* (Wyoming Big Sagebrush), 1978, *M. Christensen* (**holotype** DAOM 985255, dried specimen, ex-type culture DAOMC 256940 = IBT 24433 = IBT 14073 = CMW 57231).

DNA barcodes: ITS = KY989136, *BenA* = KY989011, *CaM* = KY989077, *RPB2* = PP993258.

Additional materials examined: **USA**, Wyoming, Snowy Mountain Range, Table Rock Rd, soil under *Artemisia tridentata* subspecies *wyomingensis* (Wyoming Big Sagebrush), 10 May 1994, *J.C. Frisvad*, culture DAOMC 256943 = IBT 17868 = CMW 57202 = CN093E4; ibid., culture DAOMC 256944 = IBT 18067 = CMW 57203 = CN093E5.

Notes: See notes under *P. algidum* above. *P. wyomingense* differs from other species of the *P. ribis* species complex by the production of several unknown metabolites as observed from the presence of unique mass features (unknown block 7; Fig. 4) derived from the untargeted metabolomics analysis. *Penicillium ribis* produces a substantially different extrolite profile as compared to *P. wyomingense* characterized by the production of trypostatin B, andrastin E, atlantinones A & B, cycloaspeptides, psychrophilins, mangrovamide G, and norlichexanthone.

DISCUSSION

A polyphasic approach to taxonomy is essential in speciose genera like *Penicillium*, where characterization of secondary metabolite production provides diagnostic characters useful to support the description of new species. However, use of secondary metabolites as phenotypic characters is somewhat constrained as, in a historical context, much of the fungal secondary metabolite chemical diversity has yet to be characterised. The application of metabolome phenotyping tools, such as untargeted metabolomics, allows for the comparison of inter- and infra-species chemical diversity that takes into consideration not only structurally characterised molecules, but also molecules of unknown chemistry, to generate a more holistic comparison.

Although a putative chemical phenotype can be assembled from observed mass features, the complete correlation of all detected mass features with known chemistry remains elusive. In the current study, diagnostic mass features (MS^2 fragmentation patterns) were compared to online spectral databases (for matching with experimentally derived and *in silico* predicted metabolite standards), allowing for the annotation of 86 metabolites. All the metabolites reported from the new species in this survey were previously found to be produced by other *Penicillium* species; however, the combination of secondary metabolites produced are unique for each of the new species described. Molecular networking analysis of MS^2 spectra was also successfully applied to detect deviations in structural moieties from known secondary metabolite products (e.g. cycloaspeptides and fungal 'statins'), providing insight into an increased diversity of new metabolite analogues or the production of distinct molecules sharing comparable structural motifs. Further experimental work is required to complete the annotation of many of the unknown mass features in this study – work that requires purification of sufficient quantities for structure elucidation efforts for characterization by, for example, NMR. However, as the candidate unknown mass features were not annotated using extensive molecular prediction tools, it is likely that the unknown mass features represent novel chemistry awaiting complete structural elucidation.

Secondary metabolite (extrolite) diversity in *Penicillium* is associated with diverse biological activities

Many of the secondary metabolites produced by the new *Penicillium* species described here have reported biological activity. Several have known cytotoxic effects against mammalian cells lines (or living animals) and therefore are considered mycotoxins, such as the roquefortines, the penitrems, viomellein and xanthomegnin (Robbers *et al.* 1978, Coton *et al.* 2020). Other metabolites have been evaluated as antiproliferative candidates in the screening for cancer therapeutics, such as asperphenamate, pseurotin A, the tryprostatins, the chaetoglobosins, the communesins, and the psychrophilins (Cui *et al.* 1995, Dalsgaard *et al.* 2005, Liu *et al.* 2016, Pompeo *et al.* 2019). Other metabolites, including chrysogenamide A produced by *P. discoense*, exhibit promising neuroprotective effects against oxidative stress-induced neurocyte death (Lin *et al.* 2008). The quinolactacins produced by *P. algidum* are potent acetylcholinesterase inhibitors that suppress inflammatory immune system responses involved in conditions such as Crohn's disease and ulcerative colitis (Kakinuma *et al.* 2000).

Many of the observed metabolites have associated antimicrobial activities, such as asperfuran, the chaetoglobosins, funiculosin, synerazol, the melearorides and PF1163 analogues, and griseofulvin and associated analogues (Nelson *et al.* 1977, Pfefferle *et al.* 1990, Ando *et al.* 1991, Huang *et al.* 2016, Okabe *et al.* 2016). Of the antimicrobial secondary metabolites observed in this survey, griseofulvin (produced by *P. discoense*, *P. algidum*, *P. turcosum*, and *P. rivulorum*) is the only example of a commercial antifungal drug in widespread clinical use to treat superficial, dermatophytic fungal infections in both animals and humans. Although the exact mode of action for griseofulvin remains inconclusive, research indicates that it interferes with cellular mitosis by interacting with the microtubule mitotic machinery in fungi (Petersen *et al.* 2014).

Cholesterol lowering therapeutics

Several of the secondary metabolites observed are lead candidate molecules or were developed as drugs for the treatment of hypercholesterolemia. Pyripyropene A (produced by *P. aquamarinum*) is a selectively potent, orally active sterol O-acyltransferase 2 / acyl-coenzyme A:cholesterol acyltransferase 2 inhibitor. It was developed as an antiatherogenic lead compound and attenuates hypercholesterolemia and atherosclerosis in vivo (Ohshiro *et al.* 2011). The fungal 'statins' represent another class of secondary metabolites produced by several of our *Penicillium* species and now currently used as drugs for the management of hypercholesterolemia.

Fungal 'statins' (and 'statin'-inspired molecules) reduce the amount of low-density lipoprotein cholesterol in the blood by competitively inhibiting 3-hydroxy-3-methylglutaryl coenzyme A reductase, which catalyses a rate limiting step in the hepatic biosynthesis of cholesterol (Campbell & Vederas 2010, Azemawah *et al.* 2019). First generation fungal 'statins' were discovered in the 1970's and early 1980's from several different fungi, including

Aspergillus terreus, *Monascus ruber*, *P. solitum* (misidentified as *P. brevicompactum* and *P. citrinum*) (Alberts *et al.* 1980, Brown *et al.* 1976, Endo *et al.* 1976, Endo 1979, Frisvad & Filtenborg 1989), although multiple different names often were assigned to the same molecules (i.e. lovastatin is also known as mevinolin and monacolin K; and compactin is also known as mevastatin and ML-236B). Metabolomic phenotyping in this study revealed numerous 'statin' molecules produced by *P. aquamarinum*, *P. oreophilum*, and *P. turcosum* – where observed molecules represented not only biosynthetic end products, but also various biosynthesis associated intermediates and potential shunt products. MS/MS ion network analysis also revealed multiple mass features representing additional undescribed 'statin'-associated analogues, some of which are likely stereoisomers.

The biosynthesis of fungal 'statins' was characterised from different producing organisms – lovastatin biosynthesis in *Aspergillus terreus* (Kennedy *et al.* 1999) and compactin biosynthesis in *P. solitum* (misidentified as *P. citrinum*) (Abe *et al.* 2002) – where associated biosynthetic gene clusters contain homologs of five different genes that encode for specific enzymes that are essential for biosynthesis. Enzymatic biosynthesis occurs in two steps, first a highly reducing iterative type I PKS produces the decalin containing nonaketide structural backbone of the molecule. Because the PKS lacks an enoyl reductase domain, enoyl reduction occurs by a separate enoyl reductase and additional hydroxylation/oxidation occurs by a cytochrome P450 monooxygenase at subsequent biosynthetic steps to generate various intermediate products (i.e. ML236A). The diketide side chain is biosynthesized by a second PKS that is condensed onto the decalin ring by an esterase to form the final product (Abe *et al.* 2002, Campbell & Vederas 2010). Interestingly, although the enzymes for both lovastatin and compactin biosynthetic gene clusters are analogous, the methyl transferase domain in the highly reducing iterative type I PKS (MlcA in *P. citrinum*) is thought to be inactive and therefore results in the absence of the C-6 methyl in compactin as compared to lovastatin (Abe *et al.* 2002). Historical reports of fungal 'statin' production favour the specific production of either lovastatin or compactin as final end products of biosynthesis. Researchers have hypothesised that predicted differences in the conserved methyl transferase domain between LovB in *A. terreus* and MlcA in *P. citrinum* might account for the lack of methyltransferase activity of MlcA (Abe *et al.* 2002); however, this hypothesis has never been proven. All three of the fungal 'statin' producing Penicillia in our study (*P. aquamarinum*, *P. oreophilum*, and *P. turcosum*) produce both compactin and lovastatin (and their associated intermediates), indicating that there is some level of fluidity occurring during biosynthesis, resulting in a diversity of products.

Insecticides and anthelmintics

Eight of the eleven psychrotolerant species (ten new species and *P. ribis*) that we studied produced secondary metabolites with associated insecticidal/anthelmintic activity. Insecticidal effects of the communesins (produced by *P. rivulorum*) were observed in oral feeding experiments with silkworm instar larvae (Hayashi *et al.* 2014). Chaetoglobosin A, produced by *P. aquamarinum* and *P. jugorum*, is reported from various fungal genera and linked with nematicidal effects and reduces fecundity of various agricultural cyst nematode pathogens, prompting suggestion for potential use for biocontrol applications in integrated management of cyst nematodes (Hu *et al.* 2012, Ashrafi *et al.* 2017).

Penitrems, produced by *P. algidum*, are also associated with insecticidal activity and reduced fecundity against a broad range of agricultural insect pests from the orders *Lepidoptera*, *Diptera* and *Hemiptera*, for which their use as an insecticide was patented (González *et al.* 2003, Hou *et al.* 2022). Penitrems affect the nervous systems of vertebrates through the blockage of ion channels, resulting in tremors and convulsions (Hou *et al.* 2022). Convulsions and mortality also occur in exposed invertebrate pests, probably associated with similar disruption of ion channel function.

Penigequinolone A and yaequinolones B, F, and J1, produced by *P. oreophilum*, are associated with mortality of arthropods and nematodes (Uchida *et al.* 2005, Uchida *et al.* 2006, Kusano *et al.* 2014); the insecticidal/anthelmintic activity of quinolone alkaloids is attributed to their unique chemical structure, due to the presence of appended oxidized prenyl groups to the quinolone chemical scaffold (Zou *et al.* 2015). The quinazolinobenzodiazepine alkaloids, sclerotigenin and circumdatin F, produced by *P. marthae*, have insecticidal effects against *Helicoverpa zea*, the maize earworm pest (Joshi *et al.* 1999), probably a consequence of inhibition of the mitochondrial respiratory chain (López-Gresa *et al.* 2005) by interference with proton-translocating NADH:ubiquinone oxidoreductase activity (Lümmen 1998).

The structurally related marcfortines and paraherquamides, prenylated heptacyclic spiro-oxindole cyclodipeptides produced by *P. aquamarinum* and *P. turcosum* respectively, were patented as anthelmintics; paraherquamides were also developed as a veterinary therapeutic (López-Gresa *et al.* 2006). The broad-spectrum anthelmintic activity of the paraherquamides occurs through disruption of L-type nicotinic acetylcholine receptors, leading to nematode paralysis by blockage of cholinergic neuromuscular transmission (Koizumi *et al.* 2023). Pyripyropenes produced by *P. aquamarinum* are also reported as insecticidal against sucking insect pests like aphids and whiteflies (*Hemiptera)*, with a mode of action that prompted some to suggest they might represent a novel class of insecticide (Goto *et al.* 2019).

First described as having moderate antiplasmodial activity against the malarial parasite, *Plasmodium falciparum* (Dalsgaard *et al.* 2005), the cycloaspeptides, in particular cycloaspeptide E, have attracted attention for their insecticidal activity against Lepidopteran crop pests. Production of cycloaspeptides is prevalent in *Penicillium* section *Ramosum*, and we detected them in *P. algidum*, *P. jugorum*, *P. oreophilum*, *P. ribis* and *P. turcosum.* They were previously reported from other section *Ramosum* species *P. jamesonlandse* and *P. soppii* (Frisvad *et al.* 2006). Cycloaspeptides have also been reported from other genera such as *Trichothecium* and insect pathogens in *Isaria* (Lewer *et al.* 2006, Zhang *et al.* 2009). Cycloaspetides biosynthesis involves a 5-module NRPS that incorporates different amino acids (including *N*-methylated amino acids) into a cyclic pentapeptide molecule; however, the cycloaspeptide NRPS lacks integral *N*-methyltransferase domains. Instead, amino acid *N*-methylation occurs via a separate trans-acting *N*-methyltransferase, prior to incorporation into the elongating pentapeptide during biosynthesis (de Mattos-Shipley *et al.* 2018). Both the 3rd and 5th module adenylation domains of the cycloaspeptide NRPS have a strong preference for *N*-methylated amino acids, although those residues also will accept and incorporate non-methylated amino acids during cyloaspeptide biosynthesis (de Mattos-Shipley *et al.* 2018). The first NRPS module incorporates anthranilic acid, the second, alanine (or serine), the third phenylalanine (or tyrosine), the fourth leucine (or valine) and the fifth either a tyrosine or phenylalanine. The unique biosynthesis of the cycloaspeptides – in terms of

external amino acid *N*-methylation and promiscuity of the NRPS adenylation domains regarding amino acid incorporation – produces a variety of cycloaspeptides analogues. We observed at least five new cycloaspeptide analogues using ion molecular networks in *P. algidum*, *P. jugorum*, *P. oreophilum*, *P. ribis* and *P. turcosum*, and presumably more analogues await discovery. The presence of a phenylalanine instead of tyrosine in position 5 of the cycloaspeptide molecule (as is observed in cycloaspeptide E), appears to be necessary for insecticidal properties (Lewer *et al.* 2006).

Integrating metabolomics and genomics tools to advance polyphasic taxonomy

Combining untargeted metabolomics with genome mining is a powerful approach to assess the secondary metabolite potential of inter- and infra-species populations (Witte *et al.* 2021). Untargeted metabolomic analysis can be considered a 'bottom up' approach, where, as was demonstrated in this study, consensus metabolomic phenotypes are constructed taking into account both known and unknown secondary metabolites. However, there are limitations to such an approach, because secondary metabolite production is often modulated by global transcriptional regulators, hence biosynthetic gene cluster transcription (and ultimately secondary metabolite production) is medium/growth condition dependent. Therefore, it is imperative to use diverse growth conditions to stimulate the maximal secondary metabolite potential of a given strain or species.

Genome sequencing and genome mining tools represent a powerful 'top down' approach to characterise the secondary metabolite potential of a given strain or species. A 'top down' approach provides information on all or nearly all secondary metabolite biosynthetic gene clusters in a genome, even if their transcription remains 'silent' under laboratory conditions. Moreover, if the makeup of biosynthetic gene clusters can be compared between species where homologous synthase genes are found, observed differences in the content of genes associated with 'tailoring enzymes' (such as hydroxylases, methyltransferases, dehydrogenases, prenyltransferases, etc.) in the biosynthetic gene clusters, can be predicted to give rise to structurally similar, yet different secondary metabolites.

Comparative genome analysis might also reveal events of pseudogenization of some secondary metabolite synthase genes, which would render the pathway inoperable. However, this would provide evidence that the species at one time had the ability to produce a particular secondary metabolite, even though production is no longer detectable. Although secondary metabolite biosynthetic gene clusters can be predicted from a genomic sequence, and compared among strains and species, linking them to specific secondary metabolites is often not possible, because few secondary metabolite products are currently linked with their respective biosynthetic gene clusters and for many biosynthetic gene clusters an associated secondary metabolite product is not known.

An additional advantage to inclusion of a 'top down' approach to characterising species diversity is that genomic analysis provides an opportunity to identify relevant phylogenetically useful markers [such as universal single copy ortholog genes (Manni *et al.* 2021)], rather than the somewhat arbitrarily selected single or multiple genes currently being applied in taxonomic descriptions and biosystematics studies. Inclusion of a greater diversity of genes in phylogenetic analyses will provide greater taxonomic resolution, especially for genera where typical barcoding genes are less effective. With the costs of genome sequencing becoming more and more affordable, the future of fungal taxonomy is phylogenomics, where hundreds of genes from whole genomes will be compared and used to define new species and their potential to produce secondary metabolites.

Psychrotrophic penicillia represent an underexplored source of fungal and chemical diversity

Many of the newly described psychrotrophic species of *Penicillium* are classified in subgenus section *Ramosa*. All of the species we described in this section (*P. algidum*, *P. discoense*, *P. jugorum*, *P. oreophilum*, *P. rivulorum*, *P. turcosum*, and *P. wyomingense*) share commonalities in secondary metabolites. All strains produced asperphenamates, most produced griseofulvin (and associated intermediate metabolites) and cycloaspeptides, and many produced asperfuran and psychrophilins. Phylogenetically, based on several barcoding genes, *P. algidum*, *P. rivulorum*, *P. turcosum* and *P. wyomingense* form a clade with *P. ribis*, and represent a "species complex" in section *Ramosum* series *Lanosa*. Although similarities in secondary metabolite production were observed (with *P. algidum* and *P. turcosum* being the most similar), each of the proposed new species produces unique secondary metabolite consensus phenotypes that differ from *P. ribis*. Further work towards resolving and expanding the *P. ribis* species complex will require focused isolations from psychrotrophic habitats, followed by genome comparisons to help elucidate evolutionary relationships in and between these species. This will also help to explain why variation in ITS, *BenA* and *CaM* is low in the complex, but *RPB2* follow groupings observed in the chemistry of these species.

As global warming advances, frozen or ice-covered regions of both arctic and high alpine environments are progressively more exposed. These areas represent a potential resource of unexplored fungal and chemical diversity. The potential chemical diversity of psychrotolerant fungi is quite high, as is shown in this study. Not only did the ten new species produce a wide spectrum of biologically active chemical compounds, they also produced numerous metabolites that were unknown, representing potential new secondary metabolites. With warming soil temperatures and increased water content of soil from melt waters, psychrotolerant species will need to proliferate and compete for resources, not only with other fungi but also prokaryotes and arthropod predators prevalent in cold environments during warmer months. Focusing upon the isolation and screening of psychrotolerant fungi will increase understanding of fungal biodiversity and unveil new secondary metabolite diversity. As the results from this study reveal, psychrotrophic Penicillia are an excellent source of structurally diverse molecules – especially associated with insecticidal and anthelminthic activities.

ACKNOWLEDGEMENTS

Funding for this research was provided by the Science & Technology Branch of Agriculture & Agri-Food Canada [Project J-002272 "Fungal and Bacterial Biosystematics – bridging taxonomy and "omics" technology in agricultural research and regulation"] to DPO; the Alfred P. Sloan Foundation Program on the Microbiology of the Built Environment and the European Union's Horizon 2020 research and innovation program (RISE) [under the Marie Skłodowska-Curie grant agreement No. 101008129, project acronym "Mycobiomics"] to CMV; and the Danish Research Council to JCF.

DATA AVAILABILITY

The sequences generated in this study are deposited with NCBI GenBank (See Table 1). The aligned DNA sequence datasets, partitioning schemes and tree files were uploaded to the University of Pretoria's research data repository hosted on Figshare https://doi.org/10.25403/UPresearchdata.27117037.

DECLARATION ON CONFLICT OF INTEREST

The authors declare that there is no conflict of interest.

REFERENCES

Abadi S, Azouri D, Pupko T, *et al.* (2019). Model selection may not be a mandatory step for phylogeny reconstruction. *Nature Communications* **10**: 934. https://doi.org/10.1038/s41467-019-08822-w

Abe Y, Suzuki T, Ono C, *et al.* (2002). Molecular cloning and characterization of an ML-236B (compactin) biosynthetic gene cluster in *Penicillium citrinum*. *Molecular Genetics and Genomics* **267**: 636–646. https://doi.org/10.1007/s00438-002-0697-y

Alberts AW, Chen J, Kuron G*, et al.* (1980). Mevinolin: a highly potent competitive inhibitor of hydroxymethylglutaryl-coenzyme A reductase and a cholesterol-lowering agent. *Proceedings of the National Academy of Sciences (USA)* **77**: 3957–3961. https://doi.org/10.1073/pnas.77.7.3957

Ando O, Satake H, Nakajima M, *et al.* (1991). Synerazol, a new antifungal antibiotic. *The Journal of Antibiotics* **44**: 382–389. https://doi.org/10.7164/antibiotics.44.382

Arenz BE, Held BW, Jurgens JA, *et al.* (2006). Fungal diversity in soils and historic wood from the Ross Sea Region of Antarctica. *Soil Biology and Biochemistry* **38**: 3057–3064. https://doi.org/10.1016/j.soilbio.2006.01.016

Ashrafi S, Helaly S, Schroers H-J, *et al.* (2017). *Ijuhya vitellina sp. nov.*, a novel source for chaetoglobosin A, is a destructive parasite of the cereal cyst nematode *Heterodera filipjevi*. *PLoS ONE* **12**: e0180032. https://doi.org/10.1371/journal.pone.0180032

Azemawah V, Movahed MR, Centuori P, *et al.* (2019). State of the art comprehensive review of individual statins, their differences, pharmacology, and clinical implications. *Cardiovascular Drugs and Therapy* **33**: 625–639. https://doi.org/10.1007/s10557-019-06904-x

Azmi O, Spepelt R (1997). Fungi of the Windmill Islands, continental Antarctica. Effect of temperature, pH and culture media on the growth of selected microfungi. *Polar Biology* **18**: 128–134. https://doi.org/10.1007/s003000050167

Brown AG, Smale TC, King TJ, *et al.* (1976). Crystal and molecular structure of compactin, a new antifungal metabolite from *Penicillium brevicompactum*. *Journal of the Chemical Society, Perkin Transactions* **1**: 1165–1170. https://doi.org/10.1039/p19760001165

Campbell CD, Vederas JC (2010). Biosynthesis of lovastatin and related metabolites formed by fungal iterative PKS enzymes. *Biopolymers* **93**: 755–763. https://doi.org/10.1002/bip.21428

Cantrell SA, Dianese JC, Fell J, *et al.* (2017). Unusual fungal niches. *Mycologia* **103**: 1161–1174. https://doi.org/10.3852/11-108

Coton E, Coton M, Hymery N, *et al.* (2020). *Penicillium roqueforti*: an overview of its genetics, physiology, metabolism and biotechnological applications. *Fungal Biology Reviews* **34**: 59–73. https://doi.org/10.1016/j.fbr.2020.03.001

Crous PW, Carnegie AJ, Wingfield MJ*, et al.* (2019). Fungal Planet description sheets: 868–950. *Persoonia* **42**: 291–473. https://doi.org/10.3767/persoonia.2019.42.11

Crous PW, Osieck ER, Jurjević Ž, *et al.* (2021). Fungal Planet description sheets: 1284–1382. *Persoonia* **47**: 178–374. https://doi.org/10.3767/persoonia.2021.47.06

Cui C-B, Kakeya H, Okada GEN, *et al.* (1995). Tryprostatins A and B, novel mammalian cell cycle inhibitors produced by *Aspergdlus fumigatus*. *The Journal of Antibiotics* **48**: 1382–1384. https://doi.org/10.7164/antibiotics.48.1382

Dalsgaard PW, Larsen TO, Christophersen C (2005). Bioactive cyclic peptides from the psychrotolerant fungus *Penicillium algidum*. *The Journal of Antibiotics* **58**: 141–144. https://doi.org/10.1038/ja.2005.16

Dalsgaard PW, Larsen TO, Frydenvang K, *et al.* (2004). Psychrophilin A and Cycloaspeptide D, novel cyclic peptides from the psychrotolerant fungus *Penicillium ribeum*. *Journal of Natural Products* **67**: 878–881. https://doi.org/10.1021/np0303714

de Hoog GS, Gerrits van den Ende AH (1998). Molecular diagnostics of clinical strains of filamentous *Basidiomycetes*. *Mycoses* **41**: 183–189. https://doi.org/10.1111/j.1439-0507.1998.tb00321.x

de Mattos-Shipley Kate MJ, Greco C, Heard DM*, et al.* (2018). The cycloaspeptides: uncovering a new model for methylated nonribosomal peptide biosynthesis. *Chemical Science* **9**: 4109–4117. https://doi.org/10.1039/c8sc00717a

Donhauser J, Frey B (2018). Alpine soil microbial ecology in a changing world. *FEMS Microbiology Ecology* **94**: fiy099. https://doi.org/10.1093/femsec/fiy099

dos Santos GS, Teixeira TR, Colepicolo P, *et al.* (2021). Natural products from the poles: structural diversity and biological activities. *Revista Brasileira de Farmacognosia* **31**: 531–560. https://doi.org/10.1007/s43450-021-00203-z

Ellis-Evans JC (1996). Microbial diversity and function in Antarctic freshwater ecosystems. *Biodiversity and Conservation* **5**: 1395–1431. https://doi.org/10.1007/bf00051985

Endo A (1979). Monacolin K, a new hypocholesterolemic agent produced by a *Monascus species*. *The Journal of Antibiotics* **32**: 852–854. https://doi.org/10.7164/antibiotics.32.852

Endo A, Kuroda M, Tsujita Y (1976). ML-236A, ML-236B, and ML-236C, new inhibitors of cholesterogensis produced by *Penicillium citrinum*. *The Journal of Antibiotics* **29**: 1346–1348. https://doi.org/10.7164/antibiotics.29.1346

Frisvad JC, Filtenborg O (1989). Terverticillate Penicillia: Chemotaxonomy and mycotoxin production. *Mycologia* **81**: 837–861. https://doi.org/10.1080/00275514.1989.12025674

Frisvad JC, Larsen TO, Dalsgaard PW, *et al.* (2006). Four psychrotolerant species with high chemical diversity consistently producing cycloaspeptide A, *Penicillium jamesonlandense sp. nov.*, *Penicillium ribium sp. nov.*, *Penicillium soppii* and *Penicillium lanosum*. *International Journal of Systematic and Evolutionary Microbiology* **56**: 1427–1437. https://doi.org/10.1099/ijs.0.64160-0

Frisvad JC, Samson RA (2004). Polyphasic taxonomy of *Penicillium* subgenus *Penicillium*. A guide to identification of food and air-borne terverticillate Penicillia and their mycotoxins. *Studies in Mycology* **49**: 1–174.

Glass NL, Donaldson GC (1995). Development of premier sets designed for use with the PCR to amplify conserved genes from filamentous *Ascomycetes*. *Applied and Environmental Microbiology* **61**: 1323–1330. https://doi.org/10.1128/aem.61.4.1323-1330.1995

Gonçalves MFM, Santos L, Silva BMV, *et al.* (2019). Biodiversity of *Penicillium* species from marine environments in Portugal and description of *Penicillium lusitanum sp. nov.*, a novel species isolated from sea water. *International Journal of Systematic and Evolutionary Microbiology* **69**: 3014–3021. https://doi.org/10.1099/ijsem.0.003535

González MC, Lull C, Moya P, *et al.* (2003). Insecticidal activity of penitrems, including penitrem G, a new member of the family isolated

from *Penicillium crustosum*. *Journal of Agricultural and Food Chemistry* **51**: 2156–2160. https://doi.org/10.1021/jf020983e

Goto K, Horikoshi R, Nakamura S, *et al.* (2019). Synthesis of pyripyropene derivatives and their pest-control efficacy. *Journal of Pesticide Science* **44**: 255–263. https://doi.org/10.1584/jpestics.D19-032

Gu Z, Eils R, Schlesner M (2016). Complex heatmaps reveal patterns and correlations in multidimensional genomic data. *Bioinformatics* **32**: 2847–2849. https://doi.org/10.1093/bioinformatics/btw313

Hassan N, Rafiq M, Hayat M, *et al.* (2016). Psychrophilic and psychrotrophic fungi: a comprehensive review. *Reviews in Environmental Science and Bio/Technology* **15**: 147–172. https://doi.org/10.1007/s11157-016-9395-9

Hayashi H, Matsumoto H, Akiyama K (2014). New insecticidal compounds, communesins C, D and E, from *Penicillium expansum* Link MK-57. *Bioscience, Biotechnology, and Biochemistry* **68**: 753–756. https://doi.org/10.1271/bbb.68.753

Hong SB, Go SJ, Shin HD, *et al.* (2005). Polyphasic taxonomy of *Aspergillus fumigatus* and related species. *Mycologia* **97**: 1316–1329. https://doi.org/10.3852/mycologia.97.6.1316

Hou Y, Chen M, Sun Z, *et al.* (2022). The biosynthesis related enzyme, structure diversity and bioactivity abundance of indole-diterpenes: A review. *Molecules* **27**: 6870. https://doi.org/10.3390/molecules27206870

Houbraken J, Kocsube S, Visagie CM, *et al.* (2020). Classification of *Aspergillus*, *Penicillium*, *Talaromyces* and related genera (*Eurotiales*): an overview of families, genera, subgenera, sections, series and species. *Studies in Mycology* **95**: 5–169. https://doi.org/10.1016/j.simyco.2020.05.002

Houbraken J, Wang L, Lee HB, *et al.* (2016). New sections in *Penicillium* containing novel species producing patulin, pyripyropens or other bioactive compounds. *Persoonia* **36**: 299–314. https://doi.org/10.3767/003158516x692040

Hu Y, Zhang W, Zhang P, *et al.* (2012). Nematicidal activity of chaetoglobosin A produced by *Chaetomium globosum* NK102 against *Meloidogyne incognita*. *Journal of Agricultural and Food Chemistry* **61**: 41–46. https://doi.org/10.1021/jf304314g

Huang S, Chen H, Li W, *et al.* (2016). Bioactive chaetoglobosins from the mangrove endophytic fungus *Penicillium chrysogenum*. *Marine Drugs* **14**: 172. https://doi.org/10.3390/md14100172

Joshi BK, Gloer JB, Wicklow DT, *et al.* (1999). Sclerotigenin: a new antiinsectan benzodiazepine from the sclerotia of *Penicillium sclerotigenum*. *Journal of Natural Products* **62**: 650–652. https://doi.org/10.1021/np980511n

Kakinuma N, Iwai H, Takahashi S, *et al.* (2000). Quinolactacins A, B and C: Novel quinolone compounds from *Penicillium* sp. EPF-6. I. Taxonomy, production, isolation and biological properties. *The Journal of Antibiotics* **53**: 1247–1251. https://doi.org/10.7164/antibiotics.53.1247

Katoh K, Standley DM (2013). MAFFT multiple sequence alignment software version 7: improvements in performance and usability. *Molecular Biology and Evolution* **30**: 772–780. https://doi.org/10.1093/molbev/mst010

Kennedy J, Auclair K, Kendrew SG, *et al.* (1999). Modulation of polyketide synthase activity by accessory proteins during lovastatin biosynthesis. *Science* **284**: 1368–1372. https://doi.org/10.1126/science.284.5418.1368

Koizumi W, Otsubo S, Furutani S, *et al.* (2023). Determinants of subtype-selectivity of the anthelmintic paraherquamide A on *Caenorhabditis elegans* nicotinic acetylcholine receptors. *Molecular Pharmacology* **103**: 299–310. https://doi.org/10.1124/molpharm.122.000601

Kornerup A, Wanscher JH (1967). *Methuen Handbook of Colour*. 2nd edn. Methuen & Co Ltd, London, England.

Kusano M, Koshino H, Uzawa J, *et al.* (2014). Nematicidal alkaloids and related compounds produced by the fungus *Penicillium* cf. *simplicissimum*. *Bioscience, Biotechnology, and Biochemistry* **64**: 2559–2568. https://doi.org/10.1271/bbb.64.2559

Lewer P, Graupner PR, Hahn DR, *et al.* (2006). Discovery, synthesis, and insecticidal activity of cycloaspeptide E. *Journal of Natural Products* **69**: 1506–1510. https://doi.org/10.1021/np060219c

Lin Z, Wen J, Zhu T, *et al.* (2008). Chrysogenamide A from an endophytic fungus associated with *Cistanche deserticola* and its neuroprotective effect on SH-SY5Y cells. *The Journal of Antibiotics* **61**: 81–85. https://doi.org/10.1038/ja.2008.114

Litova K, Gerginova M, Peneva N, *et al.* (2014). Growth of Antarctic fungal strains on phenol at low temperatures. *Journal of Bioscience and Biotechnology* **SE/ONLINE**: 43–46.

Liu Q, Li W, Sheng L, *et al.* (2016). Design, synthesis and biological evaluation of novel asperphenamate derivatives. *European Journal of Medicinal Chemistry* **110**: 76–86. https://doi.org/10.1016/j.ejmech.2016.01.020

López-Gresa MP, González MC, Ciavatta L, *et al.* (2006). Insecticidal activity of paraherquamides, including paraherquamide H and paraherquamide I, two new alkaloids isolated from *Penicillium cluniae*. *Journal of Agricultural and Food Chemistry* **54**: 2921–2925. https://doi.org/10.1021/jf0530998

López-Gresa MP, González MC, Primo J, *et al.* (2005). Circumdatin H, a new inhibitor of mitochondrial NADH Oxidase, from *Aspergillus ochraceus*. *The Journal of Antibiotics* **58**: 416–419. https://doi.org/10.1038/ja.2005.54

Loque CP, Medeiros AO, Pellizzari FM, *et al.* (2009). Fungal community associated with marine macroalgae from Antarctica. *Polar Biology* **33**: 641–648. https://doi.org/10.1007/s00300-009-0740-0

Lümmen P (1998). Complex I inhibitors as insecticides and acaricides. *Biochimica et Biophysica Acta (BBA) - Bioenergetics* **1364**: 287–296. https://doi.org/10.1016/s0005-2728(98)00034-6

Ma L-J, Rogers SO, Catranis CM, *et al.* (2000). Detection and characterization of ancient fungi entrapped in glacial ice. *Mycologia* **92**: 286–295. https://doi.org/10.1080/00275514.2000.12061156

Manni M, Berkeley MR, Seppey M, *et al.* (2021). BUSCO update: novel and streamlined workflows along with broader and deeper phylogenetic coverage for scoring of eukaryotic, prokaryotic, and viral genomes. *Molecular Biology and Evolution* **38**: 4647–4654. https://doi.org/10.1093/molbev/msab199

Masclaux F, Guého E, de Hoog GS, *et al.* (1995). Phylogenetic relationships of human-pathogenic *Cladosporium* (*Xylohypha*) species inferred from partial LS rRNA sequences. *Journal of Medical and Veterinary Mycology* **33**: 327–338. https://doi.org/10.1080/02681219580000651

McRae CF, Hocking AD, Seppelt RD (1999). *Penicillium* species from terrestrial habitats in the Windmill Islands, East Antarctica, including a new species, *Penicillium antarcticum*. *Polar Biology* **21**: 97–111. https://doi.org/10.1007/s003000050340

Minh BQ, Schmidt HA, Chernomor O, *et al.* (2020). IQ-TREE 2: new models and efficient methods for phylogenetic inference in the genomic era. *Molecular Biology and Evolution* **37**: 1530–1534. https://doi.org/10.1093/molbev/msaa015

Nelson BD, Walter P, Ernster L (1977). Funiculosin: An antibiotic with antimycin-like inhibitory properties. *Biochimica et Biophysica Acta (BBA) - Bioenergetics* **460**: 157–162. https://doi.org/10.1016/0005-2728(77)90162-1

Ohshiro T, Matsuda D, Sakai K, *et al.* (2011). Pyripyropene A, an acyl–Coenzyme A:cholesterol acyltransferase 2–selective inhibitor, attenuates hypercholesterolemia and atherosclerosis in murine models of hyperlipidemia. *Arteriosclerosis, Thrombosis, and Vascular Biology* **31**: 1108–1115. https://doi.org/10.1161/atvbaha.111.223552

Okabe M, Sugita T, Kinoshita K, *et al.* (2016). Macrolides from a marine-

derived fungus, *Penicillium meleagrinum* var. *viridiflavum*, showing synergistic effects with fluconazole against azole-resistant *Candida albicans*. *Journal of Natural Products* **79**: 1208–1212. https://doi.org/10.1021/acs.jnatprod.6b00019

Panda SS, Girgis AS, Aziz MN, *et al.* (2023). Spirooxindole: a versatile biologically active heterocyclic scaffold. *Molecules* **28**: 618. https://doi.org/10.3390/molecules28020618

Petersen AB, Rønnest MH, Larsen TO, *et al.* (2014). The chemistry of griseofulvin. *Chemical Reviews* **114**: 12088–12107. https://doi.org/10.1021/cr400368e

Pfefferle W, Anke H, Bross M, *et al.* (1990). Asperfuran, a novel antifungal metabolite from *Aspergillus oryzae*. *The Journal of Antibiotics* **43**: 648–654. https://doi.org/10.7164/antibiotics.43.648

Pluskal T, Castillo S, Villar-Briones A, *et al.* (2010). MZmine 2: Modular framework for processing, visualizing, and analyzing mass spectrometry-based molecular profile data. *BMC Bioinformatics* **11**: 395. https://doi.org/10.1186/1471-2105-11-395

Pompeo MM, Cheah JH, Movassaghi M (2019). Total synthesis and anti-cancer activity of all known communesin alkaloids and related derivatives. *Journal of the American Chemical Society* **141**: 14411–14420. https://doi.org/10.1021/jacs.9b07397

Robbers JE, Hong S, Tuite J, *et al.* (1978). Production of xanthomegnin and viomellein by species of *Aspergillus* correlated with mycotoxicosis produced in mice. *Applied and Environmental Microbiology* **36**: 819–823. https://doi.org/10.1128/aem.36.6.819-823.1978

Rong C, Ma Y, Wang S, *et al.* (2016). *Penicillium chroogomphum*, a new species in *Penicillium* section *Ramosa* isolated from fruiting bodies of *Chroogomphus rutilus* in China. *Mycoscience* **57**: 79–84. https://doi.org/10.1016/j.myc.2015.09.001

Schmid R, Petras D, Nothias LF, *et al.* (2021). Ion identity molecular networking for mass spectrometry-based metabolomics in the GNPS environment. *Nature Communications* **12**: 3832. https://doi.org/10.1038/s41467-021-23953-9

Sonjak S, Frisvad JC, Gunde-Cimerman N (2006). *Penicillium* mycobiota in arctic subglacial ice. *Microbial Ecology* **52**: 207–216. https://doi.org/10.1007/s00248-006-9086-0

Sonjak S, Uršič V, Frisvad JC, *et al.* (2007). *Penicillium svalbardense*, a new species from Arctic glacial ice. *Antonie van Leeuwenhoek* **92**: 43–51. https://doi.org/10.1007/s10482-006-9133-3

Tsugawa H, Cajka T, Kind T, *et al.* (2015). MS-DIAL: data-independent MS/MS deconvolution for comprehensive metabolome analysis. *Nature Methods* **12**: 523–526. https://doi.org/10.1038/nmeth.3393

Tsugawa H, Kind T, Nakabayashi R, *et al.* (2016). Hydrogen rearrangement rules: computational MS/MS fragmentation and structure elucidation using MS-FINDER software. *Analytical Chemistry* **88**: 7946–7958. https://doi.org/10.1021/acs.analchem.6b00770

Uchida R, Imasato R, Shiomi K, *et al.* (2005). Yaequinolones J1 and J2, novel insecticidal antibiotics from *Penicillium* sp. FKI-2140. *Organic Letters* **7**: 5701–5704. https://doi.org/10.1021/ol052458h

Uchida R, Imasato R, Tomoda H, *et al.* (2006). Yaequinolones, new insecticidal antibiotics produced by *Penicillium* sp. FKI-2140. I. Taxonomy, fermentation, isolation and biological properties. *The Journal of Antibiotics* **59**: 652–658. https://doi.org/10.1038/ja.2006.87

Visagie CM, Hirooka Y, Tanney JB, *et al.* (2014a). *Aspergillus*, *Penicillium* and *Talaromyces* isolated from house dust samples collected around the world. *Studies in Mycology* **78**: 63–139. https://doi.org/10.1016/j.simyco.2014.07.002

Visagie CM, Houbraken J, Frisvad JC, *et al.* (2014b). Identification and nomenclature of the genus *Penicillium*. *Studies in Mycology* **78**: 343–371. https://doi.org/10.1016/j.simyco.2014.09.001

Visagie CM, Yilmaz N, Kocsubé S, *et al.* (2024). A review of recently introduced *Aspergillus*, *Penicillium*, *Talaromyces* and other *Eurotiales* species. *Studies in Mycology* **107**: 1–66. https://doi.org/10.3114/sim.2024.107.01

Wang M, Carver JJ, Phelan VV, *et al.* (2016). Sharing and community curation of mass spectrometry data with Global Natural Products Social Molecular Networking. *Nature Biotechnology* **34**: 828–837. https://doi.org/10.1038/nbt.3597

Witte TE, Overy DP (2022). Untargeted metabolomic profiling of fungal species populations. In: *Proteomics in Systems Biology: Methods and Protocols* (Geddes-McAlister J, ed Springer Nature, New York: 349–365. https://doi.org/10.1007/978-1-0716-2124-0_24

Witte TE, Villeneuve N, Boddy CN, *et al.* (2021). Accessory chromosome-acquired secondary metabolism in plant pathogenic fungi: the evolution of biotrophs into host-specific pathogens. *Frontiers in Microbiology* **12**: 664276. https://doi.org/10.3389/fmicb.2021.664276

Yang JY, Sanchez LM, Rath CM, *et al.* (2013). Molecular networking as a dereplication strategy. *Journal of Natural Products* **76**: 1686–1699. https://doi.org/10.1021/np400413s

Zaleski K (1927). Uber die in Polen gefunden Arten der Gruppe Penicillium Link. II. *Bulletin International de l'Academie des Sciences de Cracovie. Classe des Sciences Mathematiques et Naturelles. Serie B* **1927**: 459–513.

Zhang Y, Liu S, Liu H, *et al.* (2009). Cycloaspeptides F and G, cyclic pentapeptides from a *Cordyceps*-colonizing isolate of *Isaria farinosa*. *Journal of Natural Products* **72**: 1364–1367. https://doi.org/10.1021/np900205m

Zhao F, Liu Z, Yang S, *et al.* (2020). Quinolactacin biosynthesis involves NRPSs catalyzed Dieckmann condensation to form the quinolone-γ-lactam hybrid. *Angewandte Chemie (International ed. in English)* **59**: 19108–19114. https://doi.org/10.1002/anie.202005770

Zou Y, Zhan Z, Li D, *et al.* (2015). Tandem prenyltransferases catalyze isoprenoid elongation and complexity generation in biosynthesis of quinolone alkaloids. *Journal of the American Chemical Society* **137**: 4980–4983. https://doi.org/10.1021/jacs.5b03022

Zucconi L, Canini F, Temporiti ME, *et al.* (2020). Extracellular enzymes and bioactive compounds from Antarctic terrestrial fungi for bioprospecting. *International Journal of Environmental Research and Public Health* **17**: 6459. https://doi.org/10.3390/ijerph17186459

Supplementary Material: https://studiesinmycology.org/

Fig. S1. MS-FINDER annotation of asperfuran based on in silico MS2 fragmentation prediction. Experimentally obtained spectrum is in black while in silico predicted spectral scores are in red. **A.** Asperfuran *m/z* 219.1012 [M+H]+.

Fig. S2. GNPS annotation of asperphenamates. Experimentally obtained spectra are in black, spectra from MS2 database are coloured green. **A.** Asperphenamate *m/z* 507.2263 [M+H]+. **B.** Asperphenamate Analog *m/z* 523.2209 [M+H]+.

Fig. S3. MS-FINDER annotation of aurantiamines based on in silico MS2 fragmentation prediction. Experimentally obtained spectra are in black while in silico predicted spectral scores are in red. **A.** Pre-aurantiamine *m/z* 235.119 [M+H]+. **B.** Viridamine or aurantiamine *m/z* 303.1815 [M+H]+.

Fig. S4. MS-FINDER annotation of chaetoglobosins based on MS2 fragmentation prediction/analysis. Experimentally obtained spectra are in black, in silico predicted spectral scores are in red and spectra from MS2 database are coloured green. **A.** Chaetoglobosin A *m/z* 529.2695 [M+H]+. **B.** Viomellein *m/z* 561.1392 [M+H]+. **C.** Chaetoglobosin E *m/z* 531.2850 [M+H]+. **D.** Cytoglobosin *m/z* 515.2904 [M+H]+.

Fig. S5. MS-FINDER annotation of chrysogenamide A based on in silico MS2 fragmentation prediction. Experimentally obtained spectra are in black while in silico predicted spectra are in red. **A.** Chrysogenamide

A *m/z* 448.2966 [M+H]+. **B.** Chrysogenamide A *m/z* 448.2966 [M+H]+.

Fig. S6. MS-FINDER annotation of communesins based on in silico MS2 fragmentation prediction. Experimentally obtained spectra are in black while in silico predicted spectral scores are in red. **A.** Communesin A *m/z* 457.2587 $[M+H]^+$. **B.** Communesin F. *m/z* 441.2634 $[M+H]^+$. **C.** Communesin G *m/z* 471.2739 $[M+H]^+$. **D.** Communesin H *m/z* 485.2898 $[M+H]^+$.

Fig. S7. MS-FINDER annotation of fungal statins based on comparison to experimentally-derived MS2 spectra (compactin and compactin open forms) and in silico MS2 fragmentation prediction (lovastatin and pravastatin). Experimentally obtained spectra are in black, spectra from MS2 database are coloured green, and in silico predicted spectral scores are in red. **A.** Compactin *m/z* 391.2481 [M+H]+. **B.** Compactin Open Form *m/z* 391.2480 [M+H-H2O]+. **C.** Compactin Open Form *m/z* 391.2482 [M+H-H2O]+. **D.** Lovastatin *m/z* 405.2639 [M+H]+. **E.** Pravastatin *m/z* 447.2355 [M+Na]+.

Fig. S8. MS-FINDER annotation of additional fungal statins based on comparison to experimentally-derived MS2 spectra (ML236A) and in silico MS2 fragmentation prediction (CNP0217257, CNP0429426 and ML236A). Experimentally obtained spectra are in black, spectra from MS2 databases are coloured green while in silico predicted spectral scores are in red. **A.** CNP0217257 *m/z* 405.2635 [M+H-H2O]+. **B.** CNP0217257 *m/z* 423.2744 [M+H]+. **C.** CNP0429426 *m/z* 325.2013 [M+H]+. **D.** ML236A *m/z* 307.1905 [M+H]+. E) ML236A *m/z* 307.1905 [M+H]+.

Fig. S9. MS-FINDER annotation of cycloaspeptides based on comparison to experimentally-derived MS2 spectra (cycloaspeptide A and H) and in silico MS2 fragmentation prediction (cycloaspeptide B/C/D and E). Experimentally obtained spectra are in black, spectra from MS2 databases are coloured green, while in silico predicted spectral scores are in red. **A.** Cycloaspeptide A *m/z* 642.3283 [M+H]+. **B.** Cycloaspeptide B/C/D *m/z* 628.3127 [M+H]+. **C.** Cycloaspeptide E *m/z* 626.3339 [M+H]+. **D.** "Cycloaspeptide H_130057" *m/z* 672.3394 [M+H]+ (see text for discussion on cycloaspeptide H annotation).

Fig. S10. MS-FINDER annotation of cycloaspeptide G based on in silico MS2 fragmentation prediction. Experimentally obtained spectra are in black while in silico predicted spectral scores are in red. **A.** Cycloaspeptide G *m/z* 658.3240 [M+H]+. **B.** Cycloaspeptide G *m/z* 658.3240 [M+H]+.

Fig. S11. MS-FINDER annotation of marcfortines based on in silico MS2 fragmentation prediction. Experimentally obtained spectra are in black, spectra from MS2 database are coloured green, and in silico predicted spectral scores are in red. **A.** Fellutanine A *m/z* 373.166 [M+H]+. **B.** Fellutanine B *m/z* 448.2597 [M+H]+. **C.** Fellutanine C *m/z* 509.291 [M+H]+. **D.** Amauromine *m/z* 509.2914 [M+H]+.

Fig. S12. MS-FINDER annotation of funiculosins based on in silico MS2 fragmentation prediction. Experimentally obtained spectra are in black while in silico predicted spectral scores are in red. **A.** Funiculosin *m/z* 492.2958 [M+H]+. **B.** Funiculosin- like *m/z* 476.3013 [M+H]+.

Fig. S13. GNPS annotation of griseofulvins based on based on comparison to standard-derived MS2 spectra. Experimentally obtained spectra are in black and spectra from MS2 database are coloured green. **A.** Griseofulvin *m/z* 353.0784 [M+H]+. **B.** Dechlorogriseofulvin *m/z* 319.1176 [M+H]+.

Fig. S14. MS-FINDER annotation of mangrovamides based on in silico MS2 fragmentation prediction. Experimentally obtained spectra are in black while in silico predicted spectral scores are in red. **A.** Mangrovamide F *m/z* 432.2646 [M+H]+. **B.** Mangrovamide G or VM-55599 *m/z* 350.2226 [M+H]+.

Fig. S15. MS-FINDER annotation of marcfortines based on in silico MS2 fragmentation prediction. Experimentally obtained spectra are in black while in silico predicted spectral scores are in red. **A.** Marcfortine A *m/z* 478.2704 [M+H]+. **B.** Marcfortine B *m/z* 464.2546 [M+H]+. **C.** Marcfortine C *m/z* 448.2597 [M+H]+.

Fig. S16. MS-FINDER annotation of melearoride A and PF 1136B based on in silico MS2 fragmentation prediction. Experimentally obtained spectra are in black while in silico predicted spectral scores are in red. **A.** Melearoride A *m/z* 486.3577 [M+H]+. **B.** PF 1163B *m/z* 462.3219 [M+H]+.

Fig. S17. MS-FINDER annotation of prenylated cyclodipeptides based on in silico MS2 fragmentation prediction. Experimentally obtained spectra are in black while in silico predicted spectral scores are in red. **A.** Penigequinolone A *m/z* 450.2286 [M+H-H2O]+. **B.** Peniciherquamide *m/z* 494.2647 [M+H]+.

Fig. S18. MS-FINDER annotation of penitrems based on in silico MS2 fragmentation prediction. Experimentally obtained spectra are in black while in silico predicted spectral scores are in red. **A.** Penitrem B *m/z* 584.3372 [M+H]+. **B.** Penitrem D *m/z* 568.3423 [M+H]+. **C.** Penitrem E *m/z* 600.3321 [M+H]+. **D.** Penitrem F *m/z* 618.2979 [M+H]+.

Fig. S19. MS-FINDER annotation of pseurotin A and synerazol based on in silico MS2 fragmentation prediction. Experimentally obtained spectra are in black while in silico predicted spectral scores are in red. **A.** Pseurotin A *m/z* 432.1644 [M+H]+. **B.** Synerazol *m/z* 414.1544 [M+H]+.

Fig. S20. MS-FINDER annotation of psychrophilins based on in silico MS2 fragmentation prediction. Experimentally obtained spectra are in black while in silico predicted spectral scores are in red. **A.** Psychrophilin A *m/z* 433.1499 [M+H]+. **B.** Psychrophilin B *m/z* 435.1652 [M+H]+. **C.** Psychrophilin C *m/z* 407.134 [M+H]+. **D.** Psychrophilin D *m/z* 449.1820 [M+H]+.

Fig. S21. MS-FINDER annotation of pyripyropenes based on in silico MS2 fragmentation prediction. Experimentally obtained spectra are in black while in silico predicted spectral scores are in red. **A.** Pyripyropene A *m/z* 584.2513 [M+H]+. **B.** Pyripyropene C *m/z* 598.263 [M+H]+. **C.** Pyripyropene E *m/z* 452.2432 [M+H]+. **D.** dehydroxylpyripyropene A *m/z* 568.2538 [M+H]+. E) 1-Deacetylpyripyropene A / 7-Deacetylpyripyropene A *m/z* 542.2381 [M+H]+.

Fig. S22. MS-FINDER annotation of quinolactacins based on in silico MS2 fragmentation prediction. Experimentally obtained spectra are in black while in silico predicted spectral scores are in red. **A.** Quinolactacin A *m/z* 271.1436 [M+H]+. **B.** Quinolactacin B *m/z* 257.1282 [M+H]+. **C.** Quinolactacin C *m/z* 287.1388 [M+H]+.

Fig. S23. GNPS annotation of roquefortines based on match to MS2 database spectra. Experimentally obtained spectra are in black while matched database spectra are in green. **A.** Roquefortine C *m/z* 390.1922 [M+H]+. **B.** Roquefortine D *m/z* 392.2082 [M+H]+.

Fig. S24. MS-FINDER and GNPS annotation of quinazolinone alkaloids based on in silico MS2 fragmentation prediction. Experimentally obtained spectra are in black, spectra from MS2 database are coloured green (GNPS), and in silico predicted spectra are in red (MS-FINDER). **A.** Sclerotigenin *m/z* 278.0923 [M+H]+. **B.** Circumdatin F *m/z* 292.1079 [M+H]+.

Fig. S25. GNPS annotation of tryprostatin B based on MS2 fragmentation prediction. Experimentally obtained spectra are in black while database-matched spectra are in green. **A.** Tryprostatin B *m/z* 352.2011 [M+H]+.

Fig. S26. MS-FINDER annotation of unguisins based on in silico MS2 fragmentation prediction. Experimentally obtained spectra are in black while in silico predicted spectral scores are in red. **A.** Unguisin A *m/z* 759.4212 [M+H]+. **B.** Unguisin C *m/z* 775.4131 [M+H]+.

Fig. S27. MS-FINDER annotation of viridic acid. Experimentally obtained spectra are in black while in silico predicted spectral scores are in red. **A.** Viridic acid *m/z* 455.2283 [M+H]+.

Fig. S28. MS-FINDER annotation of xanthomegnins based on in silico MS2 fragmentation prediction. Experimentally obtained spectra are in black while in silico predicted spectral scores are in red. **A.** Xanthomegnin *m/z*

575.1185 [M+H]+. **B.** Viomellein *m/z* 561.1392 [M+H]+. **C.** Vioxanthin *m/z* 547.1599 [M+H]+. **D.** Norlichexanthone *m/z* 259.0601 [M+H]+.

Fig. S29. GNPS annotation of yaequinolones based on match to MS2 database spectra. Experimentally obtained spectra are in black while matched database spectra are in green. **A.** Yaequinolone B *m/z* 384.1443 [M+H]+. **B.** Yaequinolone F *m/z* 448.2123 [M-H2O+H]+. **C.** Yaequinolone J1 *m/z* 450.2286 [M+H]+.

Fig. S30. MS-FINDER annotation of prenylated cyclodipeptides based on in silico MS2 fragmentation prediction. Experimentally obtained spectra are in black while in silico predicted spectral scores are in red. **A.** Paraherquamide B *m/z* 464.2541 [M+H]+. **B.** Rhinocladin A *m/z* 368.2327 [M+H]+.

Table S1. Secondary metabolites annotated in this study. Annotation level definitions: 1 = match to *m/z* from known *Penicillium* metabolite; 2 = supported by in silico prediction of fragmentation scoring (MSFINDER); 3 = supported by match to spectra from online databases of chemical standards (using MSDIAL or GNPS); N/A = unknown structure, hypothesized by predicted chemical formula.